Inverter-Based Resources Controlled as a Virtual Synchronous Machine for Improved System Dynamic Performance and Stability

by

Randupama T. Gunasekara

A Thesis submitted to the Faculty of Graduate Studies of
The University of Manitoba
in partial fulfilment of the requirements of the degree of

Doctor of Philosophy

Department of Electrical and Computer Engineering
University of Manitoba
Manitoba, Canada

Abstract

The large-scale penetration of Renewable Energy Resources (RES) will displace conventional synchronous machine-based power generation, reducing the overall system inertia and resulting in lower Short Circuit Levels (SCLs) at the locations where RES connect to the grid. RES, such as wind and solar PV, are interfaced with the power system through power electronic inverters. Operating inverter-based equipment under low inertia and SCLs presents several challenges, including poor fault recovery response, unstable oscillatory interactions, and the impact on torsional oscillations of thermal generating units. This research investigates the effectiveness of inverters controlled as Virtual Synchronous Machines (VSMs) in addressing some of these issues.

In this research a Battery Energy Storage System (BESS) inverter is controlled as a VSM, with input signals derived from solving the time-domain equations of a synchronous machine. The responses of the exciter, governor, and power system stabilizer are also incorporated into the VSM control strategy. The dynamic characteristics of the proposed VSM are validated using a Single Machine Infinite Bus (SMIB) test model. The effectiveness of the VSM approach in mitigating specific technical challenges is verified through dynamic response studies conducted on several test systems, including a representative European transmission system. The VSM's response is compared to that of a conventional synchronous machine in all test cases, demonstrating a close correlation in dynamic behaviour. Additionally, the proposed VSM concept was implemented on a solar PV plant inverter operating in grid-following mode. The simulation results highlighted a hybrid method that combines the technical advantages of both typical grid-following and VSM-based inverter control designs. In all test scenarios, the simulation results confirm that the VSM performs as expected and can effectively mitigate stability issues related to low system inertia and low short circuit strength. Furthermore, this research explores the adaptability of VSM controls in

providing essential functionalities, such as inertial and fast frequency response, to enhance grid stability, improve operational efficiency, and ensure compliance with grid code requirements.

Copyright Forms

I would like to acknowledge the use of the following publications in preparation of this thesis. Chapter 3 ©2022 IEEE. Content was used, with permission, from R. T. Gunasekara, S. Filizadeh, and D. Muthumuni, "Battery Energy Storage System Controlled as a Virtual Synchronous Machine for Improved System Stability," in 2022 IEEE Power & Energy Society General Meeting (PESGM), Denver, CO, USA.

In reference to IEEE copyrighted material, which is used with permission in this thesis, the IEEE does not endorse any of University of Manitoba's products or services. Internal or personal use of this material is permitted. If interested in reprinting/republishing IEEE copyrighted material for advertising or promotional purposes or for creating new collective works for resale or redistribution, please go to https://www.ieee.org/publications/rights/index.html to obtain information on how to obtain a License.

Chapter 4 reprinted with the permission from R. T. Gunasekara, S. Filizadeh, D. Muthumuni, D. Kho, B. Marshall, B. Ponnalagan, O. D. Adeuyi, "A novel virtual synchronous machine implementation and verification of its effectiveness to mitigate renewable generation connection issues at weak transmission grid locations," in IET Renewable Power Generation, vol. 17, no. 10, pp. 2436-2457, 2022. Please visit https://creativecommons.org/licenses/by-nc-nd/4.0/ for more information on licensing agreements regarding reprinting the content.

Chapter 5 "Application of the Virtual Synchronous Machine Approach to Control a Solar PV Power Plant for Improved System Stability," reprinted with permission from CIGRE Canada Conference & Exhibition, Vancouver, BC, Canada, 2023, ©2023.

Chapter 6 “Performance testing of a solar PV system controlled as a virtual synchronous machine to verify grid code compliance”, reprinted with permission from IET International Conference on AC and DC Power Transmission, Birmingham, UK, 2025 ©2025.

Acknowledgements

I would like to express my deepest gratitude to my supervisor, Professor Filizadeh, for his unwavering support, invaluable guidance, and insightful feedback throughout my Ph.D. journey. His thoughtful advice and continuous support have been crucial to the success of my work.

I am also profoundly thankful to Dr. Dharshana Muthumuni, whose industry expertise and encouragement have been a tremendous help throughout this process. His mentorship has been instrumental in shaping both my academic and professional growth.

I would also like to extend my heartfelt thanks to my husband, Sajith Perera, for his patience, love, and encouragement, which sustained me through the challenges of this journey. My sincere gratitude also goes to my family, and friends for their constant support.

Dedications

To my loving parents, and siblings.

Table of Contents

List of Figures

List of Tables

List of Symbols

P_{ref}	active power reference
Q_{ref}	reactive power reference
V_{ref}	voltage reference
PF_{ref}	power factor reference
p_m	measured active power
q_m	measured reactive power
$v_{rms,m}$	measured voltage (rms)
f_m	measured frequency
$p_{inv,ref}$	inverter active power reference
$q_{inv,ref}$	inverter reactive power reference
v_{dref}	voltage reference (direct axis)
v_{qref}	voltage reference (quadrature axis)
$v_{d,m}$	voltage measured (direct axis)
$v_{q,m}$	voltage measured (quadrature axis)
$i_{d,m}$	current measured (direct axis)
$i_{q,m}$	current measured (quadrature axis)
$i_{d,ref}$	current reference (direct axis)
$i_{q,ref}$	current reference (quadrature axis)
$i_{d,inj,FRT}$	current injection (direct axis) during fault ride through
$i_{q,inj,FRT}$	current injection (quadrature axis) during fault ride through
$v_{t,m}$	instantaneous voltage measured
$v_{a,ref}$, $v_{b,ref}$, $v_{c,ref}$	voltage references (phase A, phase B, and phase C)
D_f	frequency droop
D_v	voltage droop
ω_g	grid frequency
T_f	time constant of the low-pass filter
ω_n	nominal frequency
v_n	nominal voltage
T_m	mechanical torque

T_e	electrical torque
J	moment of inertia
ω	machine speed
H	inertia constant
P_m	mechanical power
P_e	electrical power
i_{ref}	reference current
λ_d	flux linkage (d axis)
λ_q	flux linkage (q axis)
λ_f	flux linkage (field winding)
R_s	stator resistance
R_f	field resistance
E_f	field voltage
i_f	field current
λ_{kq}	flux linkage (damper winding quadrature axis)
λ_{kd}	flux linkage (damper winding direct axis)
R_{kq}	resistance (damper winding quadrature axis)
R_{kd}	resistance (damper winding direct axis)

List of Abbreviations

AC	alternating current
VSM	virtual synchronous machine
BESS	battery energy storage system
POI	point of interconnection
PV	photo voltaic
DC	direct current
EMT	electro-magnetic transient
SCR	short circuit ratio
HVDC	high voltage direct current
IGBT	insulated gate bipolar transistor
FACTS	flexible alternating current transmission system
LV	low voltage
MV	medium voltage
HV	high voltage
CI	control interactions
SSTI	sub-synchronous torsional interactions
SSCI	sub-synchronous control instability
IBR	Inverter based resources
EMT	electromagnetic transient
SMIB	single machine infinite bus
PLL	phase lock loop
PPC	power plant controller
PWM	pulse width modulation
VSC	voltage source converter
IGBT	insulated-gate bipolar transistor
DC	direct current
LVRT	low voltage ride through
SOC	state of charge
WF	wind farm

MQT	model quality test
HVRT	high voltage ride through
SPC	special protection scheme
SF	solar farm

Chapter 1: Introduction

1.1. Background and Motivation

Electrical energy is a critical commodity that is expected to be available to end-users with a high level of reliability. Since the early days of electrical energy systems, most nations in the world have relied on conventional power generation based on burning fossil fuels to meet the ever-growing demand for electricity. However, conventional thermal power generation has adverse effects on the environment. Almost all nations have acknowledged this impact and the need to reduce dependency on fossil fuels for power generation. 'Net zero – 2050', 'Climate-neutral by 2050', and 'Net-Zero Emissions by 2050' are a few examples of such policies initiated by several nations to lead the drive for clean, environmentally friendly energy [1 - 3]. These initiatives have encouraged and mandated a higher percentage of renewable energy in the generation mix of most countries. While there are many alternative renewable energy sources, wind and solar power have proved to be the most viable for bulk power generation. Recent advancements in Battery Energy Storage technology are also expected to play a major role in enabling intermittent energy sources such as wind and solar.

Renewable resources are interfaced to the transmission system via power electronic converters. The dynamic response characteristics of power electronic converters are much different from those of conventional generators. Power electronic-based generators do not provide some of the favorable characteristics that conventional generators provide from a power system dynamic stability point-of-view, such as inertia contribution and short circuit current contribution. Due to this reason, operation of electric networks with high penetration of wind and solar PV generation is challenging, and careful planning and consideration are necessary to ensure reliable operation

of such power system. While encouraging high percentages of penetration of renewable energy resources, national electric network operators also require maintained reliability for system operation. This has further complicated the renewable energy integration landscape. As such, it is timely to identify potential issues and investigate appropriate mitigation options to overcome them. Specifically, converter-based generators do not contribute to system inertia and, thus, can potentially make the power system vulnerable to instability following events such as transmission system faults. Renewable resources may often be located far from load centers and long transmission lines need to be used to connect the power electronic-based generation to the rest of the grid. The short circuit current or short circuit ratio (SCR) at the point of interconnection can be low, resulting in what is known as a 'weak grid' location. This is an important consideration in view of renewable integration as it can cause dynamic response issues [4]. Therefore, these stability-related issues must be identified in the design stage of new projects, and mitigation methods must be introduced.

1.2. Problem Definition and Conventional Solutions

If inverter-based generation is not carefully designed, the following stability and dynamic response related issues may arise during operation:

- Poor fault ride-through (recovery following a fault clearance) response of renewable power generation and other devices such as Flexible Alternating Current Transmission System (FACTS) equipment and High Voltage Direct Current (HVDC) systems following system disturbances.
- Undesirable interaction (commonly termed as control interactions (CI)) between dynamic devices located in close vicinity. These interactions can lead to poorly damped oscillations,

and risks are elevated when the plants are situated in a weak grid location within the network [5, 6].

- Sub-Synchronous Torsional Interactions (SSTI) – impact on thermal generator shafts. Power electronic converter-based plants can interact with thermal generator shafts and give rise to poorly damped mechanical oscillations [7].
- Sub-Synchronous Control Instability (SSCI) due to interaction with series compensated transmission lines [8].
- Concerns related to fault-current contribution.
- Concerns related to harmonics and power quality.

In this research, the primary focus is on addressing 'fault ride-through' response and undesirable interaction issues of renewable power generation under low system-strength conditions. To mitigate these problems a Battery Energy Storage System (BESS) inverter is controlled as a Virtual Synchronous Machine (VSM), thereby effectively introducing synthetic inertia to the system. In addition to improved inertial response, the VSM approach may also have the potential to address other technical issues such as SSCI and SSTI.

Different inverter topologies and control strategies have been proposed by both vendors and industry experts to address potential system stability concerns that arise from high levels of renewable energy generation. Some of these issues can be mitigated through controller tuning [9], adjustment of inverter protection settings, and other options [10]. A coordinated approach to the overall system design, considering network characteristics and the dynamic response of other plants in the local area, is essential. However, this may pose a challenge, given that these plants are often designed by different vendors and commissioned at different times. Some known mitigation measures for dynamic response issues include the following:

- Coordinated tuning of plant controls and protection [9].
- Addition of synchronous condensers [11].
- Addition of dynamic reactive power compensation (SVC, STATCOM) [12].
- Implementing operational constraints [13] or special protection schemes [14].
- Utilization of capacitor banks or shunt reactors [15].
- Utilization of transformer tap changers [16].

Other potential mitigation approaches include:

- Grid-forming technology [46], and
- Novel inverter control strategies such as the VSM approach investigated in this research.

1.3. Research Objectives and Contributions

1.3.1. Research Objectives

The primary objectives of this research are:

- To identify and analyze the system stability challenges faced by power system operators due to high renewable energy penetration, with a specific focus on evaluating its adverse impacts on system strength and overall grid stability.
- To review and evaluate existing mitigation methods, including traditional approaches and novel control strategies, used to address power system stability challenges caused by high penetration of renewable energy, assessing their effectiveness in maintaining grid reliability.
- To design and develop a novel control strategy for grid-following inverter-based resources (IBRs) that emulates the inertial and damping characteristics of synchronous machines

(Virtual Synchronous Machine implementation), thereby enhancing their ability to contribute to power system stability during high renewable energy penetration scenarios.

- To implement the proposed Virtual Synchronous Machine (VSM) control strategy in a Battery Energy Storage System (BESS) and experimentally validate its performance, with a focus on assessing its impact on grid voltage and frequency stability under high renewable energy penetration scenarios.
- To validate the proposed Virtual Synchronous Machine (VSM) control strategy by implementing it in a Battery Energy Storage System (BESS) within a practical transmission network featuring high renewable penetration. The study will evaluate the strategy's effectiveness in enhancing system stability; particularly under weak grid conditions by analyzing its impact on voltage regulation, frequency response, and overall grid resilience.
- Investigate the dynamic response of the VSM approach when applied to a solar PV plant operating in 'Grid-Following' mode.
- Investigate the adaptability and potential of VSM-controlled inverters in delivering key functionalities, such as inertial and fast frequency response, to meet essential grid code requirements.

1.4. Contributions

This research makes several contributions to the fields of renewable energy integration and power system stability, in the context of large-scale penetration of inverter-based resources. The key contributions of the thesis are summarized below:

- Development of a novel VSM control strategy that can be applied to grid-following inverters: Most of existing VSM control strategies in the literature are based on inverters

operating with the grid-forming technique and are formulated using simplified emulations of a synchronous machine. The proposed approach enables the emulation of both electromagnetic and mechanical dynamics of a synchronous machine, thus capturing its full transient behavior.

- Implementation and validation through EMT simulations: The proposed VSM control method is applied to a BESS system and rigorously tested using an Electromagnetic Transient Simulation (EMT) platform. The method is tested, and its performance is validated on several practical transmission test systems.
- Application and verification of the proposed VSM approach for large-scale transmission networks: Unlike conventional VSM methods proposed in literature that predominantly focus on grid-forming applications in isolated or microgrid networks, this research extends the VSM approach to transmission-level systems, addressing renewable integration issues in weak grid locations.
- Implementation of the VSM approach on other renewable generation applications: By implementing the VSM approach not only on BESS systems but also on solar PV plant inverters, this research demonstrated significant improvements in system stability, addressing issues such as fault recovery and unstable oscillations.
- Scalability to hybrid renewable systems: The research introduces a hybrid method that integrates the technical advantages of grid-following and VSM-based controls.
- Introduction of the concept of "un-curtailed inertia capacity" of an IBR: This research presents a framework for analyzing the factors that influence the inertial power contribution of IBRs with specific MVA ratings.

1.5. List of Publications

The contributions made in this research have resulted in the following publications.

- R. T. Gunasekara, S. Filizadeh, and D. Muthumuni, "Battery Energy Storage System Controlled as a Virtual Synchronous Machine for Improved System Stability," in Proc. IEEE Power & Energy Society General Meeting (PESGM), Denver, CO, USA, 2022, pp. 1-5.
- R. T Gunasekara, D. Muthumuni, S. Filizadeh, D. Kho, B. Marshall, B. Ponnalagan, O. D. Adeuyi, "A novel virtual synchronous machine implementation and verification of its effectiveness to mitigate renewable generation connection issues at weak transmission grid locations," *IET Renewable Power Generation*, vol. 17, no. 10, pp. 2436-2457, 2022.
- R. T. Gunasekara, D. Muthumuni, and S. Filizadeh, "Application of the Virtual Synchronous Machine Approach to Control a Solar PV Power Plant for Improved System Stability," in Proc. CIGRE Canada Conference & Exhibition, Vancouver, BC, Canada, Sept. 25–28, 2023.
- R. T. Gunasekara, D. Muthumuni, and S. Filizadeh, "Performance testing of a solar PV system controlled as a virtual synchronous machine to verify grid code compliance," in Proc. 22nd IET International Conference on AC and DC Power Transmission, Birmingham, UK, Mar. 17–19, 2025.

1.6. Thesis Outline

This thesis is organized into seven chapters, each addressing various aspects of the research conducted. The structure of the thesis is as follows:

Chapter 1 provided the background information necessary to understand the core concepts of the thesis. It included detailed problem definition, discussed conventional solutions to the identified problems, and presented the objectives and contributions of the research.

Chapter 2 provides an extensive review of the existing literature on key topics central to the research. It focuses on system strength measures, and the issues that arise from low system strength when IBRs are connected to the grid. The chapter also highlights incidents and challenges reported related to IBR integration in grids with low system strength and explores various proposed solutions aimed at addressing these issues. Additionally, the chapter discusses the concept of Virtual Synchronous Machines (VSM) technology in grid-forming mode, while also identifying the limitations of current VSM methods.

Chapter 3 explores the theoretical background and mathematical formulation of the VSM concept, focusing on its role in enhancing grid stability in systems with high penetration of renewable energy sources. It describes the detailed implementation of the VSM. The implementation is tested on a Single Machine Infinite Bus (SMIB) test system and the verification results are presented. The VSM-based BESS system is then implemented on a number of practical transmission systems. The effectiveness of the VSM based BESS in mitigating challenges is demonstrated through simulations and presented in this chapter.

Chapter 4 provides an in-depth analysis of the application and verification of the VSM concept in a practical European high-voltage network. The performance of the VSM approach is evaluated

in a real-world transmission system context, ensuring its robustness in a complex grid environment with high renewable penetration.

Chapter 5 shows the VSM approach applied to a solar PV system. The response of the system is validated through detailed analysis and simulations, demonstrating the effectiveness of the VSM concept in renewable-based power systems. In addition, the VSM concept is further extended by introducing a hybrid method that integrates the technical advantages of grid-following and VSM-based controls.

Chapter 6 provides a detailed analysis of the functional performance of a grid-following solar inverter operating as a VSM. It introduces an EMT - domain testing procedure to verify compliance with grid codes and validates the VSM control design, focusing on key functionalities such as inertial and fast frequency responses. Additionally, the chapter introduces the concept of "un-curtailed inertia capacity", offering insight into the factors influencing the inertial power contribution of IBRs.

Chapter 7 summarizes the key conclusions drawn from the investigations carried out throughout the research. It highlights the main contributions, and a list of publications completed based on the findings of this research. This chapter also discusses potential future work that could extend and build upon the findings of this thesis.

Chapter 2: Literature Review

2.1. An Overview of Grid-Following Inverter-Based Resource (IBR) Technology

The majority of inverter-based generation schemes connected to power systems worldwide operate in grid-following mode [17]. Grid-following inverters function by "following" the grid's voltage and frequency, typically using a phase-locked loop (PLL) to synchronize with the grid voltage. Figure 2.1 provides a block diagram of a typical wind farm interconnection setup to an AC system. The set point inputs to the Power Plant Controller (PPC) include the active power reference (P_{ref}) and the reactive power reference (Q_{ref}). Typically, the reactive power output is controlled by selecting one of the three control options: voltage control (V_{ref}), power factor control (PF_{ref}), or direct reactive power control (Q_{ref}). Typically, the input quantities to the PPC are the measured active power (p_m), reactive power (q_m), rms voltage ($v_{rms,m}$), and the grid frequency (f_m). Based on these inputs, the PPC determines the active power command ($p_{inv,ref}$) and reactive power command ($q_{inv,ref}$) required for the inverter-level controls. The inverter-level control then calculates the reference voltage waveforms required to generate the switching pulses for the inverter.

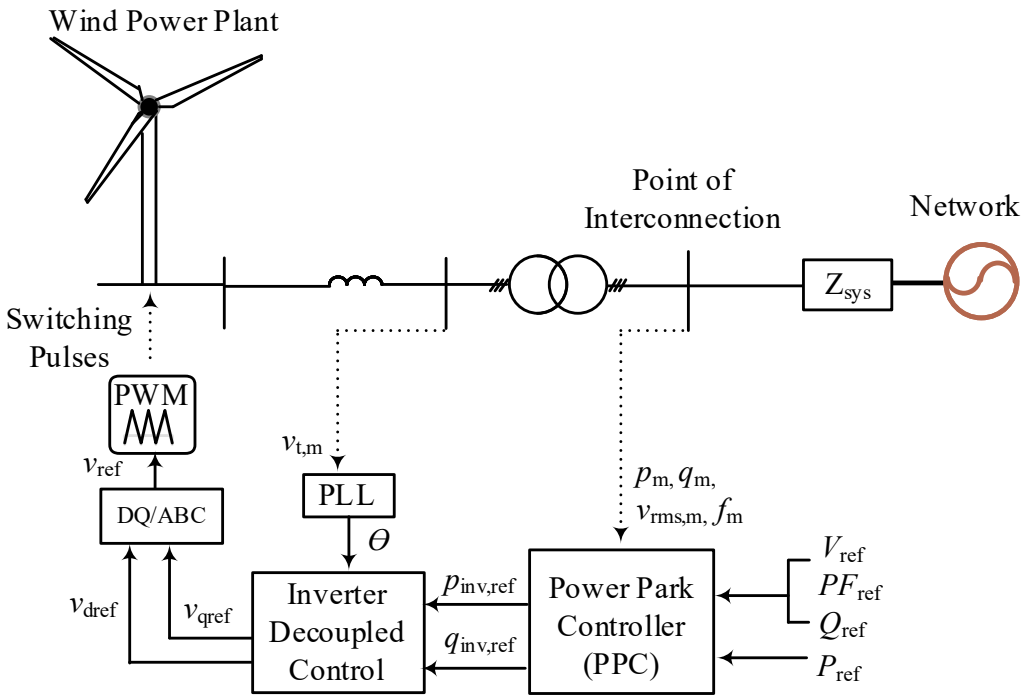

Figure 2.1: A typical block diagram of a wind power plant connecting to a power system.

Details of the PPC and the decoupled controller are shown in Figure 2.2. The operation of the Voltage Source Converter (VSC) and its controls are well established in literature [17]. For clarity, the control system is divided into several blocks for ease of understanding (Refer to Figure 2.2).

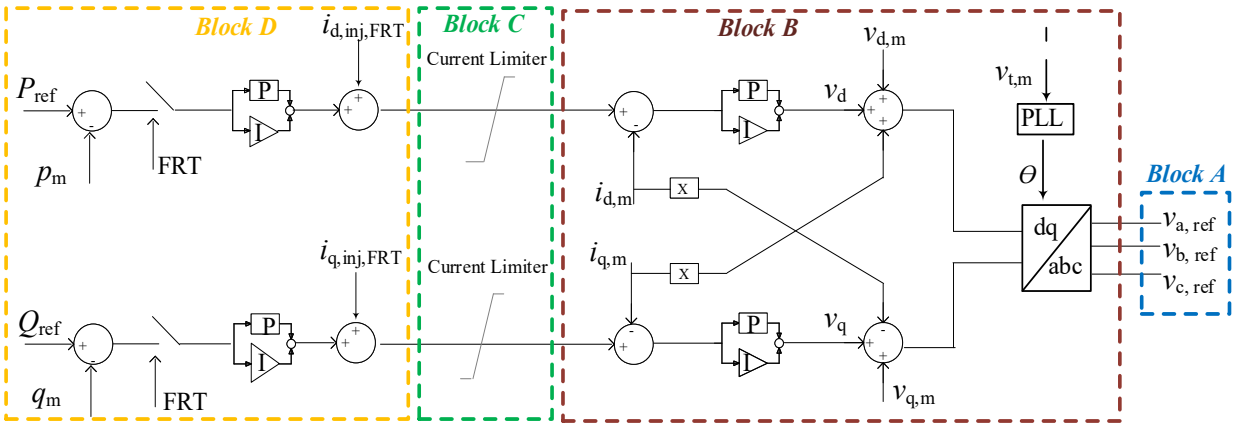

Figure 2.2: Basic layout of an inverter controller connected to an AC power system and associated controls.

Block A: Reference voltage signals that are compared with a carrier waveform to generate switching pulses for the inverter's IGBT switches.

Block B: The inner loop of the control block is referred to as the de-coupled current control block. The inputs to the de-coupled current control block are the reference currents $i_{d,ref}$ and $i_{q,ref}$ as well as measured system voltages in the d-q frame ($v_{d,m}$ and $v_{q,m}$). The de-coupled current control block outputs the reference voltages in the d-q reference frame.

Block C: Depicts the implementation of current limiting. If the current references generated by the controller are outside the rated current envelop of the inverter, they will be adjusted based on a preference mode (i_d (P) priority or i_q (Q) priority).

Block D: Typically, the outer level controls adjust the current reference to minimize the error between the reference power (or active power) and the voltage (or reactive power) output measured at the Point of Interconnection (POI). However, in other applications, the i_d reference may be derived based on other quantities such as the DC link voltage error. Likewise, i_q may also be derived based on other quantities such as the rms voltage error.

2.2. Limitations and Challenges Associated with Grid-Following IBR Schemes

There are several key reasons why special attention must be given to assess stability problems when power electronics-based renewable energy penetration assumes a large share in weak grids:

- Power electronic inverter controls rely on system measurements as inputs. Precise estimation of the instantaneous phase angle using PLLs is often essential and plays a critical role in achieving successful fault ride-through response. Accurate estimation of the system voltage is a challenge when the plant is connected at weak grid locations.

- Power electronic inverters possess the capability to deliver speedy responses (both real and reactive power). However, this capability can also be problematic in weak grid locations.
    - Fast injection of real power can lead to rapid changes in the bus voltage angle, potentially leading to PLL tracking errors and unacceptable response (e.g., tripping, reverse power flow, oscillatory response) [47].
    - Fast injection of reactive current by multiple plants in a weak local area can lead to undesirable interactions between the plants [48].
- Electric network dynamics such as DC offsets (in voltage, in particular) will have an impact on inverter performance following a fault. Rotary synchronous generators are more robust and less susceptible to network transient effects.
- Network transients will lead to voltage waveforms with high harmonic contents immediately following events such as fault clearance. The control and measurement systems of inverters that are exposed to such challenging conditions are also expected to function as intended.
- A weak grid location is an indication that synchronous generation, which provides inertia, is located relatively far from the POI. Grid-following IBRs do not provide the same inertial support that synchronous machines do. System disturbances such as fault clearance (e.g., tripping of lines or other equipment) will lead to a high rate of change of the bus voltage angle. The inverter controls can find it challenging to track fast angle changes caused by limitations in PLL response. Synchronous machines provide inertia, which help limit the rate of change of the ac system voltage at locations close to the synchronous machine connection.

- In addition to the PLL output inaccuracies described above, other input signal measurement-related points that can impact the inverter's response include:
    - Delays associated with signal transmission from the POI to the inverter unit,
    - Delays introduced by signal filtering,
    - Limitations of specific measuring techniques adopted (e.g., to estimate frequency, power, reactive power, rms voltage).
- Unplanned tripping of plants can impact the frequency stability of the system. The resulting oscillatory response can have negative impacts on grid reliability, such as unit tripping, flicker, or power quality concerns, and ultimately potential human safety concerns or equipment damage [18, 19].
- Most relays depend on a threshold level of fault current to be available. High penetration of inverter-based renewable generation (and the expected retirement of conventional generation plants) can impact the reliability of protection devices [20].

2.3. Measures of System Strength

System strength refers to a power system's ability to maintain stable voltage levels and ensure rapid voltage recovery following system disturbances. It is determined by the grid's impedance at a given location and the capacity of voltage sources, such as synchronous generators, to deliver high fault currents. A system with high strength can better withstand disruptions, while a weak system may be negatively impacted by voltage instability, poor fault recovery, or even cascading failures. Strengthening the grid often requires solutions such as synchronous condensers or strategic network reinforcements, especially as renewable energy integration grows.

System inertia is the grid's resistance to sudden frequency changes, enabled by the kinetic energy stored in the rotating masses of synchronous generators. When electricity supply and power demand are imbalanced, or under abnormal events, the rotating masses in the power system either slow down or speed up, releasing or absorbing kinetic energy to stabilize grid frequency. This slows the rate of frequency deviation until additional frequency support mechanisms activate. Traditionally, inertia has been provided by coal, gas, and hydro plants; however, modern systems with high renewable penetration, where generation is decoupled from the grid, lack this natural inertia. This increases the risk of rapid frequency instability and introduces operational challenges. To address this, modern grids may require synthetic inertia from inverter-based resources (as proposed in this thesis), fast-responding batteries, or synchronous condensers to replicate this critical stabilizing effect and ensure reliability.

The short circuit strength at the connection point of a renewable generation plant, indicated by the short circuit ratio (SCR), is an important consideration when designing power electronic inverter controls. The SCR denotes predominantly what is known as the "system strength" in industry. Typically, the SCR is estimated by calculating the fault current at a specific POI. Higher fault current levels result in higher SCRs while lower fault current levels result in low SCRs, indicating what is known as a "weak system" [21]. A weak grid implies a higher system impedance as seen from the POI (looking towards the AC network).

While there is no global industry-accepted standard, the following classification [22] is a generally reasonable indication of the system strength:

- A high SCR: SCRs greater than 3,
- A low SCR: SCRs between 2 and 3,
- A very low SCR: SCRs less than 2.

A low SCR is an indication of potential dynamic response issues with power electronic-interfaced devices and also indicates potential for overall system dynamic response concerns. Although SCR is an effective screening measure to identify potential dynamic response and stability issues for the IBR response as well as the overall system, it is only one indicator. Other measures such as overall inertia and the location of machines providing inertia (i.e., their proximity to inverter-tied devices) will also have a significant impact on the stability of inverters, and hence the power system. In this research, a few simulation-based exercises (details provided in Chapter 3) are performed to investigate the importance and effect of higher system inertia on dynamic response of renewable plants connected in presence of low SCR values [23].

2.3.1. Incidents Reported due to IBR Connection in Grids with Low System Strength

There are several issues reported worldwide due to IBR connections in power systems with low system strength. Some of these issues are listed below.

- Sustained low-frequency oscillations in the range of 8-12 Hz were observed in the Australian power system [24]. Even though these oscillations were small in magnitude, the frequency range is of concern from the standpoint of visible flicker. As a result, mitigation or operational measures (such as limiting the number of power electronic devices in operation under specific system conditions) were required. In some cases, control settings of existing (legacy) SVCs were identified as contributing factors. Based on simulation studies, enhancing the system's robustness through the incorporation of synchronous condensers was identified as a potential solution. In Chapter 3, the proposed VSM control strategy is applied to a BESS to mimic the characteristics of a synchronous condenser. The effectiveness of this approach is validated, demonstrating the BESS's capability to provide inertia emulation and support the stable operation of inverter-based resources (IBRs).

- Extreme weather conditions in 2016 resulted in five system faults on the south Australian transmission system over a period of 87 seconds [25] leading to a blackout. The outage of up to 3 lines weakened the transmission system. Due to extreme wind conditions, there was a sustained reduction in wind generation to the north of Adelaide, resulting in an increase in the interconnector power flow from the neighbouring state. The increase of imports on the interconnector resulted in the activation of interconnector's automatic loss of synchronism protection. Once the ac line interconnecting the two states tripped, the inertia of the south Australian system was insufficient to limit the rate of frequency drop. According to the findings of the AEMO investigations, there is a special 'Inverter Protection Function' that is present in most wind generation converters where the units are tripped in the event of multiple faults within a short period. This protection feature (implemented by vendors) was not known by system operators prior to this event. In Chapter 4, the proposed Virtual Synchronous Machine (VSM) control strategy is implemented on a BESS to emulate the behavior of a synchronous condenser. The analysis validates the effectiveness of the approach, demonstrating the BESS's ability to provide inertia emulation and enhance the stability of inverter-based resources (IBRs) in a wide-area network with high levels of renewable energy penetration.
- The Musselroe Wind Farm is located at Cape Portland in the far Northeast of Tasmania, Australia [4]. Due to low system strength, rate of change of frequency and anti-islanding protection concerns under weak grid conditions (reduced inertia) were experienced. Also, the system operator faced difficulty in coordinating control functions between the inverter and the power plant controller. In addition, low-voltage ride through (LVRT) issues were observed. It is shown that the VSM approach proposed in this thesis helps reduce rate of

change of frequency during transient conditions and improves voltage ride though performance (Chapter 3).

- The ERCOT Panhandle region in West Texas is far from synchronous generators and load centres and is considered a weak grid with significant wind generation [21]. The grid was experiencing high voltage sensitivity (dv/dQ) and low SCR. In addition, most of the wind projects connected in the Panhandle region are effectively linked to a 'common' POI, potentially increasing the possibility of interactions. It is shown that the VSM approach proposed in this thesis can be adopted to mitigate unstable system conditions in network regions with high IBR penetration (Chapter 4).

- A number of interaction issues were reported in the ERCOT operated region in Texas, USA. Almost all reported issues were due to power electronic devices interacting with series compensated 345 kV transmission lines. The issues are generally termed as Sub-Synchronous Control Interactions (SSCI) and are predominantly a concern when power electronic devices are radially connected to series compensated lines [25].

- High inrush currents can cause voltage dips near transformer locations. This is specifically an issue when energizing transformers at weak grid locations. The voltage dip magnitude and its duration can impact the operation of other power electronic-based plants in the local area. If the voltage dip magnitude and duration exceed the required low voltage withstand limits of the other plants, there is a risk of plant tripping [21] as this was reported by Southern Company. It is identified that such network transient issues can be mitigated by considering station equipment design such as breakers with pre-insertion resistors.

- Germany's Bard 1/BorWin Project had experienced oscillations around 250–350 Hz at power levels higher than 200 MW [21]. The BorWin harmonic instability was attributed to interactions between active elements (wind turbine generators and HVDC) with the cable system. The cable system had introduced a parallel resonance in the offshore ac network. Harmonics, of frequencies around the network resonance frequency, from the wind turbine generators and HVDC would thus interact with the ac system and distort the ac voltages, leading to harmonic voltage amplifications and potentially, harmonic instability [21].

The proposed VSM approach may be a viable mitigation option for some of the issues reported in Section 2.3.1.

2.4. VSM Technology Used in Grid-Forming Mode

If inverter-based generation is not carefully designed, it can lead to several stability and dynamic response-related issues during operation. Control systems of conventional and inverter-based generation units must be designed considering site-specific conditions and operation under a range of diverse conditions. The increase of inverter-based generation connections in power systems has necessitated the development of new control strategies. Various inverter topologies and inverter control strategies have been adopted by vendors to mitigate potential stability concerns.

The VSM methods found in literature are all based on grid-forming operation. Thus, a PLL is not necessarily required, and the reference voltage magnitude and phase angle are derived using various approaches, some of which are discussed next.

2.4.1. Droop Control Method

2.4.1.1. Direct Generation of Reference Voltage Signal

One approach to develop an inverter control strategy is to use frequency droop and voltage droop-based controllers. This methodology is commonly used in isolated power systems, and an overview of the control approach is shown in Figure 2.3 and Figure 2.4.

The error signals for the active and reactive power (i.e., the difference between the desired (P_{ref}, Q_{ref}) and measured quantities (p_m, q_m)) are sent through frequency droop (D_f), and voltage droop (D_v) control blocks. The grid frequency (ω_g) and the rms voltage at the point of connection ($v_{rms,m}$) are the feedback quantities to the frequency droop and voltage droop controller, respectively. Typically, these input quantities to the controller are measured in per unit. This information is then used to derive the reference voltage required to generate the reference voltage waveform for producing the switching pulses [26].

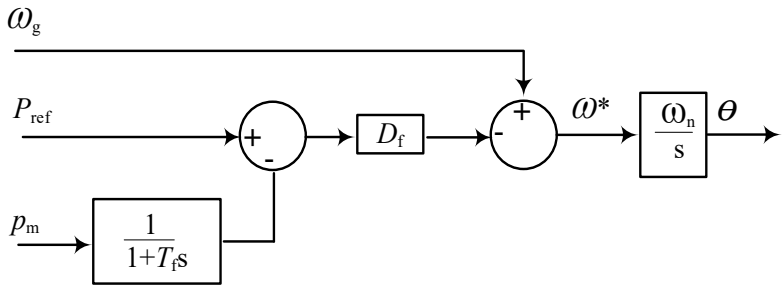

Figure 2.3: Frequency droop controller.

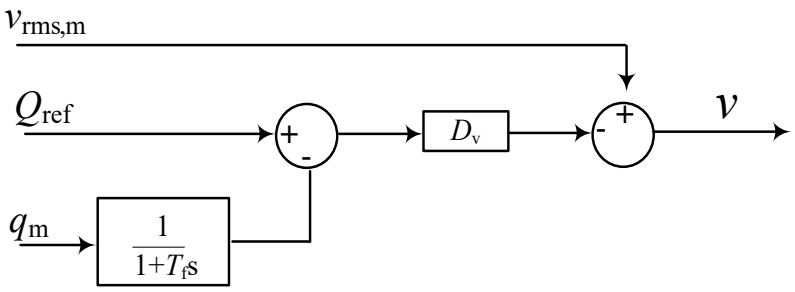

Figure 2.4: Voltage droop controller.

T_f is the time constant of the low-pass filter used in this control strategy that helps with conditioning the oscillations present in the power feedback measurements. A similar control strategy developed based on frequency and voltage droop concept is discussed in [28], wherein the low-pass filter is used to establish a delay, which is claimed to mathematically represent a virtual inertia.

2.4.1.2. Deriving the Bus Voltage Angle through a Power Droop Control Loop

Another droop controller developed for active power sharing among parallel inverters in an islanded microgrid application is discussed in [27]. The control strategy is shown in Figure 2.5. The input quantities to the droop controller are the measured active (p_m) and reactive power (q_m). The droop controller generates the angle (θ) and the reference voltage (v_{ref}). In a balanced, three-phase system, the q component of the voltage can be set to zero (this depends on the how the d-q reference frame is defined). v_n and ω_n are the nominal voltage and the grid frequency. Control reference ($v_{d,ref}$) is then sent through internal voltage and current loops, which generate voltage references in the dq frame required to generate the switching signals for the inverter. This grid-forming method was applied in an isolated microgrid application.

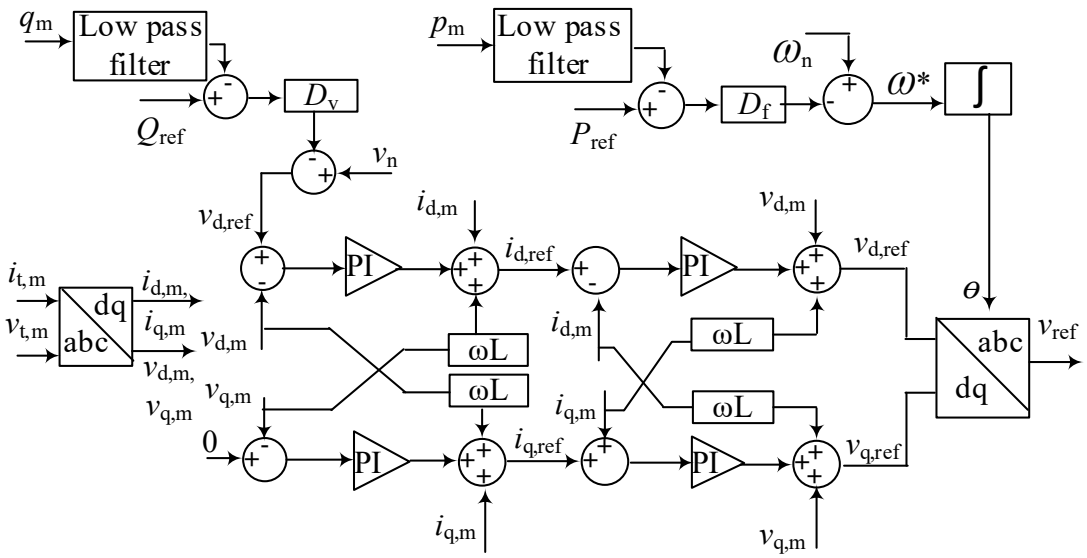

Figure 2.5: Control loops of an inverter proposed in [27].

2.4.2. Mimicking the Mechanical Response of a Synchronous Machine

2.4.2.1. Adoption of the Swing Equation

Most control methodologies proposed to mimic certain characteristics of a synchronous machine follow a grid-forming approach. In these methodologies, the voltage angle required to generate the reference voltage for inverter switching is obtained by solving the swing equation, which governs the behavior of the rotor of a synchronous machine as in (2.1).

$$T_m - T_e = J\frac{d\omega}{dt} + K_d(\omega) \tag{2.1}$$

$$J = 2H \tag{2.2}$$

where T_m is the mechanical torque, T_e is the electrical torque, J is the moment of inertia, H is the inertia constant, K_d is the damping coefficient and ω is the speed of the machine (virtual). This equation is used to derive the bus voltage angle in the grid-forming inverter. The swing equation can be further modified based on the available control inputs (e.g., active power) to the control system as shown in Figure 2.6.

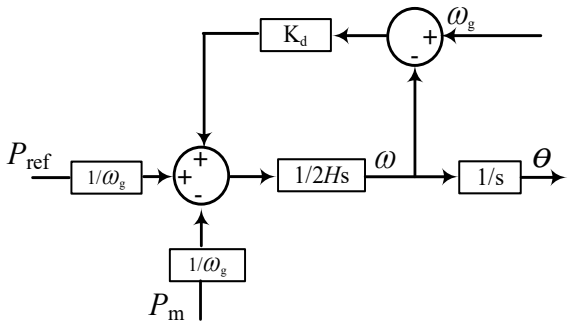

Figure 2.6: Derivation of voltage angle based on swing equation.

As discussed earlier, a desirable option to control inverters is to mimic the favorable characteristics of a synchronous machine through appropriate adaptation of the inverter control methodology. This concept is generally termed the Virtual Synchronous Machine (VSM) approach. The design approach and the level of details included in the VSM implementation vary in the approaches discussed in literature.

The VSM method introduced in [29] uses a 'voltage-to-current' control approach and a 'current-to-voltage' control approach as shown in Figure 2.7 and Figure 2.8. In this approach mechanical characteristics of a synchronous machine are mathematically represented using the swing equation, which is used to estimate the reference angle required to generate the reference waveforms required for switching. In the 'voltage-to-current' control approach switching actions are conducted using a current hysteresis controller [29]. This results in higher switching frequencies and switching losses. In the 'current-to-voltage' control approach shown in Figure 2.8 the voltage reference needed for switching is derived. The proposed methodology is introduced to overcome grid stability and power quality-related concerns. The grid used to exemplify the proposed method is a simplified microgrid described in [29].

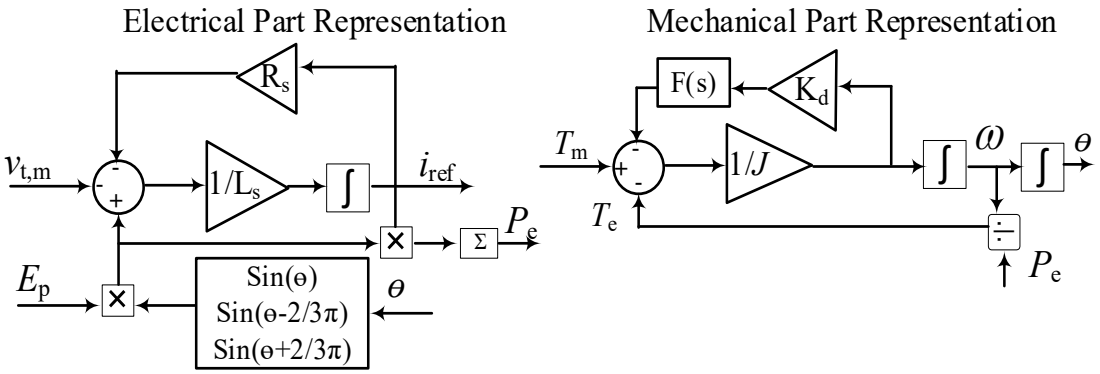

Figure 2.7: Block diagram of the VISMA method – 'voltage-to-current' model.

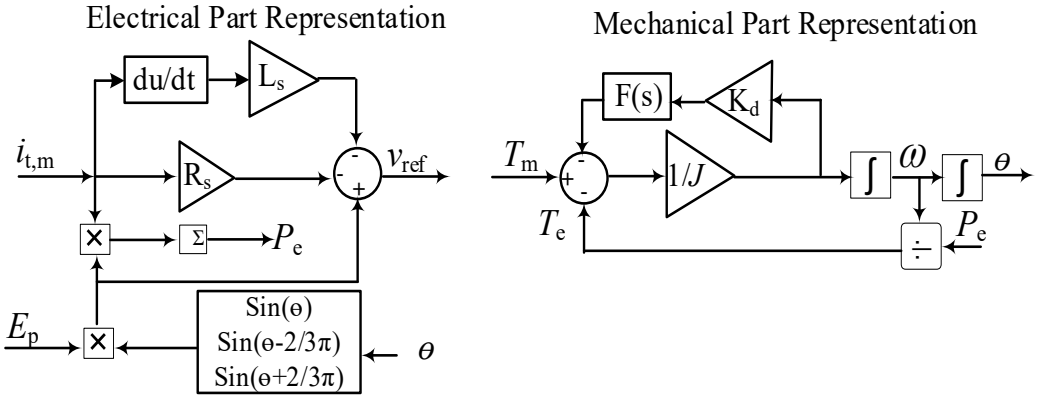

Figure 2.8: Block diagram of the VISMA method – 'current–to-voltage' model.

2.4.2.2. Adoption of the Swing Equation and Virtual Resistance

Another VSM control strategy discussed in [30] has been developed based on the swing equation of a synchronous generator as shown in Figure 2.9. In this approach a virtual resistance is introduced to reduce the decay time constant and control the output voltage of the inverter. Numerical simulation results provided in [30] confirm improved fault ride-through capability and grid stability.

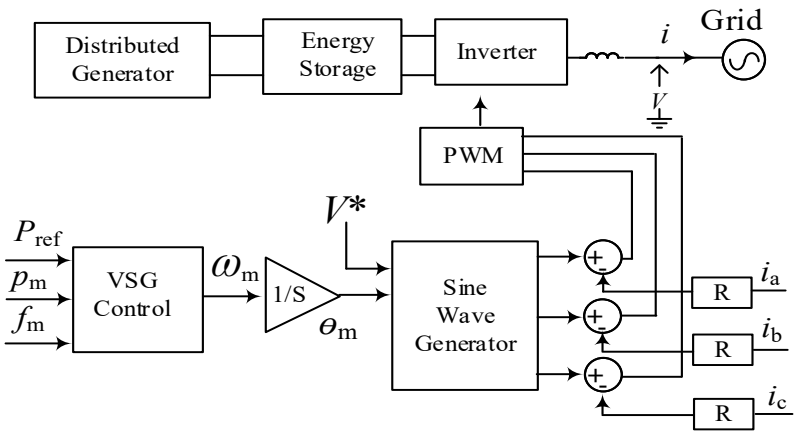

Figure 2.9: Block diagram of the technique with a virtual resistance.

2.5. Limitations of Existing VSM Methods

There are a number of VSM techniques discussed in the literature. They have been developed based on mimicking certain characteristics of a synchronous generator (mostly using simplified methods that are relying on various assumptions applicable to the mathematical modelling of synchronous machines) for different applications. One of such methods developed to suppress oscillations that emerge due to high penetration of solar PV in microgrids is discussed in [31]. Another method, developed to address low-frequency oscillations in power systems, is elaborated on in [32-34].

The inertial effect of a synchronous machine is modelled in [35] for an HVDC scheme by mimicking the machine's rotor dynamics (as discussed in Section 2.4.2.1). A similar strategy is adopted in [36], where the VSM concept is used in a microgrid setup. Another strategy designed to emulate the rotor inertia to enhance the rotor angle stability of a small system by incorporating an energy storage unit, a voltage source converter (VSC), and an LCL grid filter is shown in [37].

However, none of these methods are widely adopted in practical, transmission-level renewable energy plants. Almost all the proposed methods are tested on simplified test systems or on simple micro-grid type systems. Nearly all VSM methods proposed in literature for renewable plants are

developed based on grid-forming technology. While grid-forming technology is gaining attention and development effort, large-scale implementation of this technology may be years away from realization [38]. A number of technical issues must be resolved as system operators (e.g., ERCOT, AEMO) take a cautious approach in adopting new technologies [39].

The VSM method proposed in this research is based on grid-following techniques and considers synthesising both the electrical and mechanical characteristics of a synchronous machine. The machine's response is estimated by sampling the instantaneous bus voltage at the point of connection. Therefore, the proposed VSM technique is able to capture the transient and sub-transient behaviour, and the mechanical response, and also has flexibility to incorporate exciter, power system stabilizer and governor actions as required to improve overall system response. The proposed VSM approach is implemented on a battery energy storage converter to investigate its effectiveness and verify its capability to mitigate common issues arise with low system inertia due to high renewable penetration.

Chapter 3: VSM Background, Mathematical Implementation, Model Verification and Simulation Results

3.1. Implementation and Verification of a VSM-Based Battery Energy Storage System

In the proposed approach, a BESS inverter is controlled to mimic the response of a synchronous machine, considering both mechanical and electrical characteristics of the machine. The VSM approach adopted in this research is illustrated with the schematic diagram in Figure 3.1. The proposed VSM approach is implemented and tested in PSCAD/EMTDC simulator.

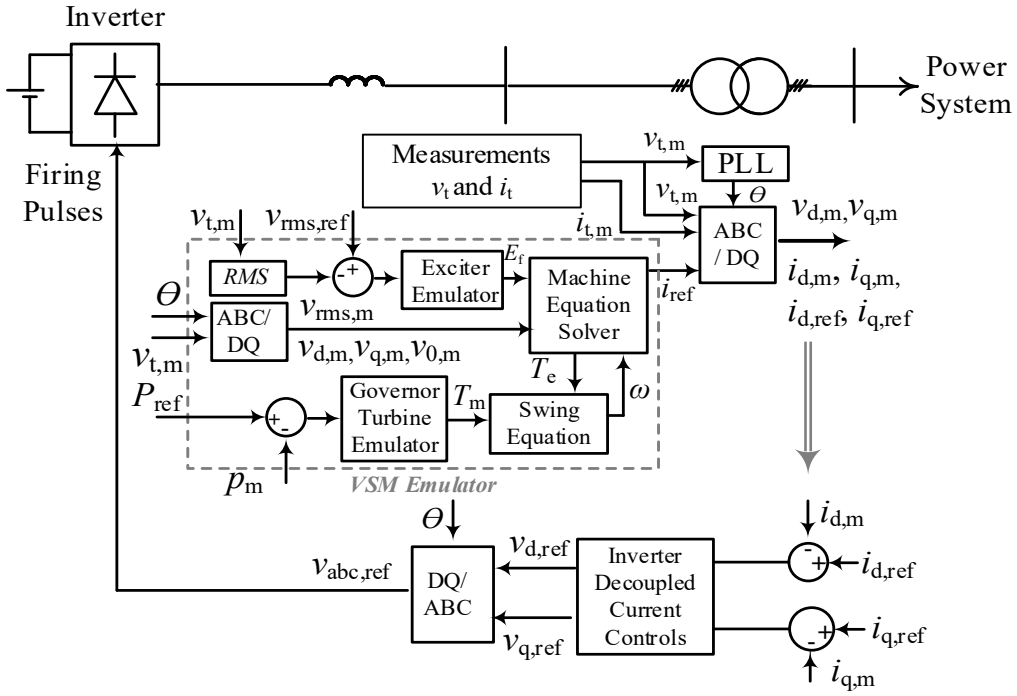

Figure 3.1: Schematic diagram of the proposed VSM approach adopted for a BESS.

Details of the VSM controller are provided section 3.1.1.

3.1.1. VSM Emulator

The inputs to the VSM emulator (shown within the dashed box in Figure 3.1) are the reference and measured active power (P_{ref} and p_m), measured instantaneous voltage ($v_{t,m}$), and reference and measured (rms) voltage ($v_{rms,ref}$, $v_{rms,m}$). Based on these input quantities the VSM Emulator estimates the reference currents that are then used as inputs to the de-coupled current control block of the inverter controller. The synchronous machine response is emulated by deriving the reference currents for the de-coupled current control block by solving machine equations.

The machine's electrical equations, implemented and solved inside the VSM Emulator block, are shown below [40]. Note that the machine equations below are represented in the dq0 reference frame. For the purpose of VSM emulation the machine equation may also be solved directly in the ABC domain.

In the equations shown below V_d, V_q, and V_0, represent the measured terminal voltages converted to the dq0 frame ($V_{d,m}$, $V_{q,m}$, and $V_{0,m}$ shown in Figure 3.1).

Stator-side equations:

$$V_d = R_s i_d + \frac{d}{dt}\lambda_d - \lambda_q \omega \tag{3.1}$$

$$V_q = R_s i_q + \frac{d}{dt}\lambda_q + \lambda_d \omega \tag{3.2}$$

$$V_0 = R_0 i_0 + \frac{d}{dt}\lambda_0 \tag{3.3}$$

Rotor-side equations:

$$E_f = R_f i_f + \frac{d}{dt}\lambda_f \tag{3.4}$$

$$0 = R_{kq} i_{kq} + \frac{d}{dt}\lambda_{kq} \tag{3.5}$$

$$0 = \mathrm{R_{kd}} i_{\mathrm{kd}} + \frac{\mathrm{d}}{\mathrm{dt}} \lambda_{\mathrm{kd}} \tag{3.6}$$

Mechanical dynamic of the rotor of the synchronous machine are represented by the equation shown below:

$$T_{\mathrm{m}} - T_{\mathrm{e}} = J \frac{\mathrm{d}\omega}{\mathrm{dt}} + D\omega \tag{3.7}$$

where

J is the total inertia of the rotating masses.

T_{m} is the mechanical torque generated by the machine.

T_{e} is the electrical torque generated by the machine.

ω is the angular speed of the virtual rotor.

D is the friction and windage loss coefficient

3.1.2. Implementation of External Synchronous Machine Controls

The proposed VSM approach captures the mechanical and electrical equations of a synchronous generator. In order to fully represent a machine, the responses of exciters and governors are also considered. This implementation includes a AC7B-type exciter (shown in Figure 3.2) and a GOV2-type governor (shown in Figure 3.3) [41,42].

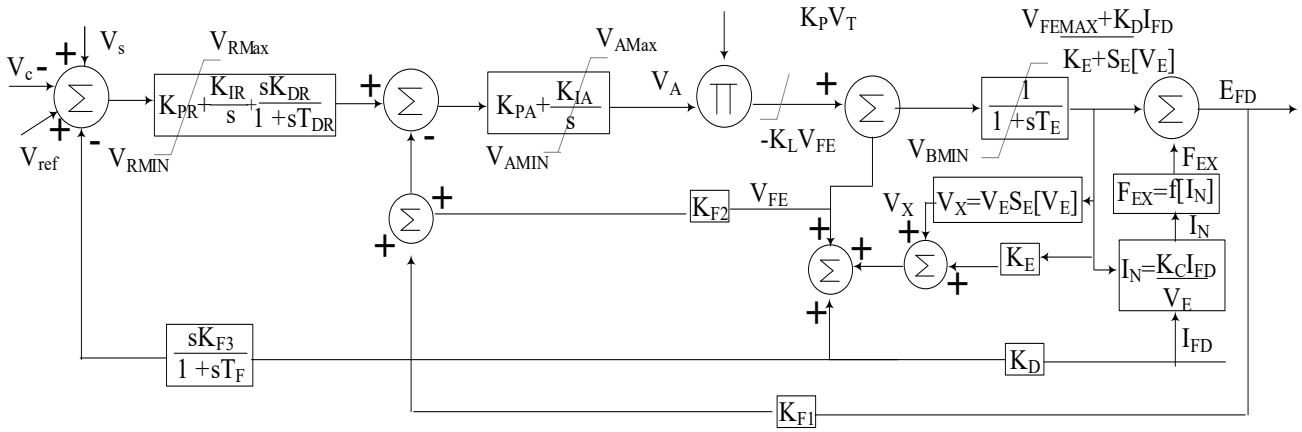

Figure 3.2: Block diagram of the AC7B exciter model.

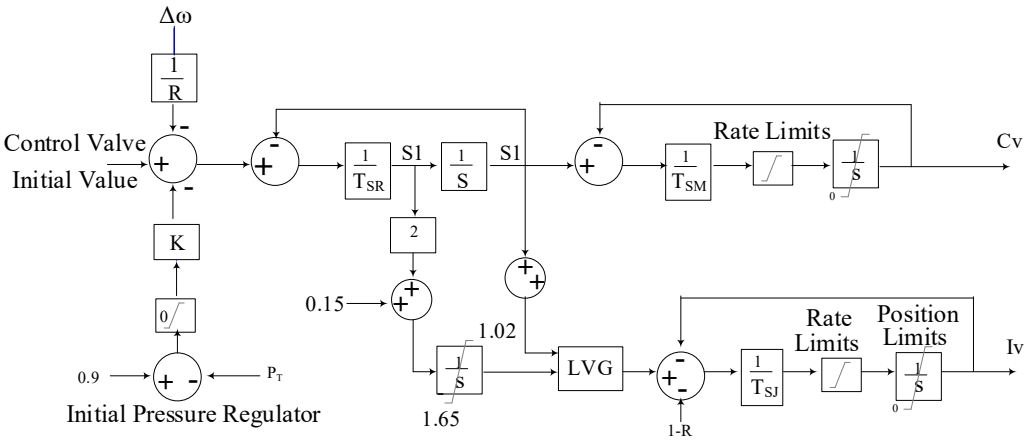

Figure 3.3: Block diagram of GOV2 governor model.

The exciter regulator gain, and time constant are set at 12 (K_{IA}) and 20 (T_E), respectively. The droop and time constant of the governor are set to at 0.05 pu (R) and 0.2 seconds (T_{SM}), respectively. These exciter and governor models were selected for illustration and any other exciter or governor type may be adopted depending on the specific technical requirements. Alternatively, constant E_f and T_m values can be used, or a simple PI controller tuned to minimize error signals (voltage error for exciter modelling, frequency error for governor modelling) can be used to derive E_f and T_m. The exciter and governor responses can be computed inside the PPC module.

The key distinction of the proposed VSM control strategy lies in its voltage angle reference generation. Unlike most VSM strategies that estimate the angle using external control methods (e.g., swing equation solutions), this approach directly extracts the voltage angle from a PLL at the point of connection for inverter control. This instantaneous measurement enables faster dynamic response compared to conventional methods.

Furthermore, the proposed strategy derives current references by solving comprehensive synchronous machine equations, allowing the inverter to replicate both electromagnetic and electromechanical characteristics of a synchronous machine. In contrast, conventional methods

typically consider only mechanical characteristics or simplified machine equations. Consequently, the proposed VSM achieves significantly closer emulation of synchronous machine behaviour.

3.1.3. The Control Philosophy of a BESS Controlled as a VSM

The overall control philosophy of the BESS operated using the proposed VSM method is summarized as follows:

- The power and voltage references (set points) are provided as inputs to the Governor and Excitor control blocks, respectively. These calculations can be inside the PPC module. The measured power and terminal voltage are also provided as inputs to the Governor and Excitor control blocks, respectively.
- The output of the Exciter block is the expected 'field voltage' of the VSM.
- The output of the Governor/Turbine block will be used as the 'input torque' to the VSM.
- Equations (3.1) – (3.7) are solved (for currents) with field voltage, input torque, and measured instantaneous terminal voltage as known inputs. The outputs of the VSM emulator block are the calculated VSM currents. These currents will act as inputs to the de-coupled current control block of the BESS inverter control system, which subsequently outputs the inverter's switching pulses.

In the proposed approach, the machine equations are solved without simplifying approximations in order to capture the behaviour of a machine as closely as possible. As such, the inputs to the control system are the instantaneous (sampled) values of the terminal voltage. Thus, measurement and signal processing delays associated with conversion to rms quantities or estimation of system frequency deviation are avoided. Thus, from an inertial response viewpoint, the proposed VSM approach does not introduce noticeable delays, which can be identified as a

key factor that would contribute to improving overall dynamic response of the plant as well as that of the system.

The VSM response of the inverter is achieved by modifying the control system hardware and software of the inverter. Thus, adopting a VSM approach should not add any significant cost to the overall cost of the plant. Normal current-limiting functions (as implemented in typical BESS, wind, or solar PV inverters) can be readily adopted irrespective of the VSM implementation to operate the inverter within its ratings.

3.1.4. Verification of the VSM Concept and Implementation

The response of the VSM is verified by comparing its simulation results with those of a comparable synchronous machine. The single-machine-infinite-bus (SMIB) test systems shown in Figure 3.4 and Figure 3.5 were used to verify the VSM concept and its implementation. The rating of the synchronous machine was set to 30 MVA and its rated voltage is 17.32 kV (L-L). The sub-transient reactance (X_d") and inertia constant (H) were set to 0.2 pu (per unitized based on machine MVA) and 4 s, respectively. The voltage source impedance was calculated to represent a 10 kA fault current contribution from the source side (1.905 Ω). The transformer is rated at 30 MVA, 17.32/33 kV and the transformer's leakage impedance is 10%. A 125 MW load is connected at the 33 kV connection point.

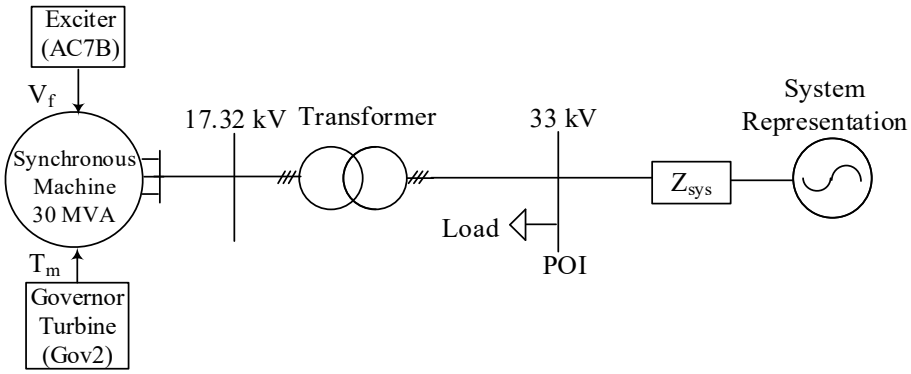

Figure 3.4: SMIB test system used to verify the proposed VSM approach.

The inverter and its transformer are rated at 1 MVA. They were then 'aggregated' to represent a 30 MVA BESS plant. The two-level inverter's PWM switching frequency was set to 1.5 kHz.

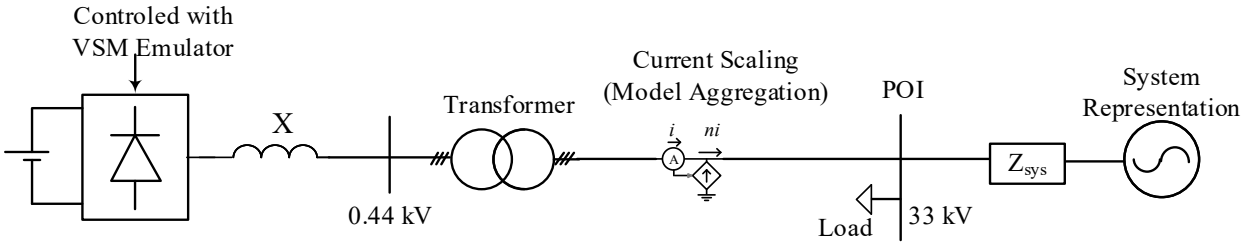

Figure 3.5: SMIB Test system developed to verify the proposed VSM approach (BESS controlled as a VSM, connected to the SMIB set up).

3.1.4.1. Fault Response Comparison

The fault current from the synchronous machine is compared with the counterpart VSM as described in Figure 3.4 and Figure 3.5. The current from the inverter is intentionally not limited as the intent of this exercise is to demonstrates the response of the VSM in comparison to that of a synchronous machine. Figure 3.6 shows the responses (current) of the machine and the VSM during and following the clearance of a three-phase-to-ground fault. The fault current from the synchronous machine and the VSM shows close conformity.

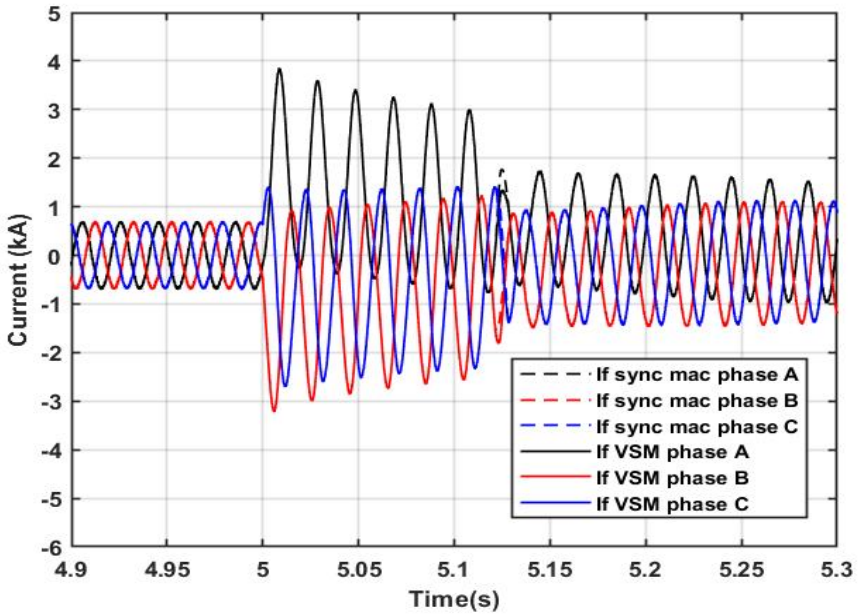

Figure 3.6: Fault current comparison – proposed VSM and the response of a comparable synchronous machine (Three-phase-to-ground fault).

Figure 3.7 shows the responses (current) of the machine and the VSM during and following the clearance of a two-phase-to-ground fault. The fault currents from the synchronous machine and the VSM show a close match (solid and dashed waveforms are overlapping).

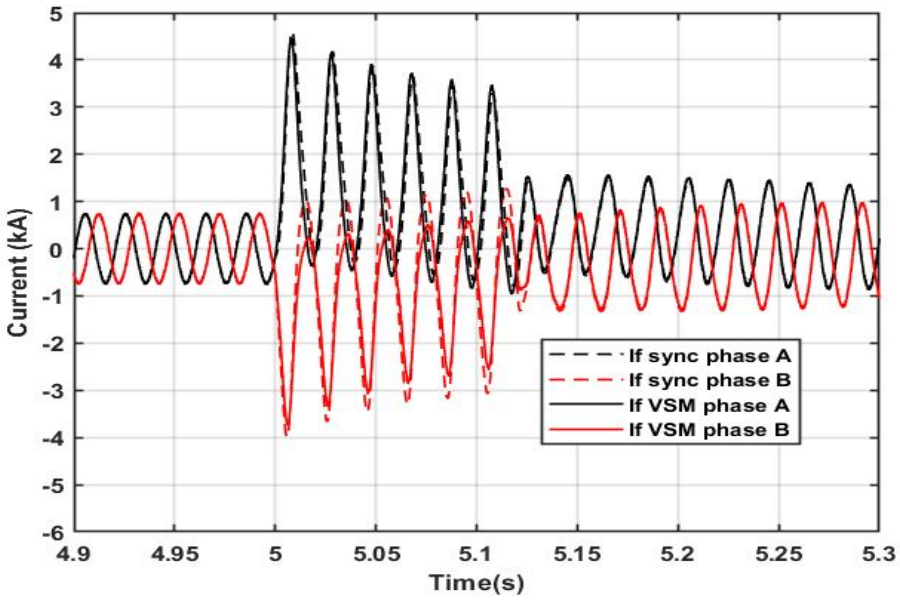

Figure 3.7: Fault current comparison – proposed VSM and the response of a comparable synchronous machine (Two-phase-to-ground fault).

Figure 3.8 shows the responses (current) of the machine and the VSM during and following the clearance of a single-phase-to-ground fault. The fault current from the synchronous machine and the VSM shows a close match.

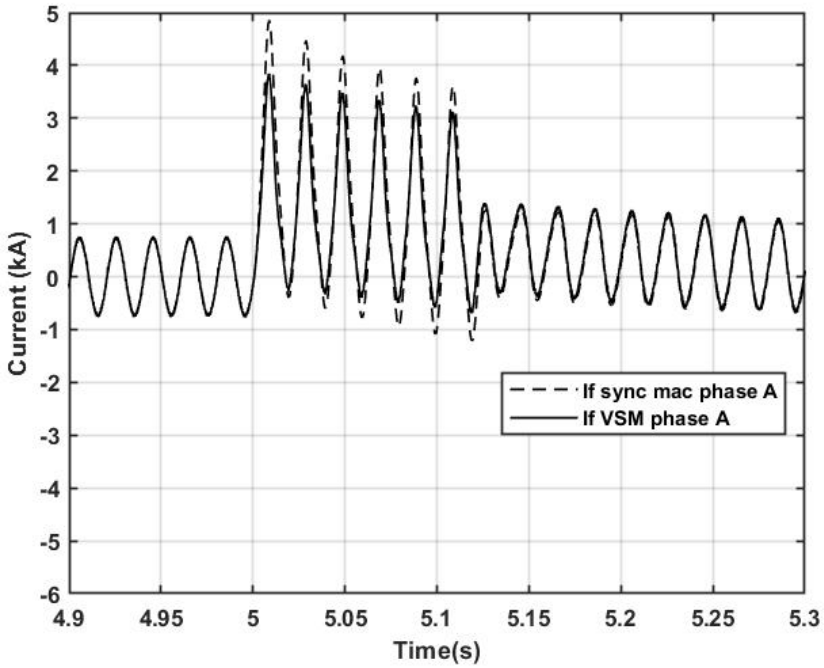

Figure 3.8: Fault current comparison – proposed VSM and the response of a comparable synchronous machine (Single-phase-to-ground fault).

The close conformity of the fault currents in Figure 3.6, Figure 3.7, and Figure 3.8 provides sufficient confirmation that the VSM concept can accurately mimic the transient and sub-transient behaviour of a synchronous machine.

It should be noted that the zero-sequence component was ignored, i.e., following the abc to dq0 transformation, only the d and q components are used as inputs to the control system. This explains the slight differences observed in fault currents during unbalanced faults. If needed, the control structure can be modified to consider the zero-sequence current component as well. However, ignoring the zero-sequence component does not impact the overall objective of providing system strength for inverter-based generation connections. This observation is evident

in the simulation results, both in the test system and the actual network model that is described in Section 3.1.4.4 and Chapter 4.

3.1.4.2. Voltage Reference Step Response

The behaviour of the VSM is further verified by comparing its response to a step change in the voltage set point with that of a synchronous machine. The voltage reference was changed from 1 pu to 1.05 pu. The simulation results are shown in Figure 3.9. The VSM response follows the synchronous machine's response closely, further verifying the VSM concept and its implementations in PSCAD/EMTDC simulator.

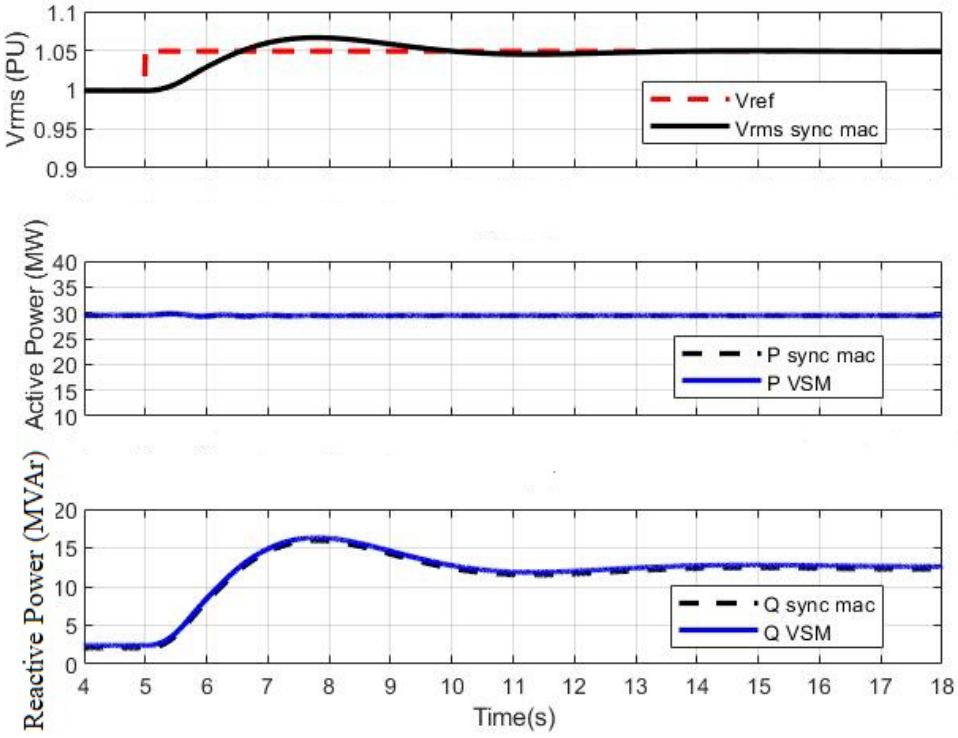

Figure 3.9: Step response comparison - proposed VSM and a comparable synchronous machine.

The exciter and governor types can be selected based on specific technical requirements. To illustrate this, a comparison was conducted between two exciter implementations in the VSM control. Figure 3.10 presents a comparison of the VSM's response to a voltage step when the

exciter is modelled as AC1A versus when it is modelled as a simple PI controller. The voltage response can be improved by tuning the gains and the time constants of the two exciter types.

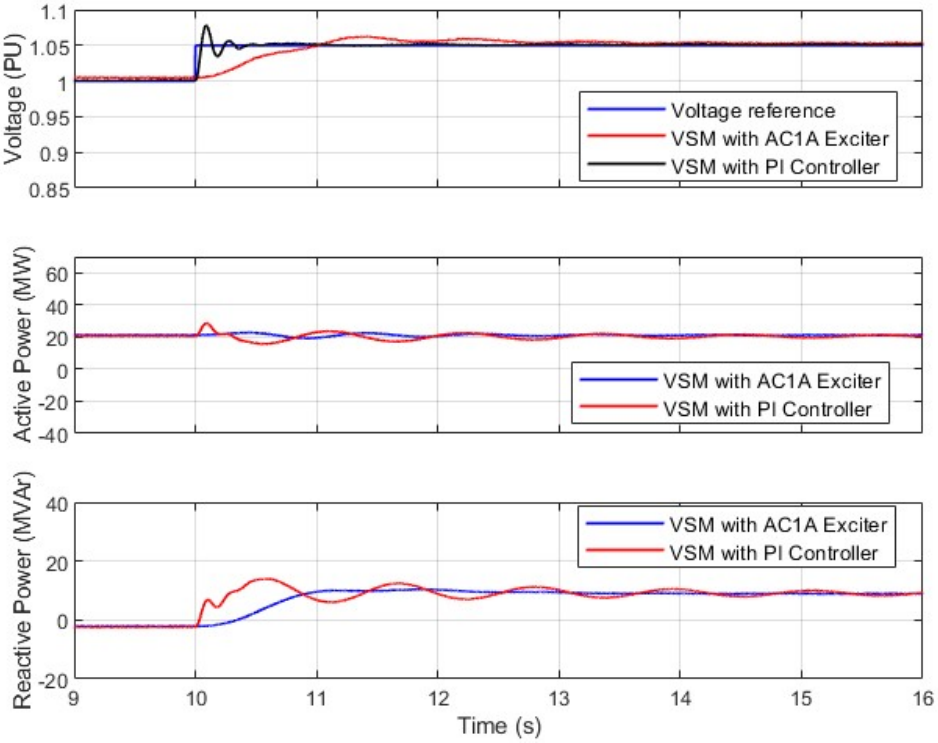

Figure 3.10: Comparison of the VSM's response to a voltage step.

3.1.4.3. Verification of the VSM Performance Based on a Simple Test System Consisting of a Power Electronic Interfaced Renewable Generation

The test system shown in Figure 3.11 is used to verify the dynamic response of the VSM with that of a comparable synchronous machine. The synchronous machine is rated at 17.32 kV, 50 MVA and is initialized to provide 25 MW to the system in steady state. A 125 MW load is connected at the POI (33 kV).

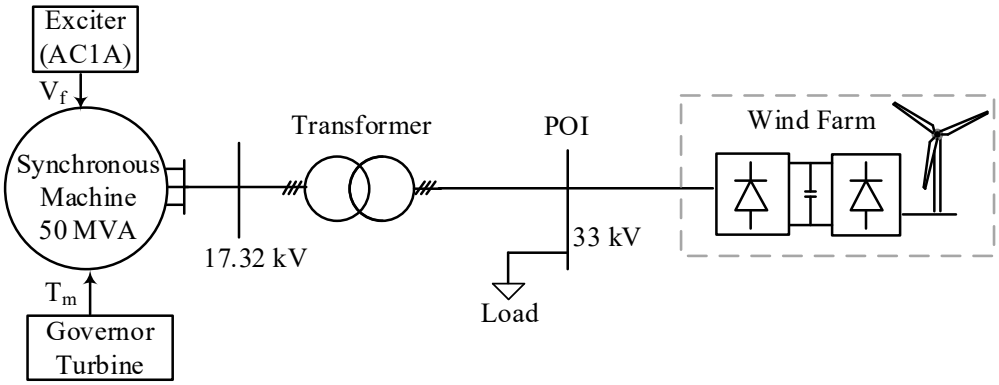

Figure 3.11: Simple test system used to verify the VSM (synchronous machine connected to the test system).

The test system shown in Figure 3.12, consists of a Type IV Wind Turbine Generator (WTG) rated at 5 MW. The detailed WTG model is scaled to represent a 100 MW wind farm connected to the rest of the circuit at 33 kV level. The wind farm is operating close to its full power rating. The sub-transient reactance of the synchronous generator is 0.28 pu (a large value is assumed to consider a worst-case scenario) and thus, the short circuit MVA at the POI is 178 MVA. The generator's inertial constant (*H*) is 3 seconds. Considering the wind farm rating of 100 MW, the SCR at the POI is 1.78.

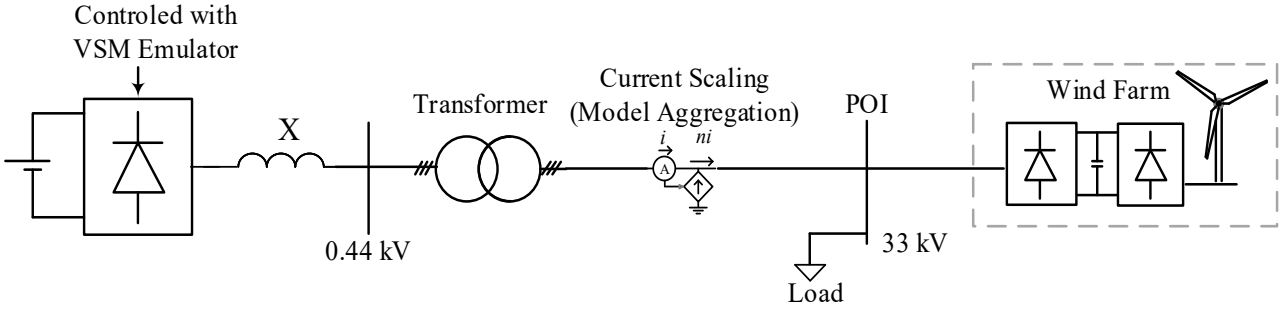

Figure 3.12: Simple test system developed to verify the VSM (BESS controlled as a VSM, connected to the test system).

Figure 3.13 shows the response of the wind farm following a three-phase-to-ground fault, applied at the POI at 5 seconds and cleared after 120 ms, and the wind farm's response is stable.

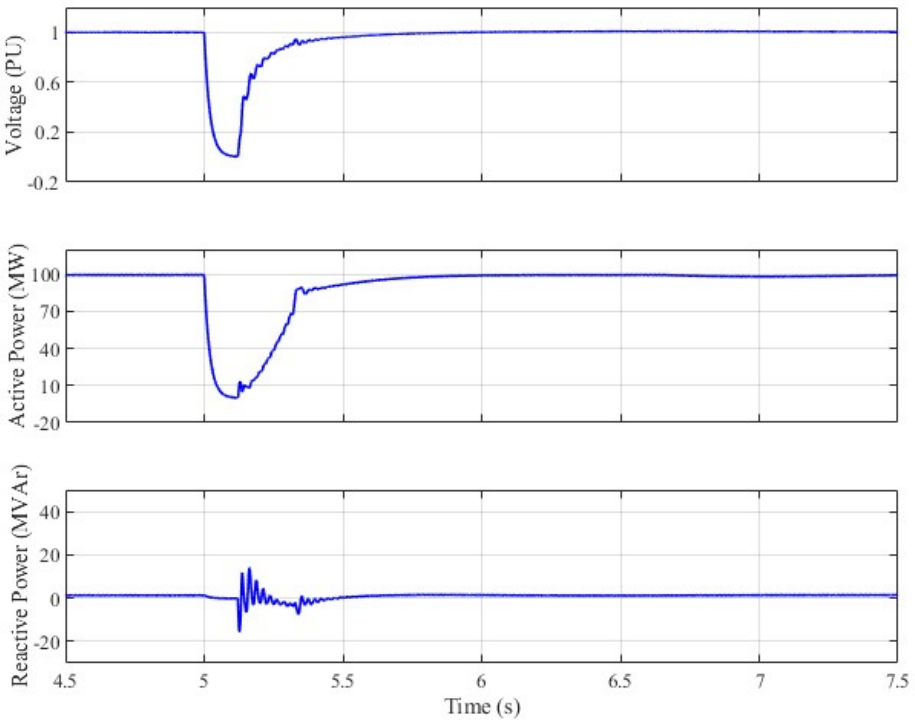

Figure 3.13: Measurements at the POI – fault recovery is successful.

If the synchronous generator rating is around 25 MVA (with identical per unit machine parameters on machine's MVA base), the SCR drops to about 0.65 and the wind farm is not able to ride through the fault successfully, as indicated by results in Figure 3.14.

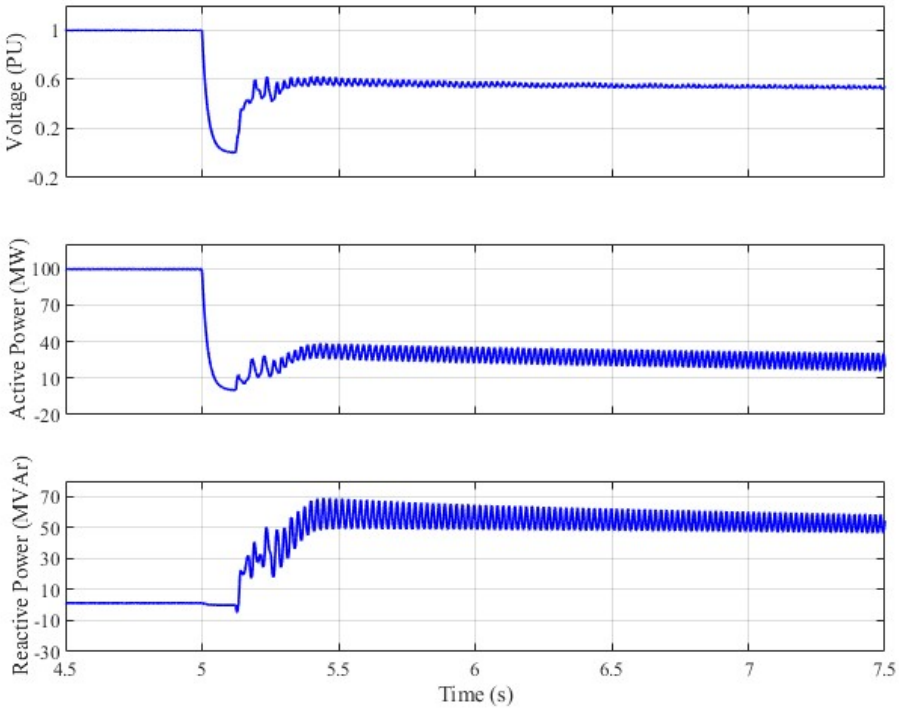

Figure 3.14: Measurements at the POI – fault recovery is unsuccessful.

However, when the inertia of the synchronous generator is increased (from 3 to 14, noting that this is not a practical value, but is used for demonstration purposes), the wind farm does recover from the 120 ms fault, as depicted in Figure 3.15.

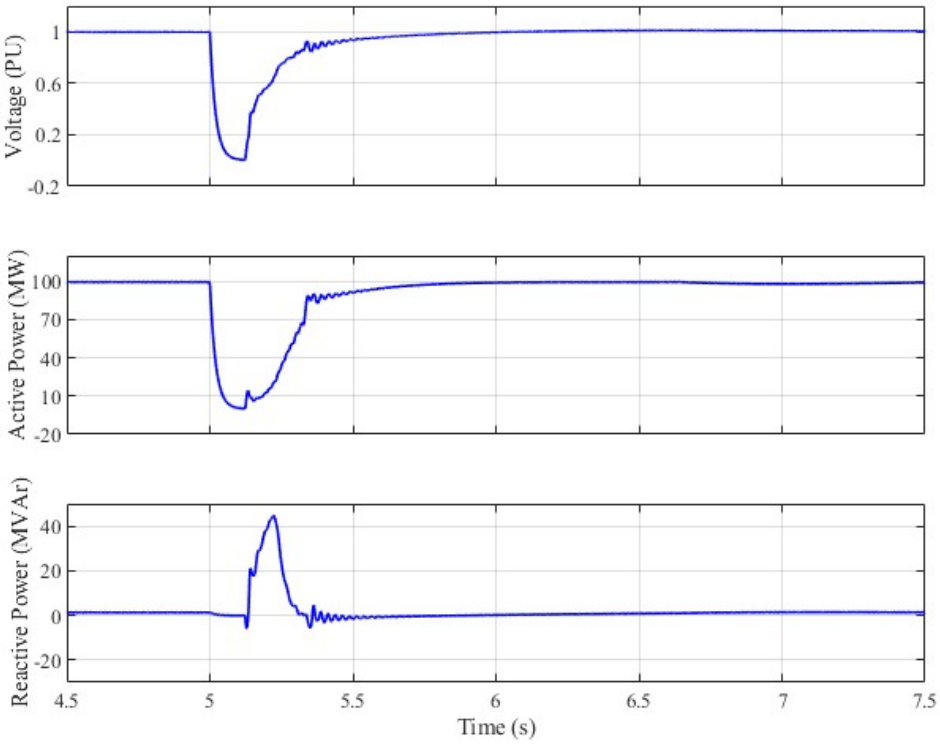

Figure 3.15: Electrical measurement at the POI with high machine inertia.

This exercise was performed to illustrate that while the SCR is an effective measure, it is only an indicative index. This is an important illustration as the power industry has used SCR as a screening measure without due consideration to other factors that can contribute to dynamic response issues in power systems with high penetration of power electronic inverter-based renewable generation [23].

Other system measures such as the overall inertia and the location of machines providing inertia (proximity to inverter-tied devices) will also have a significant impact on the stability of inverters and hence the system. The available inertia (including the location in the network where the machines are connected) determines the rate of change of voltage at the POI (specifically the voltage angle) and has a significant impact on the fault ride-through response of power electronic-based devices. This necessitates conduction of detailed simulation studies with the study model capturing a wide area of the system.

It should be noted that inverters controlled based on a VSM method can mimic very high inertia, likely at a much lower cost. VSM-based inverters can provide the inertial effects without the inverter having to contribute high fault currents (response comparable to a synchronous machine can be achieved even when the inverter current-limiting functions are active and limit the current during faults to pre-determined levels; typically, around 110% of normal rating).

Figure 3.16 shows a modified test circuit with a 5 MVA synchronous machine and a BESS mimicking a 25 MVA Virtual Synchronous Machine. In this test setup, the synchronous machine rating is low (compared to the test system of Figure 3.11), and that alone will not provide the SCR to stably connect the wind power plant. However, the connection of the BESS mimicking a 25 MVA VSM has provided the necessary system strength to operate the wind power plant stably.

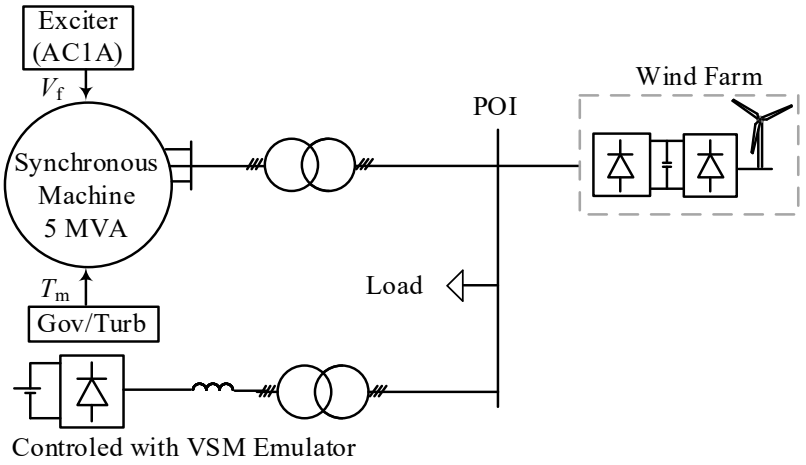

Figure 3.16: Modified test system.

The simulation results in Figure 3.17 show that the wind power plant as well as all other equipment successfully recover from the three-phase-to-ground fault (applied at 5 s) with a 120 ms fault duration.

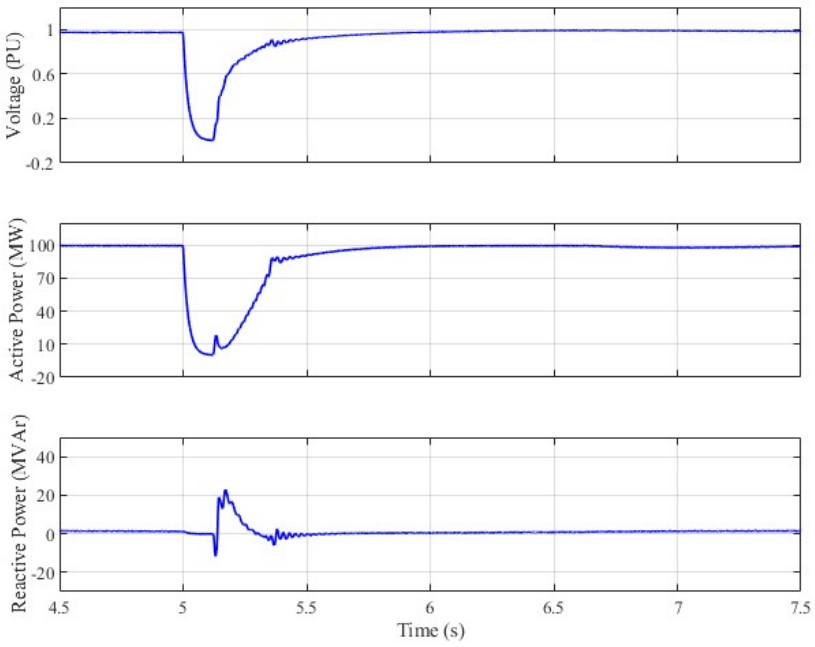

Figure 3.17: Electrical measurement at the POI (BESS is connected to the wind farm model).

This illustrates that the VSM concept can be adopted to mitigate the most challenging stability concerns of inverter-based devices connected to power systems. Note that details such as the State of Charge (SOC) of the battery are not included in the model since the transient events being considered are of very short duration. Even if the rate of change of current is limited within the DC side of the BESS (e.g., due to inherent or added inductances) these fast events will have negligible impact on the main purpose of the VSM-inertial response.

3.1.4.4. Verification of the VSM Concept on a Transmission Network Test System

The response of the VSM-based BESS plant was considered when connected to an exemplar test system. The transmission network (based on a practical high voltage system) developed to verify the proposed VSM response is shown in Figure 3.18. This test network is selected as it represents a practical network with relatively low short circuit levels near the POI (Bus 1) of a wind power plant.

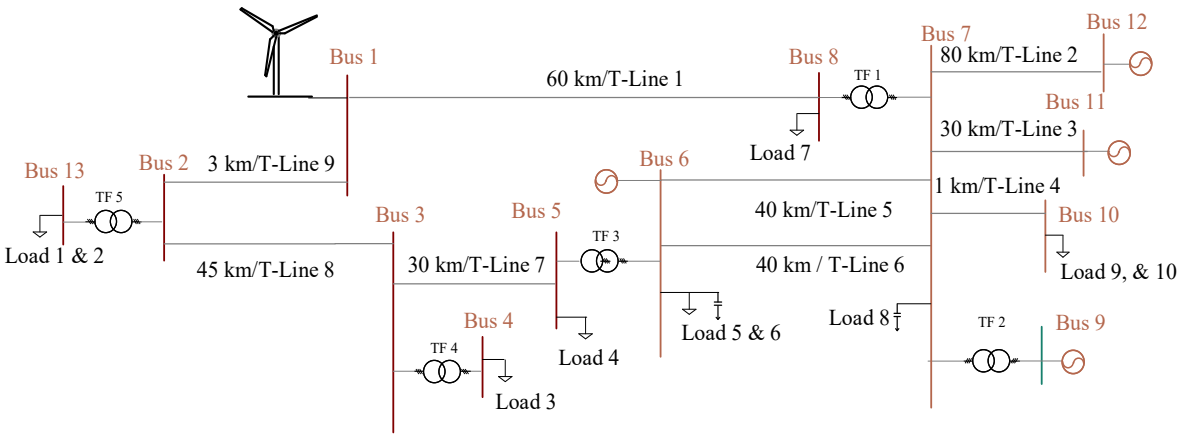

Figure 3.18: Practical transmission network test system developed to verify the proposed VSM approach.

The windfarm connected to Bus 1 is rated at 75 MVA (the power set point in the study example is set at 60 MW). The short circuit level at Bus 1 is nearly 166 MVA and thus the SCR is about 2.7. A three-phase-to-ground fault is applied (at 8 s) to the line 1 at the Bus 1 side. The fault is cleared by tripping the line breakers at 120 ms (Bus 1) and 170 ms (Bus 8) after the fault; delayed fault clearing is assumed to represent a 'worst case' condition.

When the transmission line from Bus 1 to Bus 8 is tripped, the SCR drops to about 1.2. Simulations results shown in Figure 3.19 indicate that the windfarm will not recover from a three-phase-to-ground fault.

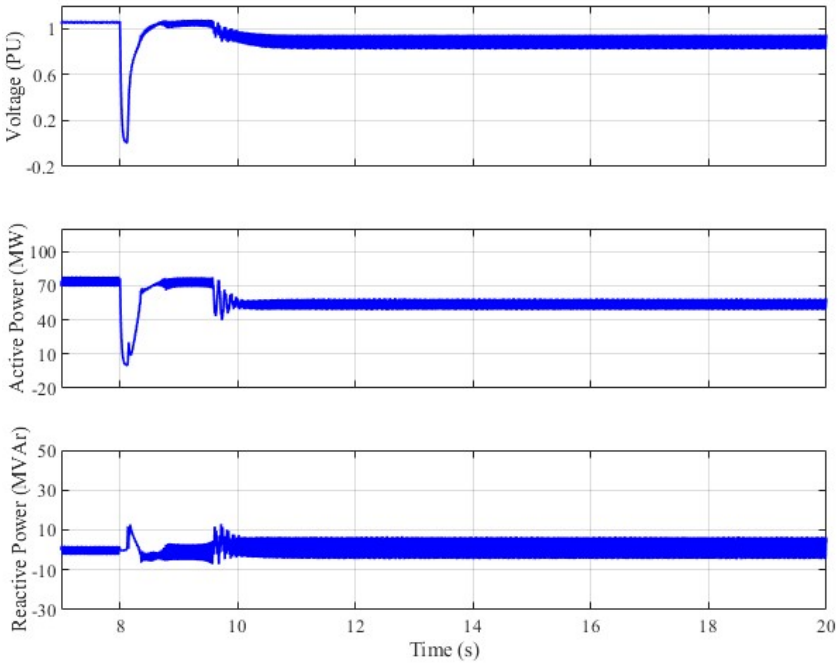

Figure 3.19: Electrical measurement at the POI.

To investigate whether the fault ride-through problem can be mitigated using a synchronous condenser connected at Bus 1, a synchronous condenser with a minimum rating (determined through a series of simulations) in the range of 50 MVA (X_d" = 0.28 pu, and H = 4 s) was connected at Bus 1. A three-phase-to-ground fault was then applied, as described in the previous test. The simulation results shown in Figure 3.20 show that when the synchronous condenser is connected at Bus 1, the wind farm is able to successfully ride through the fault.

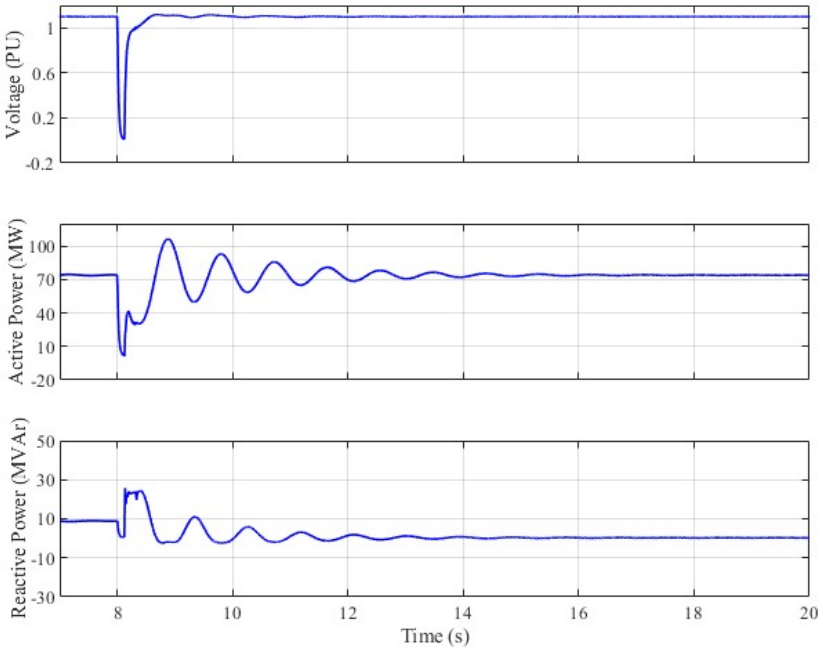

Figure 3.20: Electrical measurement at the POI with synchronous condenser.

To evaluate the effectiveness of the proposed VSM approach, the synchronous condenser was replaced by a BESS controlled using the proposed VSM method. Upon applying the same contingency as in the previous tests, successful fault ride-through behavior was observed when the BESS model, controlled as a VSM, was connected at Bus 1, replacing the synchronous condenser as seen from the simulation results shown in Figure 3.21.

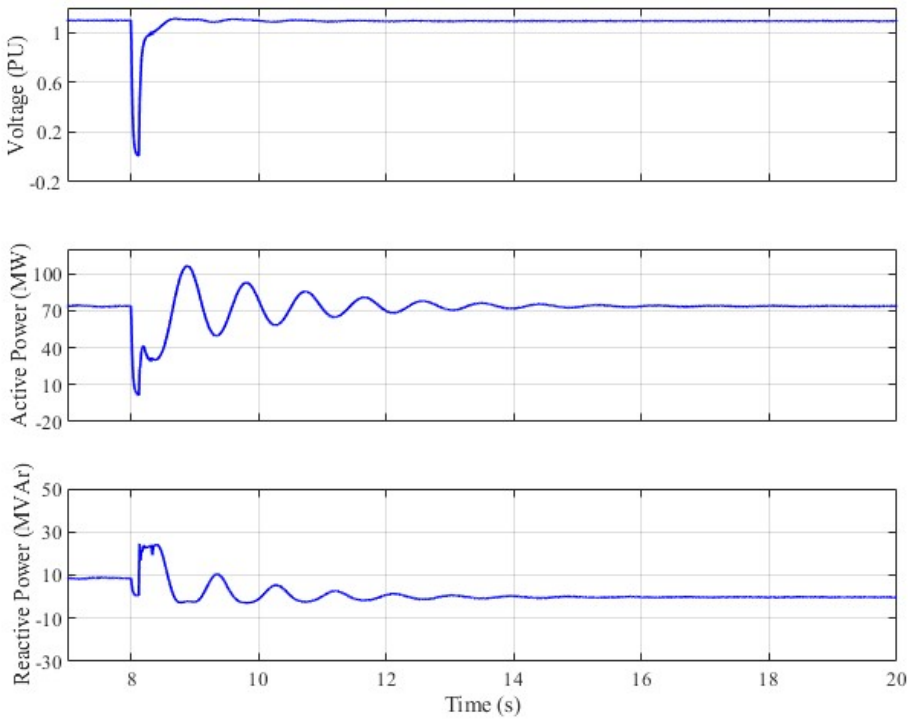

Figure 3.21: Electrical measurement at the POI with the VSM.

Figure 3.32 illustrates the comparison of phase angle behavior at the point of connection of the wind farm, both with and without the integration of a BESS controlled as a VSM. The inclusion of the VSM limits the rate of change of the phase angle, facilitating more accurate tracking by the PLL. This is a key advantage of controlling inverter-based resources using the proposed VSM strategy. By emulating inertial response, the VSM control enables the wind farm to recover effectively from faults and to inject more power at the connection point. These results demonstrate that, similar to synchronous condensers, the proposed VSM control is capable of providing vital inertial support, an essential requirement for maintaining power system stability in scenarios with high renewable energy penetration.

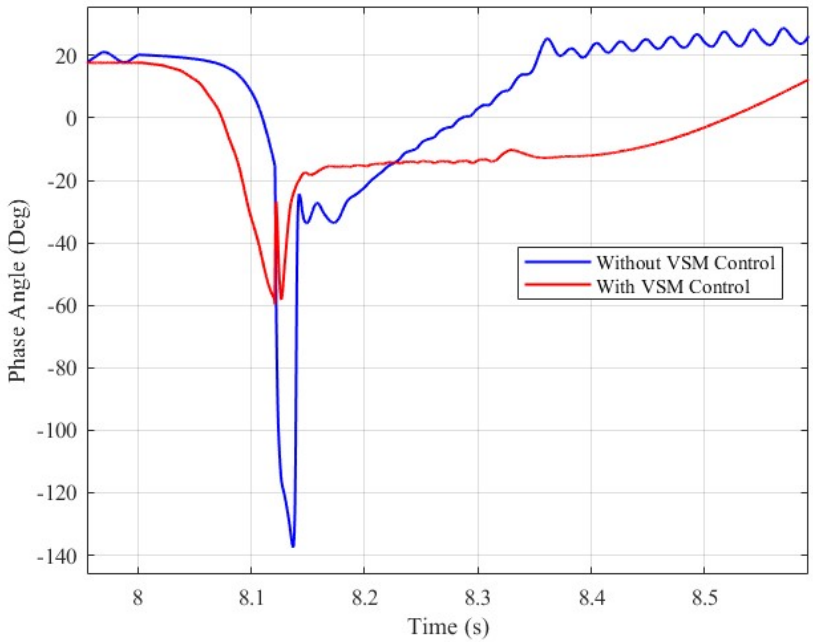

Figure 3.22: Phase angle comparison at Bus at the POC with and without VSM connected.

The VSM method can readily be adapted to implement conventional measures, such as power system stabilizers (PSS), to enhance the damping of power oscillations.

3.1.5. Improvement of the System Response with a PSS

In order to further demonstrate the flexibility of the proposed VSM approach, a simple Power System Stabilizer (PSS) was added to VSM control implementation. The PSS model adopted in the simulation is shown in Figure 3.23. The gains G_1 and G_2 are 1 and 50, respectively. The time constants T, T_1, and T_2 are 0.05 s, 0.284 s, and 0.062 s, respectively.

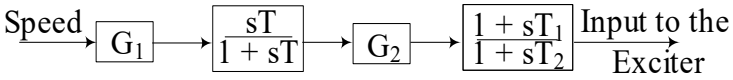

Figure 3.23: Block diagram of the PSS model.

Figure 3.24 shows a comparison of voltage, active power, and reactive power measured on the wind farm side of Bus 1. The simulation results indicate that with the PSS included in the VSM implementation, the oscillations dampen slightly faster, as expected. Identical results were

observed when the same PSS is connected to the exciter of the synchronous condenser at Bus 1. This demonstrates that the VSM concept can be further modified to incorporate additional control functions if required to meet the expected system response criteria.

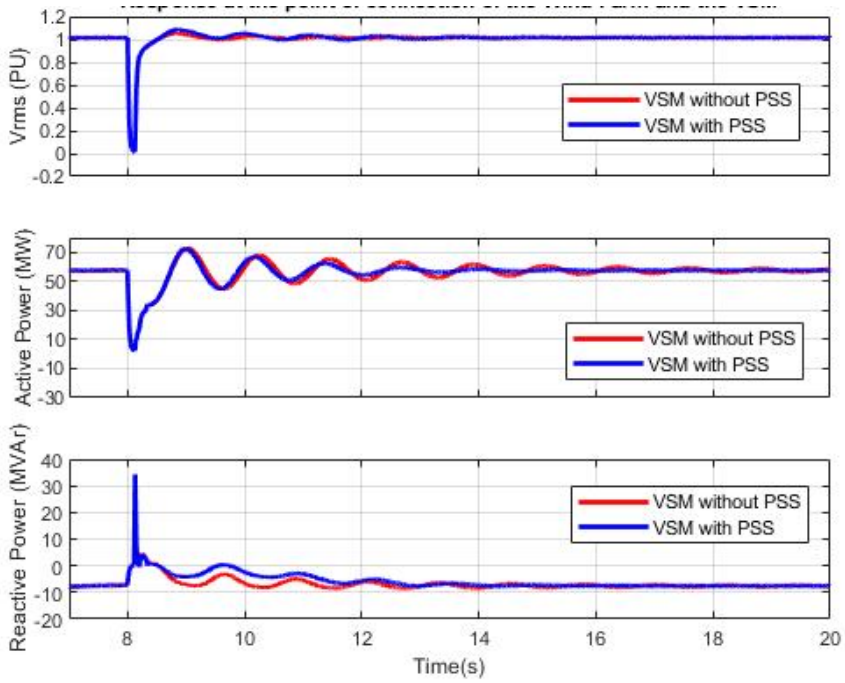

Figure 3.24: Electrical measurement at the POI of the Wind Farm and the VSM (red curve – without PSS, blue curve – with PSS).

3.1.6. Implementation of the Current-Limiting Function and Its Impact on Overall Dynamic Response

To address the inherent limitations of inverter switches, which unlike synchronous machines cannot handle currents beyond their maximum current capability (up to six times the rated value for synchronous machines), the VSM controls were modified to limit the output current to 1.1 pu of the inverter's rated current. This controller modification ensures that the inverter operates within safe limits while still providing adequate performance. The VSM response with the current limiting function implemented was tested in a SMIB set up shown in Figure 3.12. The fault current from the VSM is compared with a comparable synchronous machine fault response and the simulation results are shown in Figure 3.25.

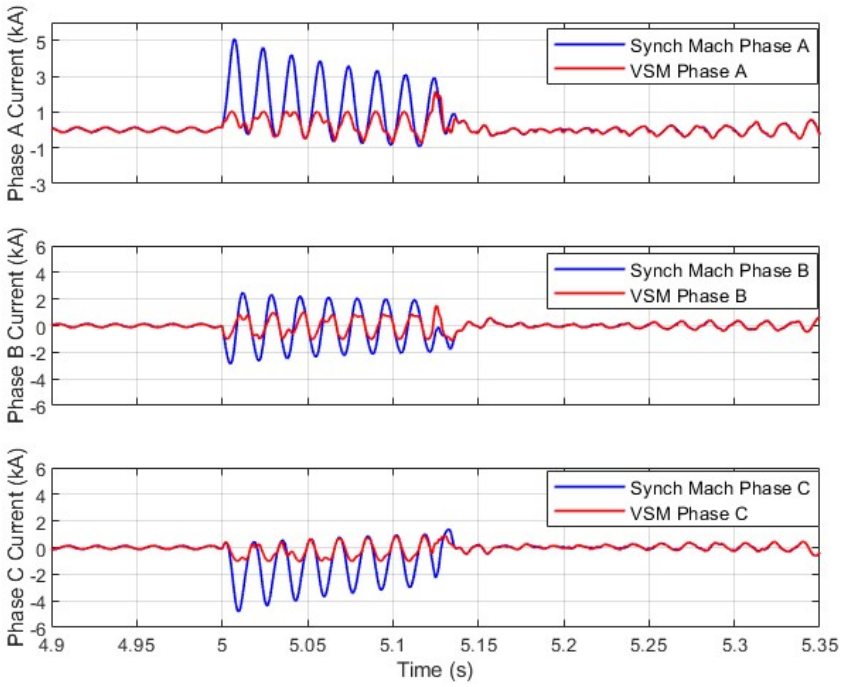

Figure 3.25: Fault current comparison –VSM and the response of a comparable synchronous machine (Three-phase-to-ground fault).

Due to current limiting in the inverter control during faults, the VSM cannot provide as high a current as a synchronous machine would; however, it remains in phase with that of a comparable synchronous machine, and following fault clearance, the VSM response closely matches the synchronous machine's behavior. Higher fault currents during faults are only required for the proper operation of protection equipment.

This is particularly significant because, despite current-limiting constraints during faults, the VSM provides benefits comparable to a synchronous machine; including in-phase fault current injection, post-fault inertial response matching, and enhanced dynamic support for nearby inverter-based resources through synthetic inertia emulation.

Next the effectiveness of the modified VSM controls with current limits was validated using the test system illustrated in Figure 3.18. To test the robustness of the VSM (with current limiting function), a three-phase-to-ground fault (at 5 s) was applied to line 1. The fault was cleared by

tripping the line breakers after 120 ms at Bus 1 (near end) and 170 milliseconds at Bus 2 (far end). Under system's intact condition, the maximum power delivery from the wind farm at the point of interconnection was 60 MW, as shown in Figure 3.26.

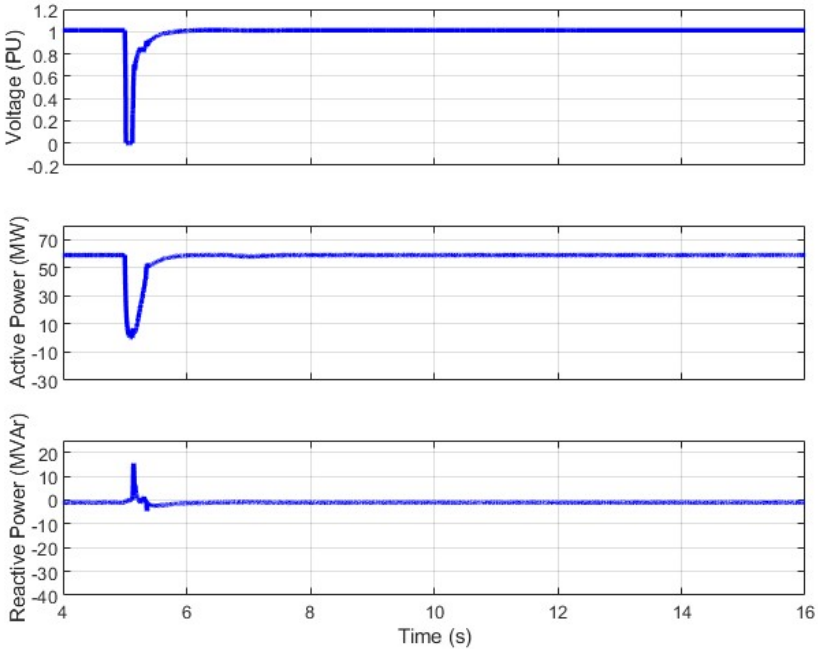

Figure 3.26: Electrical measurements at the POI of the wind farm (Power delivery 60 MW).

However, when the active power delivery from the wind farm was increased to 90 MW, the response became unacceptable, as illustrated in Figure 3.27.

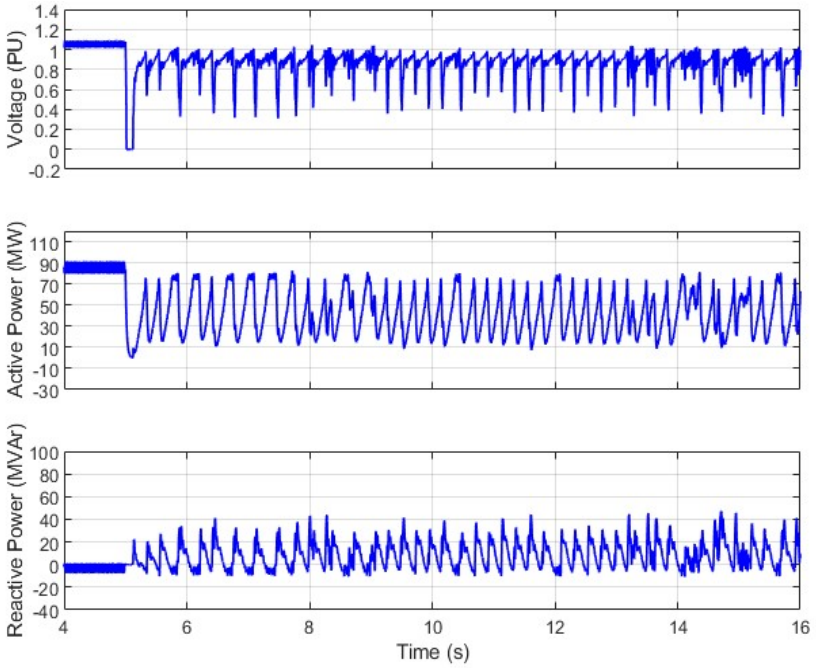

Figure 3.27: Electrical measurements at the connection point of the wind farm (Power delivery 90 MW).

To mitigate this fault ride through issue, a 50 MVA synchronous condenser was integrated into the system (at Bus 1), resulting in an acceptable response from the wind farm, as depicted in Figure 3.28.

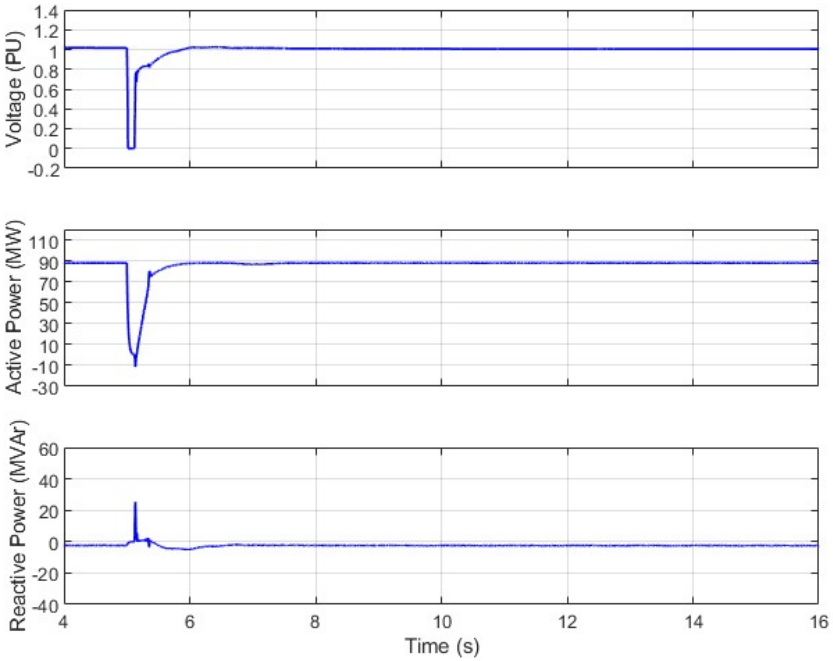

Figure 3.28: Electrical measurements at the point of interconnection of the wind farm and the synchronous condenser.

The synchronous condenser was then replaced with a BESS controlled using the proposed VSM approach with the current-limiting function. The results, shown in Figure 3.29, indicate that the fault ride-through was successful with the BESS implementation. The VSM effectively limited the current output, while still maintaining successful recovery from the fault.

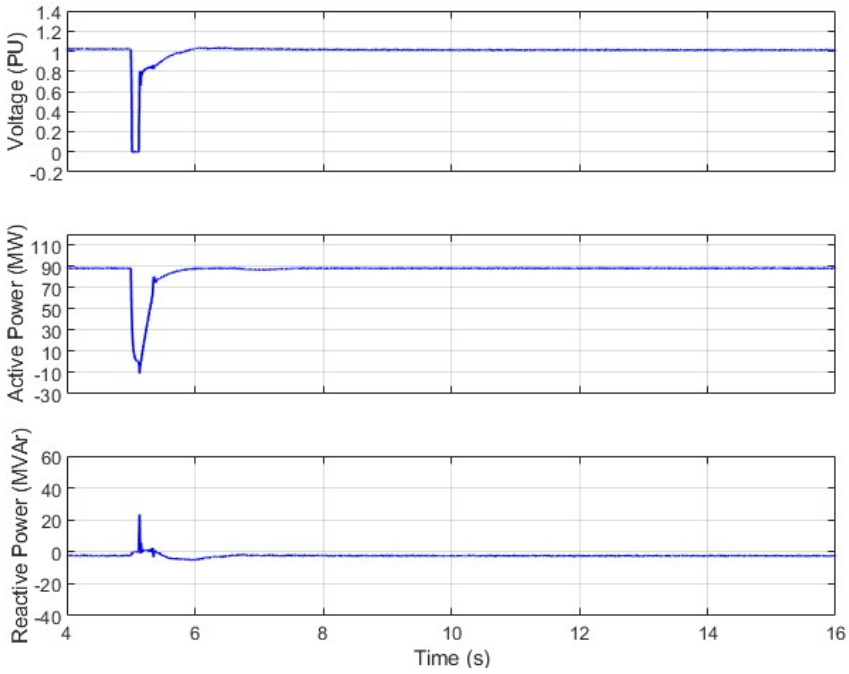

Figure 3.29: Electrical measurements at the connection point of the windfarm with the VSM.

A fault current comparison between the BESS controlled as a VSM and a comparable synchronous condenser, during the three-phase-to-ground fault, is provided in Figure 3.30. When the current-limiting function is applied to the VSM control, the fault current is effectively limited compared to the current observed with a comparable synchronous machine connected at the POI. Despite the limitation, the current remains in phase with that of the synchronous condenser, providing the necessary inertial effect to improve the wind farm's response. The response comparison after fault clearance is almost identical between the VSM (with current limits) and a comparable synchronous condenser.

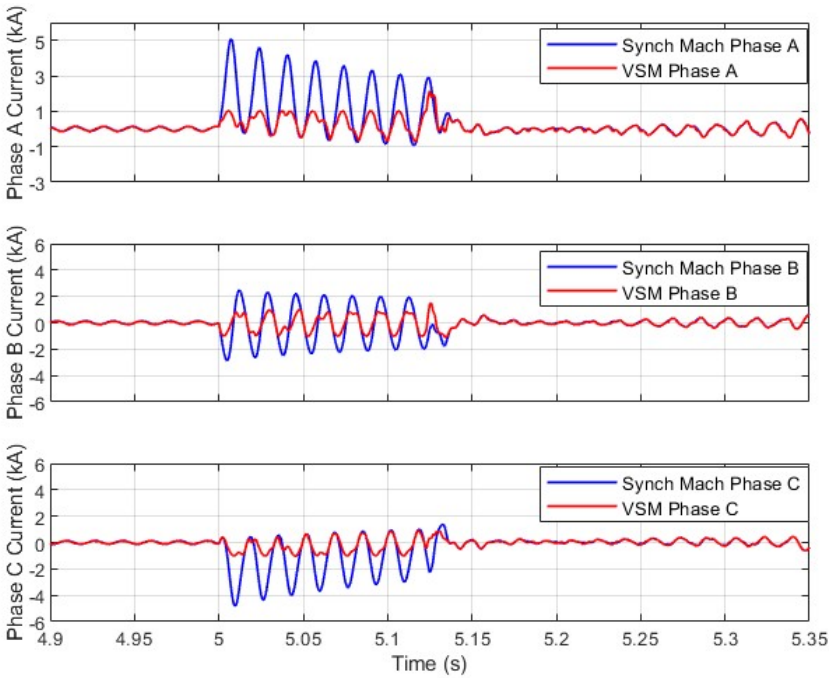

Figure 3.30: Fault current comparison –VSM and the response of a comparable synchronous machine (Three-phase-to-ground fault).

3.1.7. Impact of Frequency Changes on the DC Current of the Battery When Controlled as a VSM

In the practical test system depicted in Figure 3.18, the impact of system-side frequency changes on the DC current of the battery, when controlled as a VSM, was investigated. This test was done to assess the inertial response and the response required from the DC source to provide such inertial characteristics. A three-phase-to-ground fault was applied to line 1 at $t = 5$ s, with the line breakers tripping to clear the fault after 120 ms (at Bus 1 – near end) and 170 ms (at Bus 2 – far end). The frequency measurements at the point of interconnection of the wind farm and the BESS controlled as a VSM, as well as the DC-side current of the BESS, are plotted in Figure 3.31. Based on the simulation results, it can be observed that the DC current of the battery increases as the system frequency decreases indicating the ability to provide inertial support. Conversely, the DC current decreases as the system frequency increases.

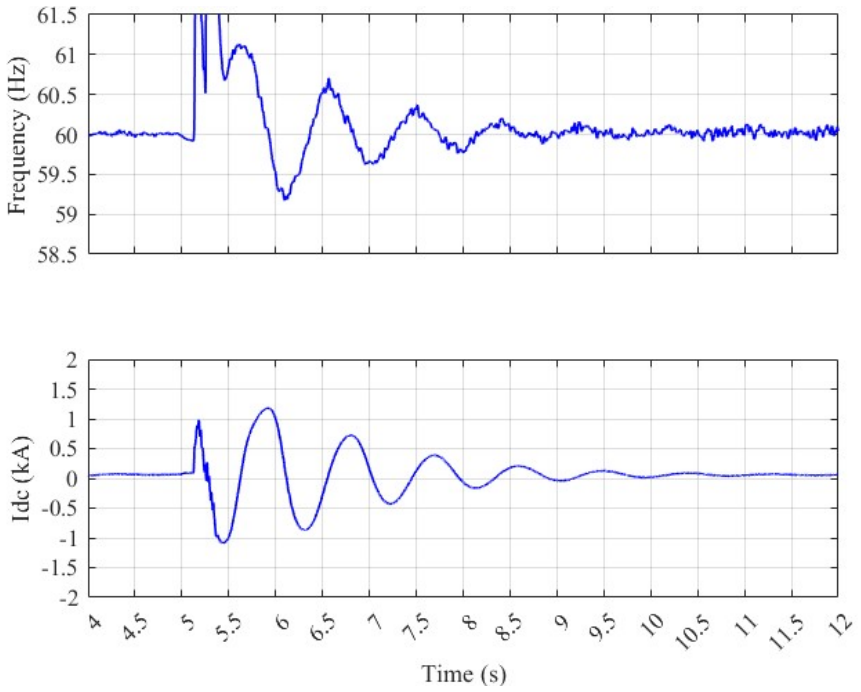

Figure 3.31: System Frequency and the DC current Measurement of the VSM.

Battery sizing for an inverter depends on both power (kW) and energy (kWh) requirements. The battery's continuous discharge rating must at least match the inverter's rated power (e.g., a 10 kW inverter requires a battery capable of sustaining ≥10 kW output). For VSM applications, the battery capacity can be sized based on the synchronous machine's inertial response time (typically 2–10 seconds, depending on virtual synchronous machine design). Consequently, the required DC-side discharge duration need not be significantly longer.

Proper sizing balances the inverter's instantaneous power demands with application-specific energy needs while accounting for the battery's discharge capability (C-rate), temperature effects, and cycle life.

3.1.8. Verification of the VSM Concept on a Modified Transmission Network Test System with High IBR

The response of the VSM-based plant was further validated using the modified practical test system shown in Figure 3.32. The modified test system consists of a 60 MW wind power plant connected at Bus 1, a 25 MW solar PV plant connected between Bus 2 and Bus 3, and a thermal generator (50 MVA) connected at Bus 6. The transformer, transmission line, and load data, as well as the equivalent source details at buses 9, 11, and 12 are given in Table 8.1 to Table 8.4.

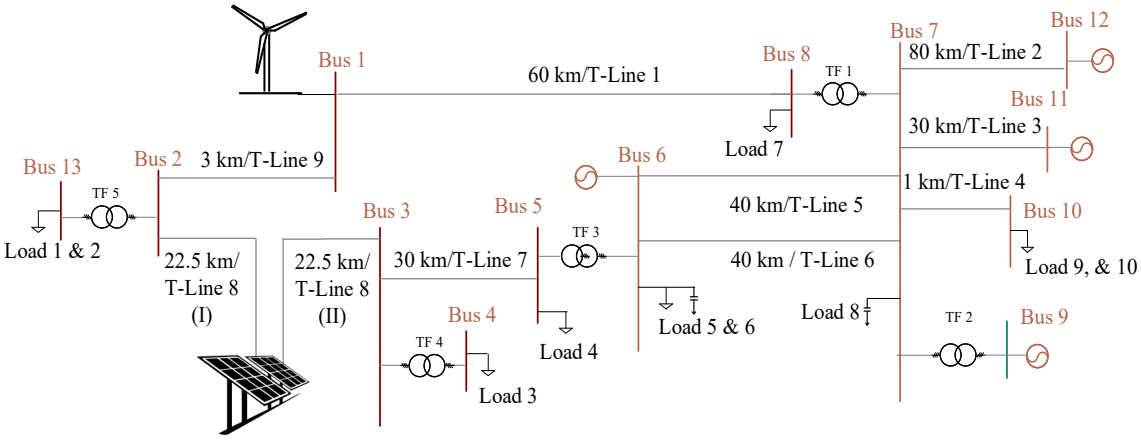

Figure 3.32: Practical transmission network test system developed to verify the proposed VSM approach.

The short circuit MVA at Bus 1 is approximately 166 MVA. With respect to the 60 MW wind plant, the effective short circuit ratio (SCR) is approximately 2.7. When the transmission line from Bus 1 to Bus 8 is tripped, the short circuit ratio drops to about 1.2 (73 MVA). This represents a very weak connection condition for the wind farm. System loads, especially those in close vicinity of the POI, can influence the dynamic response following a fault and its clearance. However, the work presented in this thesis focuses on studying the viability of the VSM concept to overcome inverter response challenges. Thus, the loads are represented as constant PQ components. A three-

phase-to-ground fault is applied (at 15 s) to line 1 and is cleared by tripping the line breakers after 120 ms (Bus 1 – near end) and 170 ms (Bus 2 – far end).

Figure 3.33 and Figure 3.34 show simulation results of wind farm and solar PV plant, respectively. It can be seen that the response of the wind farm is not acceptable and that both the wind farm and the solar farm would not recover from the fault.

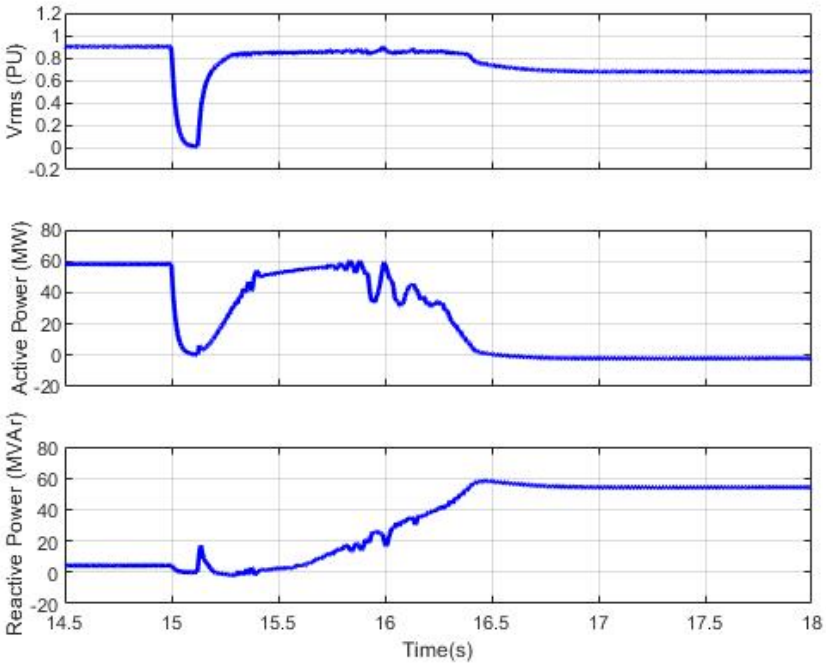

Figure 3.33: Electrical measurements at the point of interconnection of the wind farm.

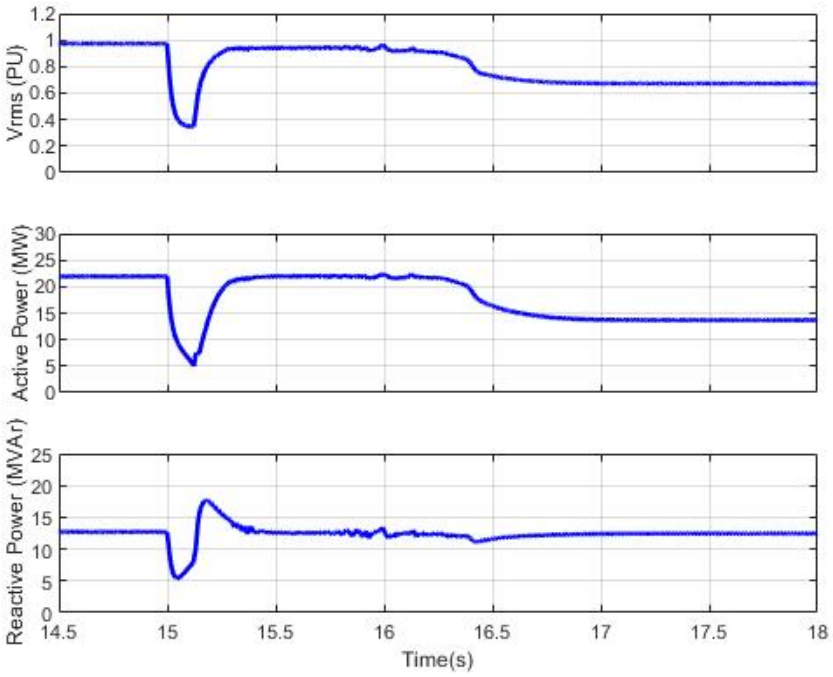

Figure 3.34: Electrical measurements at the interconnection point of solar PV plant.

Addition of a synchronous condenser is a potential measure to improve the response of the wind farm. This was verified through simulations with a synchronous condenser connected at Bus 1. Simulation studies show that a synchronous condenser with a rating of 50 MVA (minimum rating to ensure successful fault ride through) is required to ensure successful recovery of the wind and solar plants. The sub-transient reactance and the inertia of the synchronous condenser (X_d" and H) are 0.22 pu and 4 seconds, respectively.

Figure 3.35 and Figure 3.36 show the simulation results with the synchronous condenser (with AC7B exciter) connected at Bus 1. With the synchronous condenser in service, both the wind farm and the solar PV plant are able to ride through the fault and recover to operate stably.

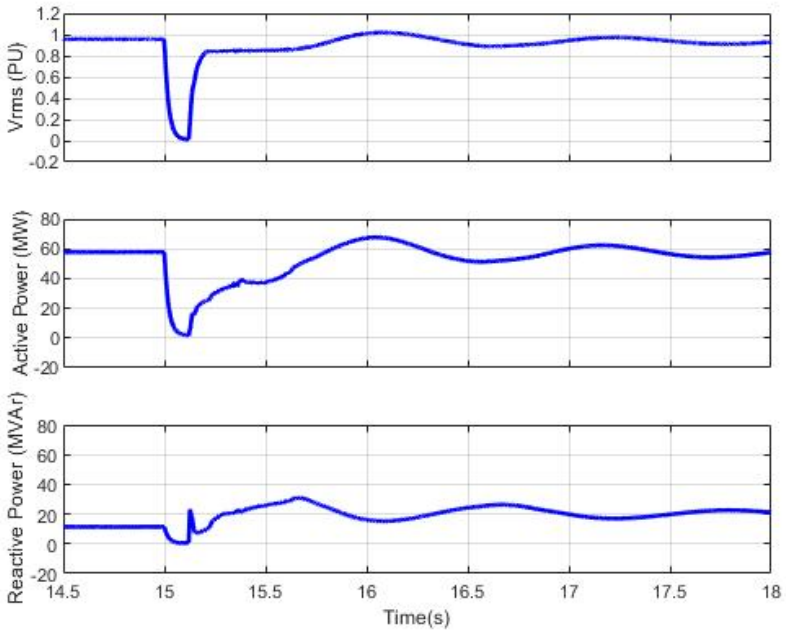

Figure 3.35: Electrical measurements at the POI of the wind farm and the synchronous condenser.

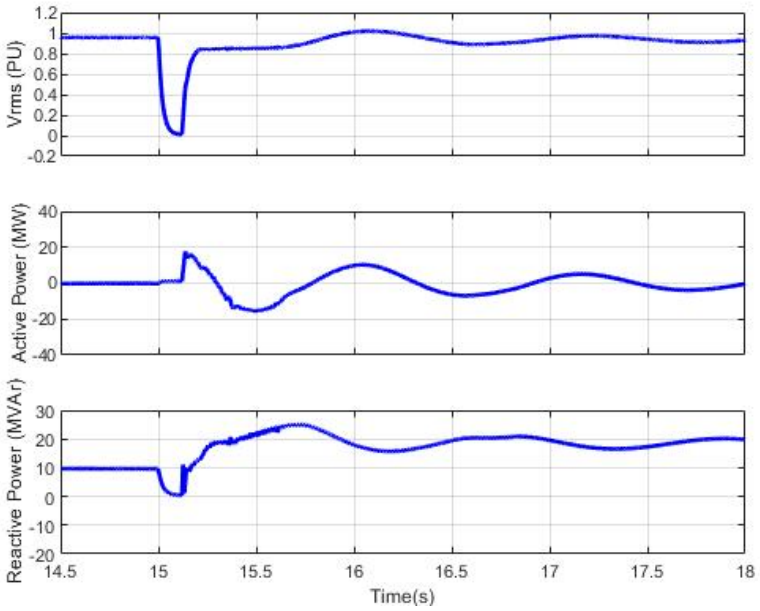

Figure 3.36: Electrical measurements at the POI of the synchronous condenser.

The synchronous condenser was then replaced by a BESS controlled as a VSM. The rating of the VSM is comparable to the synchronous condenser (50 MVA equivalent with inverter current limits implemented accordingly). Figure 3.37 and Figure 3.38 show simulation results with the BESS (controlled as a VSM) connected at Bus 1. The response of the BESS follows the response

of the synchronous condenser very closely. The overall system response is comparable to the case where the synchronous condenser was connected to Bus 1. The transient active power response following fault clearing, shown in Figure 3.38, demonstrates that the inertial response of the BESS closely follows that of a comparable synchronous condenser. The inertial response delay of the BESS (operated based on VSM approach) is insignificant. This is an important observation and an important feature of the proposed method.

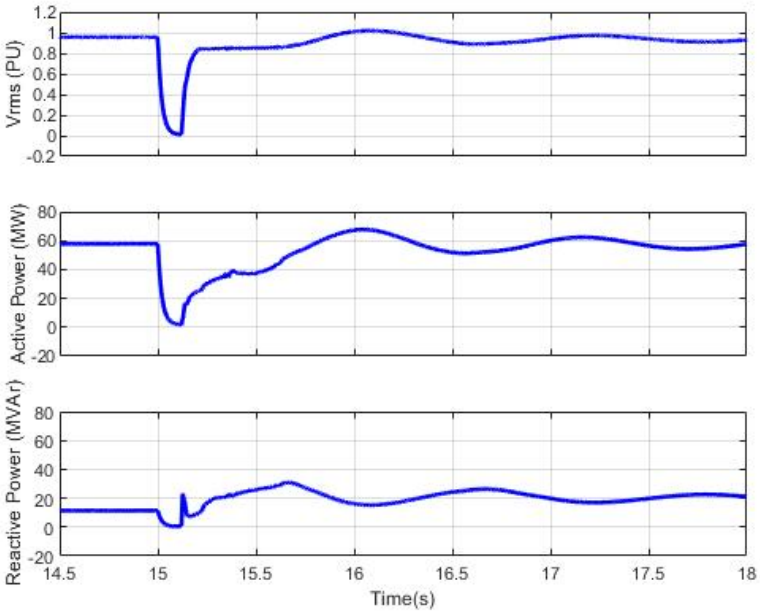

Figure 3.37: Electrical measurements at the POI of the wind farm and the synchronous condenser.

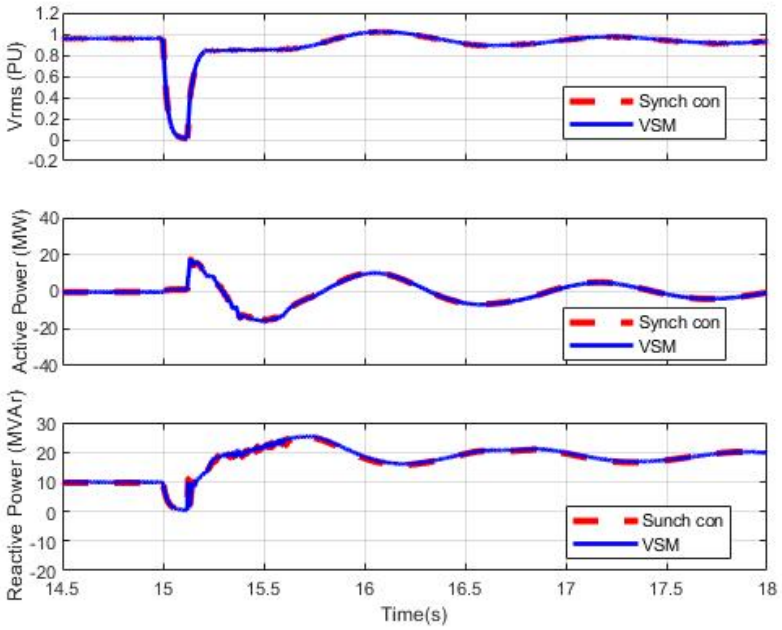

Figure 3.38: Electrical measurements at the POI of the synchronous condenser/VSM (comparison).

Simulation results show the effectiveness of the VSM approach.

3.1.9. Impact of VSM on PLL Response

The network model shown in Figure 3.39 is used to investigate the impact of the proposed VSM on the Phase-Locked Loop (PLL) response. The solar farm is configured to deliver 90 MW at the point of connection. To assess the effect of the proposed VSM approach on the PLL response, the performance of the solar farm was compared with and without a battery energy storage system controlled as a VSM.

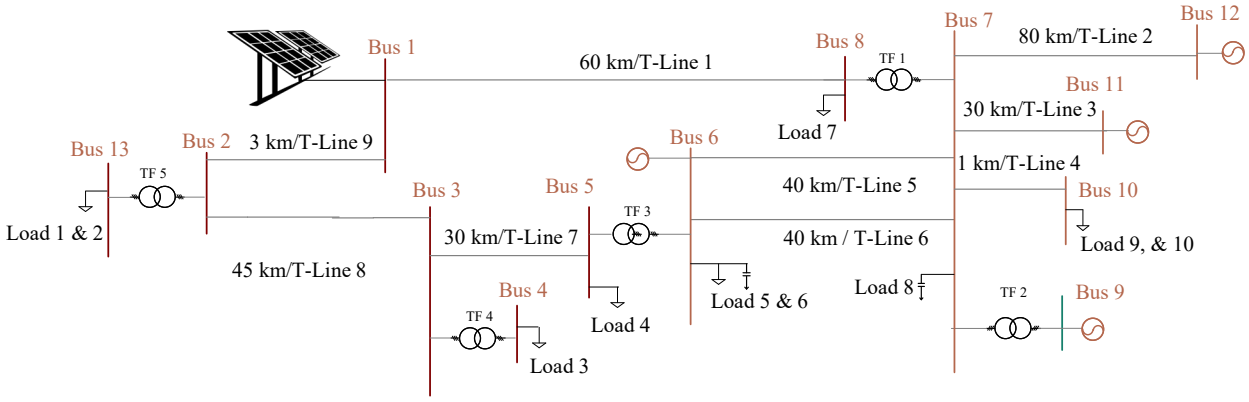

Figure 3.39: Practical transmission network test system developed to verify the effect of VSM approach on PLL Response.

Figure 3.40 shows the comparison of d and q-axis voltages, as well as the voltage phase angle at the point of connection.

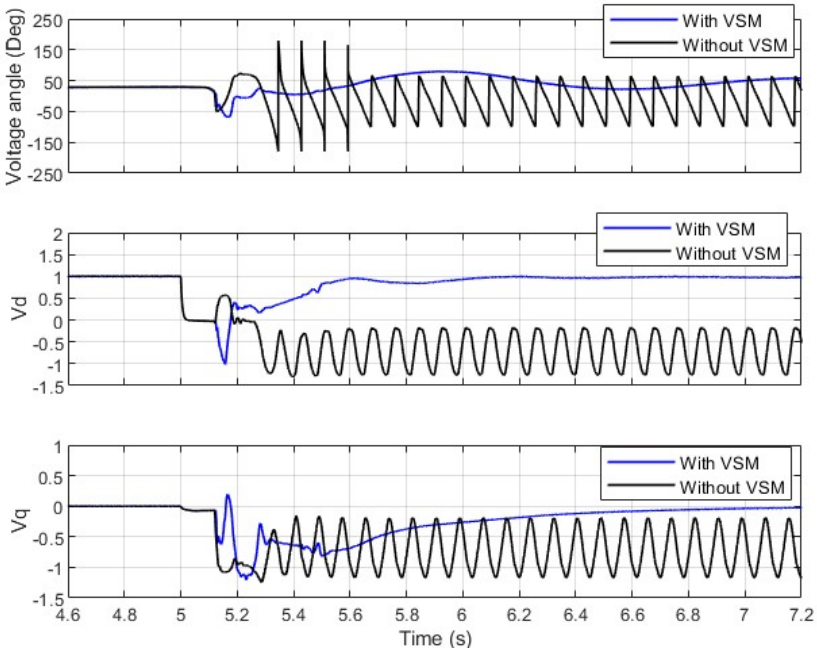

Figure 3.40: Voltage angle, and d and q-axis voltage comparison with and without VSM.

With the BESS controlled as a VSM, the rate of change of the voltage angle at the point of interconnection of the solar farm is minimal. Consequently, the PLL can accurately track the voltage angle, enabling the solar farm to provide a stable response. As the inertia of the VSM increases, the PLL response improves further as shown by Figure 3.41.

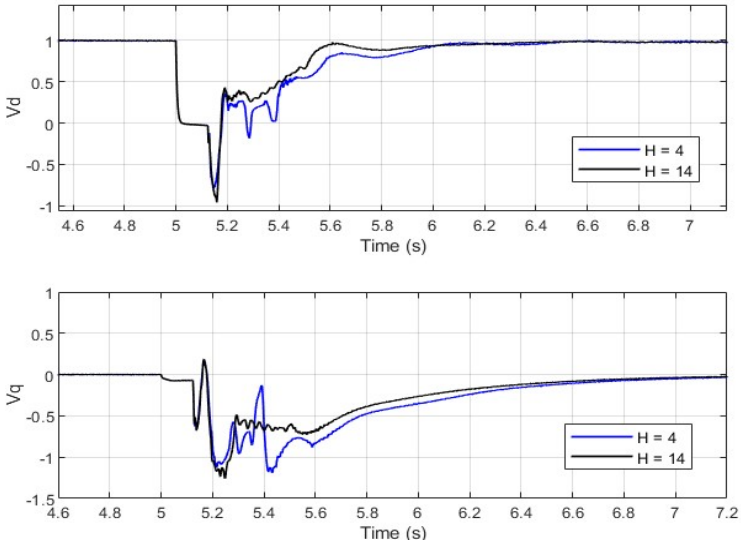

Figure 3.41: d and q-axis voltage comparison for different inertia levels.

3.1.10. Impact of the Proposed VSM on System Frequency

In the transmission network shown in Figure 3.39, the frequency at Bus 6 was measured both with and without the VSM when a three-phase-to-ground fault is applied at t = 5 s on line 1. The frequency comparison (with and without the proposed VSM) is shown in Figure 3.42. The frequency nadir improves (though marginally in this test system) when the VSM is connected during the fault.

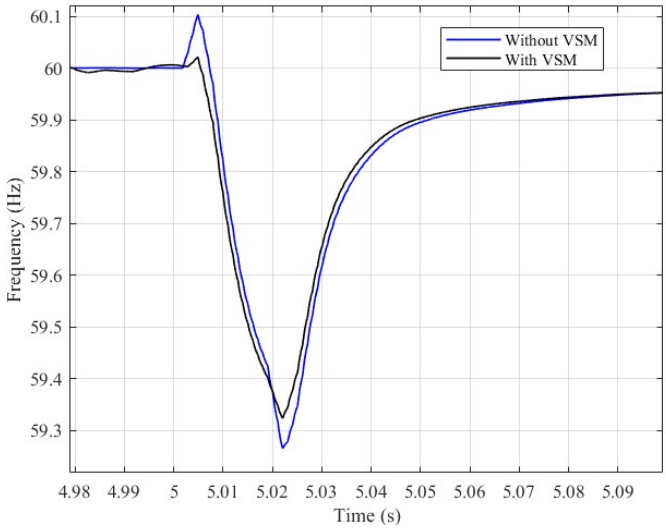

Figure 3.42: Frequency measurement at Bus 6.

Figure 3.43 shows simulation results expanded over a longer time duration.

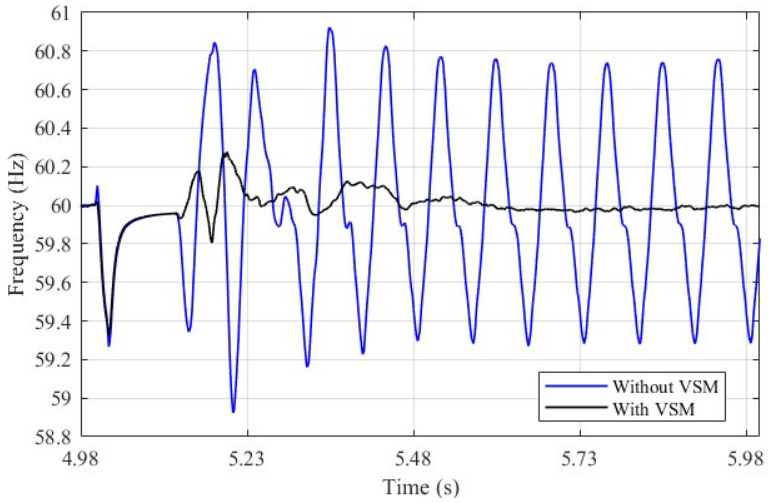

Figure 3.43: Frequency measurement at Bus 6.

Without the VSM the overall response is in fact unstable in this particular case. The simulation results show that the proposed VSM approach can significantly improve frequency stability.

3.1.11. Comparison of the Proposed VSM Approach with Existing Technologies

The proposed VSM implementation presented in this thesis is based on grid-following techniques, where a PLL is used to track the grid voltage. In contrast, most VSM methods proposed in the existing literature are based on the grid-forming approach. Additionally, many of these methods do not account for the electromagnetic characteristics of the machine (the machine winding voltage current equations described in equations (3.1) to (3.6) are not implemented). Due to these differences, a direct comparison between the proposed method and existing methods is difficult to perform. However, in this section a comparison between the proposed VSM approach and two selected VSM approaches based on the information available from the literature, is conducted.

One of the VSM techniques selected for comparison with the proposed method is developed based on the swing equation of a synchronous generator. This method is designed to suppress frequency oscillations resulting from the high penetration of solar PV in microgrids, as illustrated in reference [31]. The current references required to implement the method described in [31] are derived as shown in Figure 3.44.

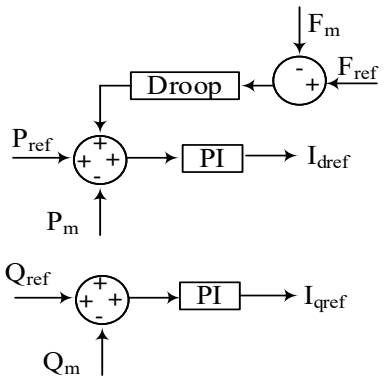

Figure 3.44: Derivation of I_d and I_q references to implement the method described in [31].

The voltage angle required to generate the voltage reference waveform for producing switching pulses was derived using (2.1), as described in [31]. The methods described in [31] and were implemented in a test system as shown in Figure 3.45 to provide an illustrative comparison.

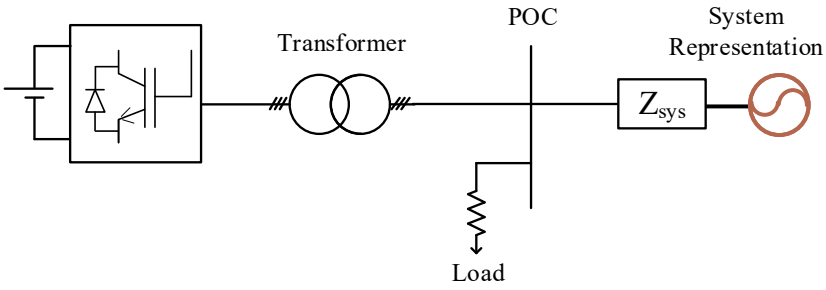

Figure 3.45: Single Machine Infinite Machine (SMIB) test system adopted for VSM technique comparison.

The proposed VSM response was compared with the method implemented in [31], and the simulation results are shown in Figure 3.46. The active power response indicates that this method does not provide effective inertia response compared to the approach presented in this research.

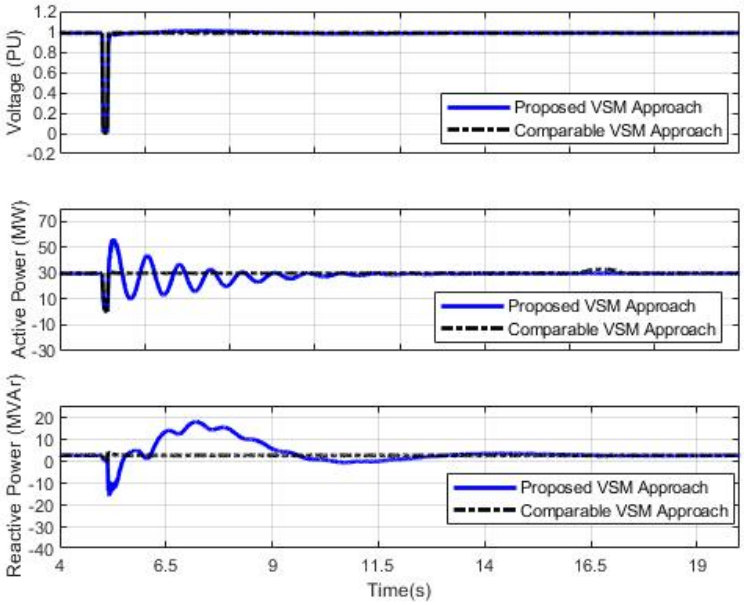

Figure 3.46: Dynamic response comparison following a three-phase fault (applied at 5 seconds) and cleared in 0.12 ms – proposed VSM and the response of a comparable VSM based on grid forming approach and with only the mechanical swing equation adopted to derive inverter control input signals.

The second method selected for comparison with the proposed VSM approach utilized the electrical equations of a synchronous machine, with sub-transient effects omitted, as described in [43]. The inertial response of the machine was implemented using (2.1), and the current references were derived by solving the machine equations, following the method outlined in [43]. This method was implemented in the test system, shown in Figure 3.45, to provide an illustrative comparison.

The proposed VSM response was compared with the method implemented in [43], and the simulation results are presented in Figure 3.47. The active power response indicates that the approach proposed in this research provides better damping.

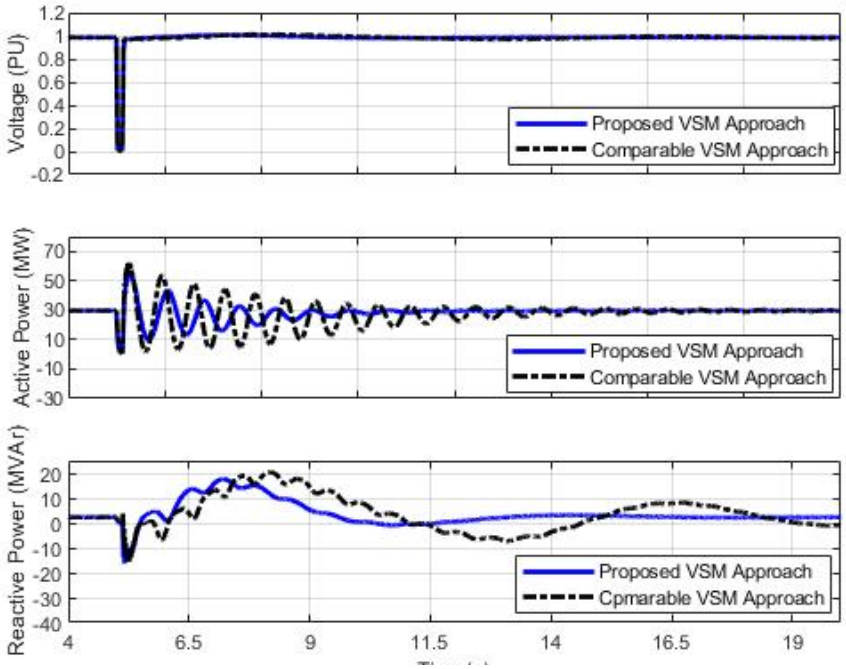

Figure 3.47: Dynamic response comparison following a three-phase fault (applied at 5 seconds) cleared in 0.12 ms – proposed VSM and the response of a comparable VSM based on grid forming approach and with mechanical swing equation and electrical equations (ignoring damper winding effects) adopted to derive inverter control input signals.

3.2. Summary of Contributions

Most existing VSM control strategies in literature are based on inverters operating with the 'grid-forming' technique, and these strategies are formulated using simplified emulation of a synchronous machine (based on numerous assumptions). In this research an advanced VSM control strategy was developed that solves the full transient equations of the machine to derive the instantaneous current references for inverter controls. This approach enables the emulation of both the electromagnetic and mechanical dynamics of a synchronous machine, capturing its full transient behavior. By incorporating key synchronous machine controls such as exciters, power system stabilizers, and governor-turbine responses, this method provides a more comprehensive and accurate emulation of synchronous machine behavior than existing simplified VSM models.

The proposed VSM control method was applied to a BESS system and rigorously tested using EMT simulation software platform. Simulations were first conducted on a SMIB-type setup where the proposed technique was verified. Then the method was further tested on several practical transmission test systems. The results demonstrated that the grid-following VSM effectively emulates the dynamic response of a synchronous machine, enhancing system stability under a variety of conditions, including low system strength and high renewable penetration.

Based on the investigations carried out in this chapter, a research paper titled "Battery Energy Storage System Controlled as a Virtual Synchronous Machine for Improved System Stability" was presented at the 2022 IEEE Power & Energy Society General Meeting (PESGM) in Denver, CO, USA.

Chapter 4: Verification of the VSM Concept on a Practical European High-Voltage Network

In this chapter, investigations conducted to further verify the proposed VSM concept are presented. The dynamic response of the proposed VSM approach is validated using the network model of a representative European transmission system [44]. The area of interest (study area) for this investigation is shown in Figure 4.1. The selected transmission network comprises conventional generation as well as converter-based plants such as onshore/offshore wind, HVDC, solar PV, battery energy storage systems, etc.

The 'study area' (capturing a radius of over 8 busses from the wind farms A, B, C, D, E, and F) of the transmission network includes 400 kV and 275 kV transmission lines with the length of the longest circuit at just above 100 km. The study area comprises the following generating plants and HVDC connections as well as two proposed synchronous condenser units (future scenario).

1. Conventional generation
    a. Gen 1 (800 MVA) and Gen 2 (800 MVA)
    b. Gen 3 (40 MVA)
2. Type III wind farms
    a. Wind farm A (75 MW)
    b. Wind farm B (48 MW)
    c. Wind farm E (180 MW)
3. Type IV wind farms
    a. Wind farm C (108 MW)
    b. Wind farm D (276 MW)

4. Wind farm F (700 MW)VSC HVDC Link

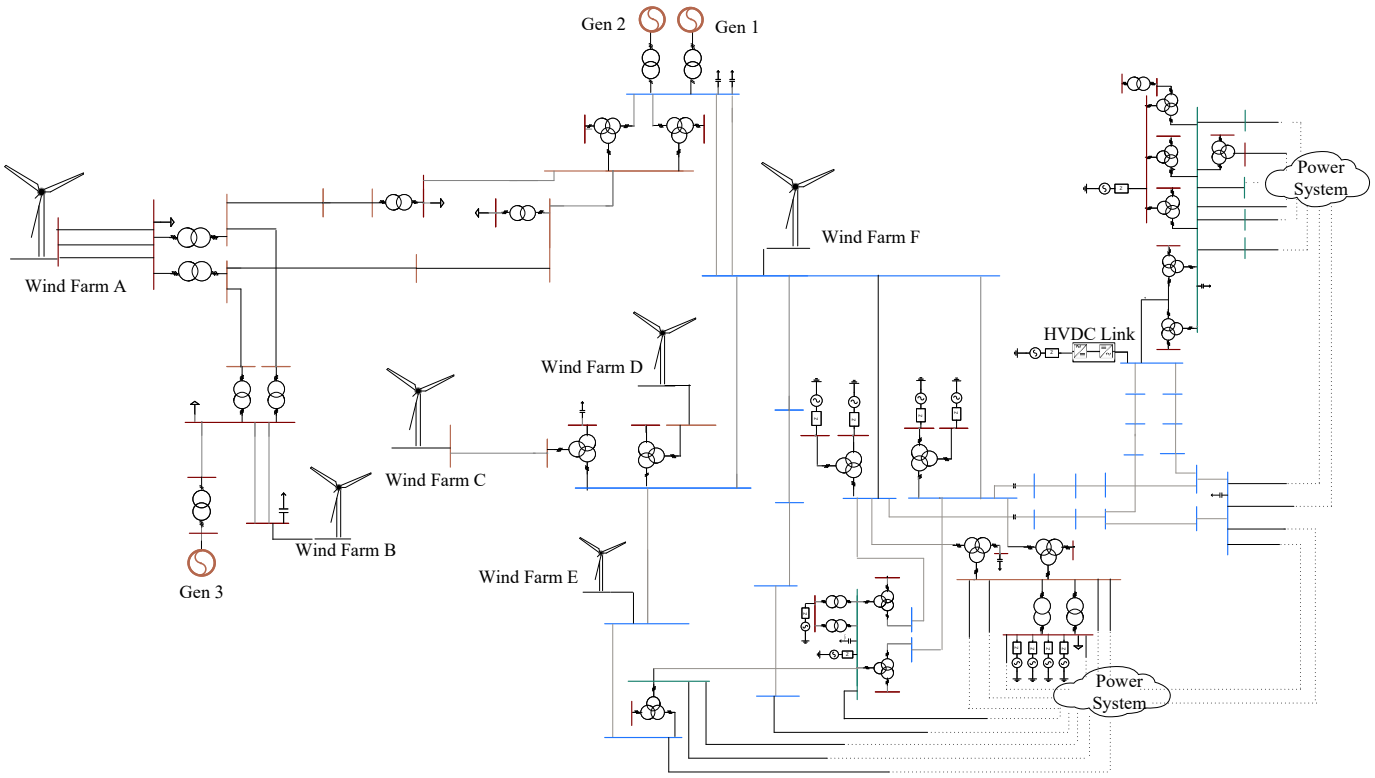

Figure 4.1: Actual transmission model used for verification of the proposed VSM approach.

Conventional synchronous generators are able to provide system inertia and fault current contribution to nearby faults. As the renewable generation increases in the network (in the study area), it is expected that some of the conventional plants will be de-commissioned or not dispatched. For example, Gen 1 and Gen 2 in the study area are due to be taken out of service, leaving Gen 3 the only conventional generator in the area. This will lower the strength of the power system, potentially triggering power system stability issues and impacting the performance of the existing AC protection systems (due to lower fault currents and due to the change in fault current characteristics). The objective is to investigate if these concerns can be mitigated using the proposed VSM approach. The study area shown in Figure 4.1 was represented in detail in PSCAD/EMTDC software.

The dynamic devices (conventional generators, wind farms and HVDC links) were represented with detailed models that mimic typical plant controller characteristics. In order to represent the remainder of the transmission network that is not explicitly modelled, network equivalent voltage sources are used. The network equivalent source impedances are derived through a matrix reduction technique, where the full system nodal admittance matrix is reduced with only the buses in the study area and the boundary buses explicitly retained.

Three network conditions and a selected fault condition were used to verify the performance of the VSM concept and assess its impact on the system's stability.

1. Scenario 1 - System intact condition: All synchronous machines, synchronous condenser and all the transmission lines in main study area kept in service.
2. Scenario 2 - Network outage condition: Three synchronous generating units (Gen 1, 2, and 3) are not in service. The lines from Bus B to Bus C, Bus F to Bus G and the two proposed hybrid synchronous condenser units connected to Bus H and G are not in service.
3. Scenario 3 - Network outage condition (described in scenario 2) with a 50 MVA synchronous condenser connected at Bus A.
4. Scenario 4 - Network outage condition (described in scenario 2) with a BESS controlled as a VSM (comparable to a 50 MVA synchronous condenser) connected at Bus A.

Under each scenario, the response of the wind plants and the system were observed following a three phase to ground fault (applied at t = 8 s) on the line between Bus D and Bus E. Fault was cleared by opening the breakers at the line ends. Near end and far end breaker operating times are 120 ms and 220 ms from the fault inception, respectively.

Scenario 1 - System intact condition

All plants and the system recovered to a stable operating state following the clearing of the fault. The response of Wind Farm A, B and E are shown in Figure 4.2, Figure 4.3, Figure 4.4.

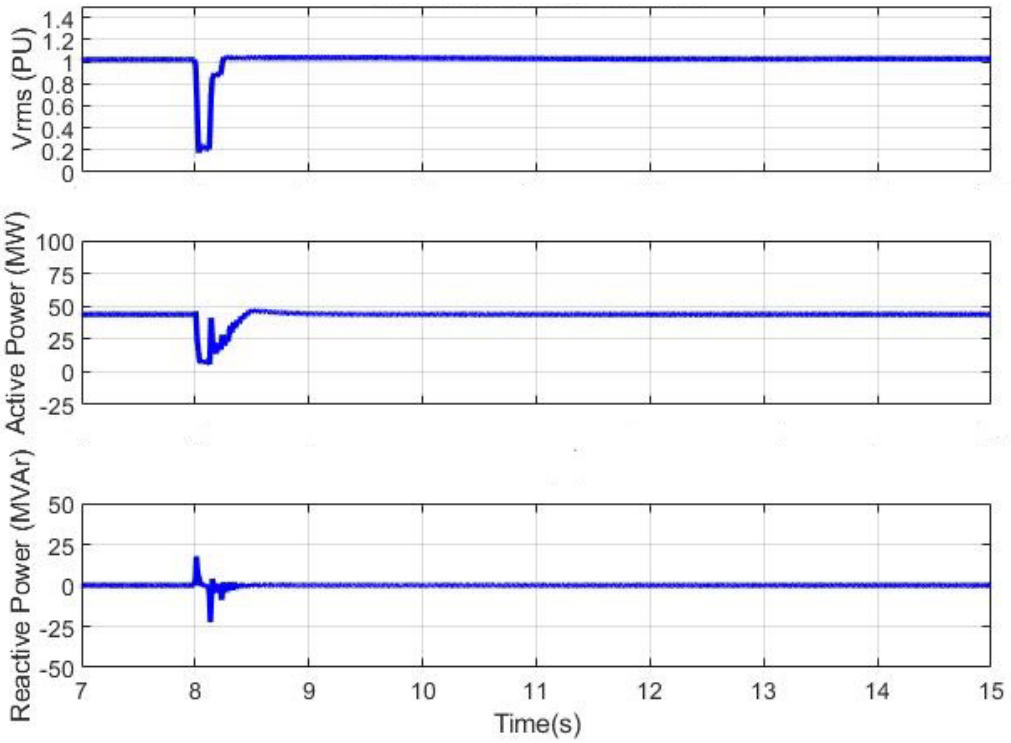

Figure 4.2: Response of Wind Farm A in Scenario 1.

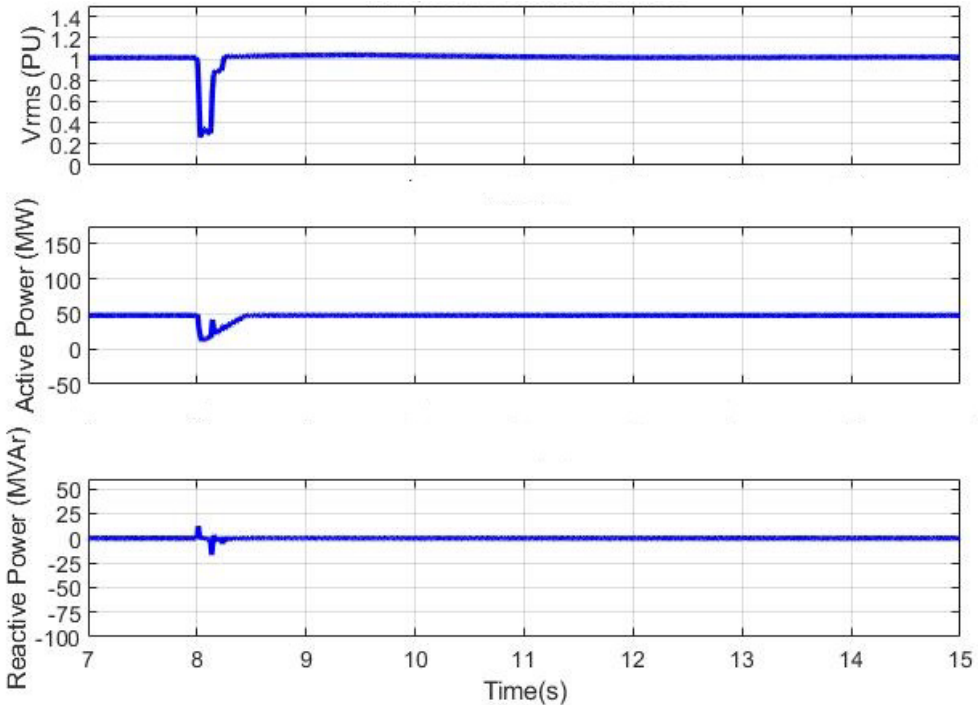

Figure 4.3: Response of Wind Farm B in Scenario 1.

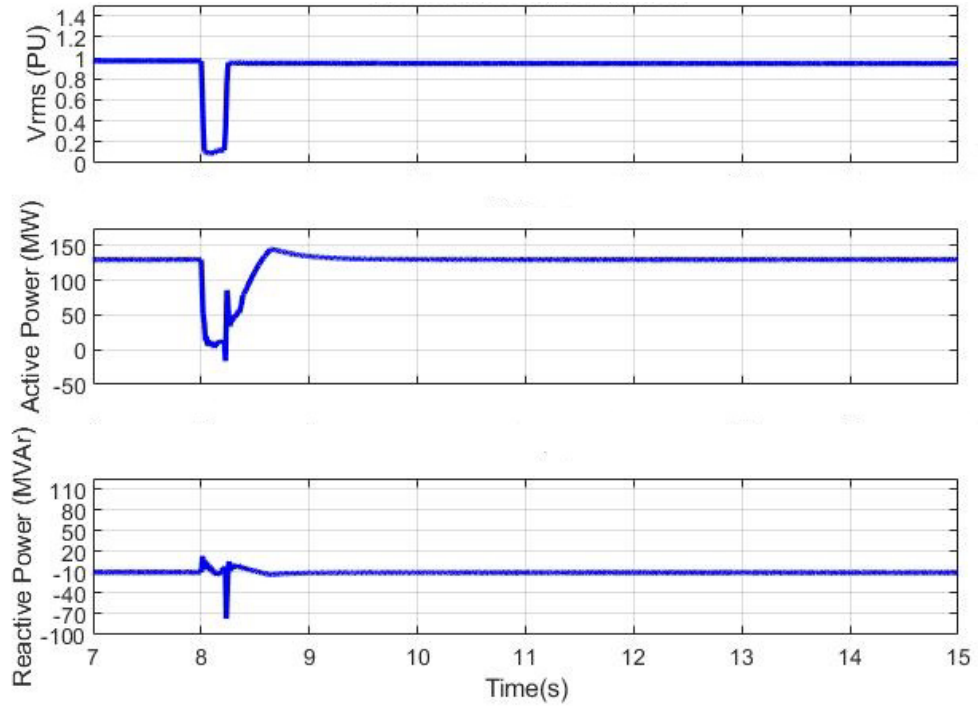

Figure 4.4: Response of Wind Farm E in Scenario 1.

Scenario 2: Network outage condition

Simulation results show that most of the wind farms in the study area will not recover from the fault. The absence (not dispatched) of the synchronous machines and the proposed synchronous condensers in the study area as well as the line outages have caused significant reduction in the system inertia and short circuit levels. The response of wind farm A (recovery unsuccessful), wind farm B (recovery unsuccessful) and wind farm E (recovery successful) are shown in Figure 4.5, Figure 4.6, and Figure 4.7, respectively.

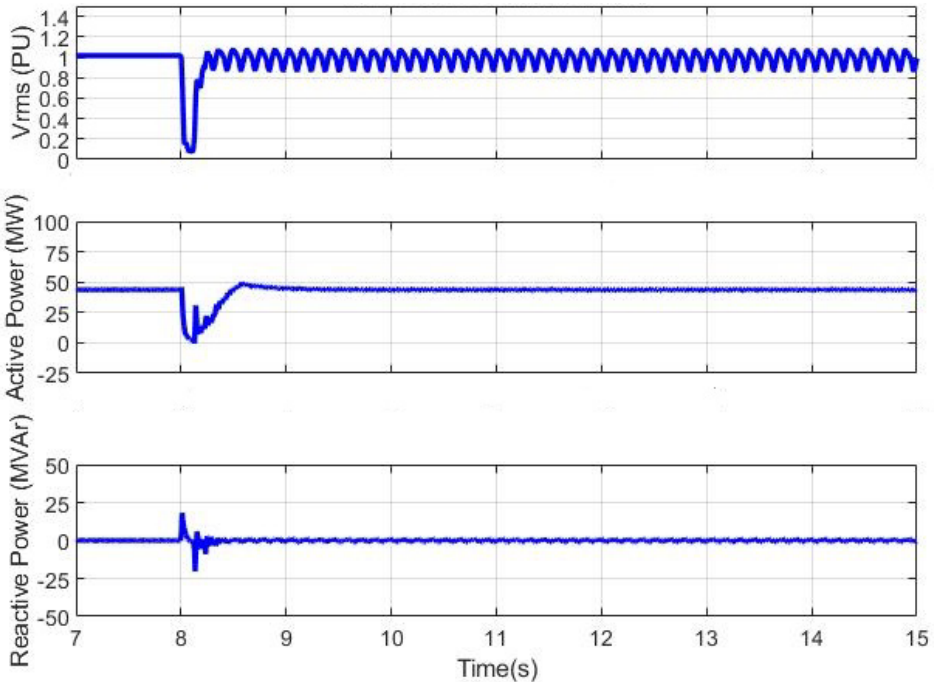

Figure 4.5: Response of Wind Farm A in Scenario 2.

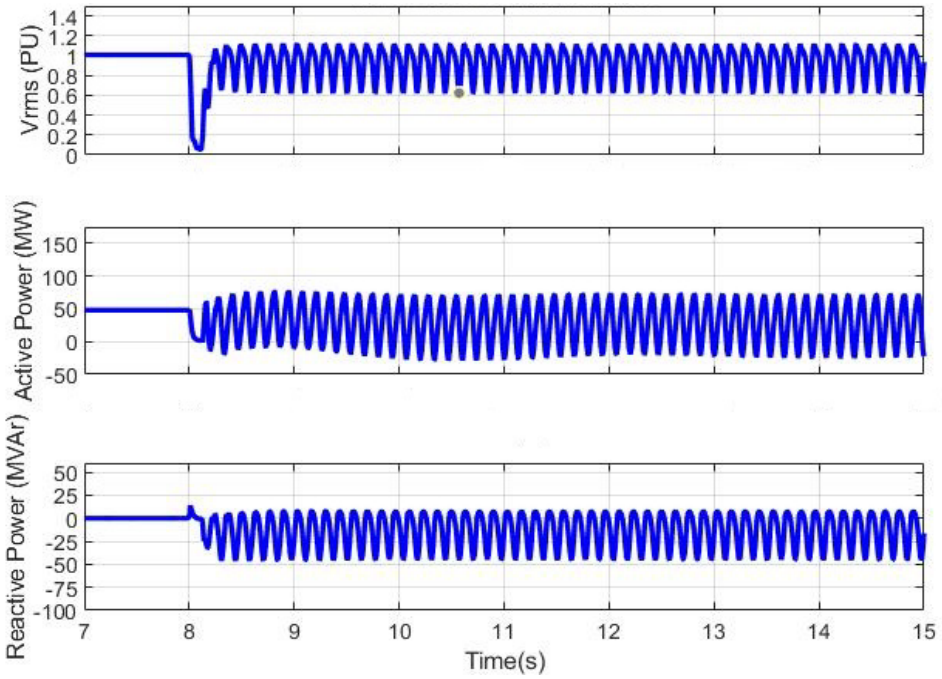

Figure 4.6: Response of Wind Farm B in Scenario 2.

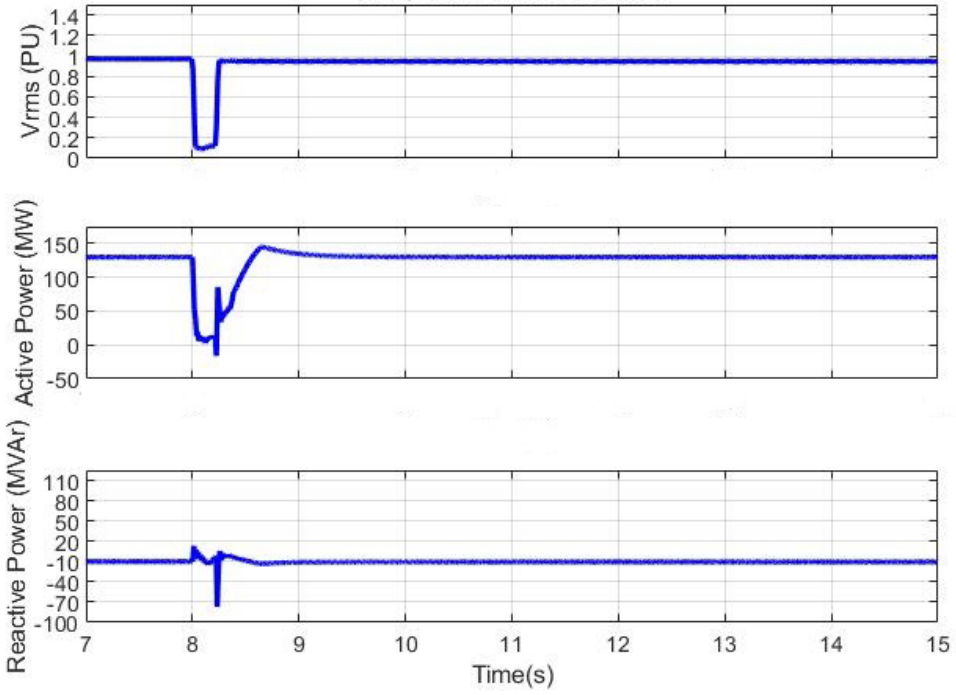

Figure 4.7: Response of Wind Farm E in Scenario 2.

Scenario 3: Network outage condition with a 50 MVA synchronous condenser connected at BUS A

In order to overcome the fault recovery issues observed under the network outage condition (scenario 2), a 50 MVA synchronous condenser (X_d" = 0.2, H = 4 s) was connected to Bus A. The simulation results shown in Figure 4.8, Figure 4.9, and Figure 4.10 show that the synchronous condenser can mitigate the fault recovery issues under generation and line outage conditions.

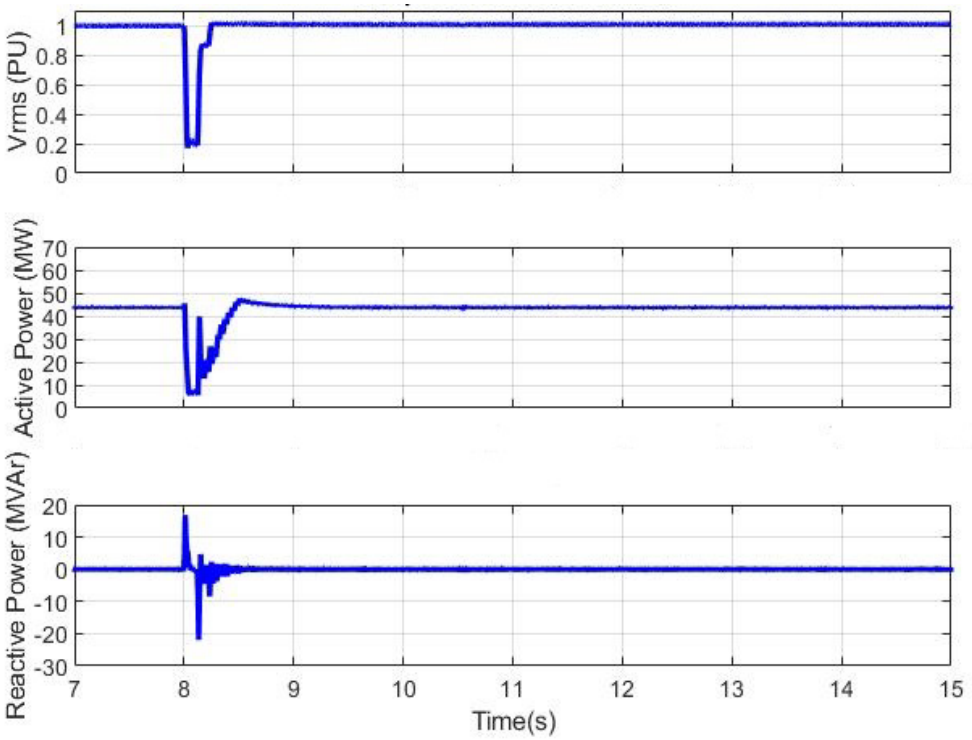

Figure 4.8: Response of WF A in Scenario 3.

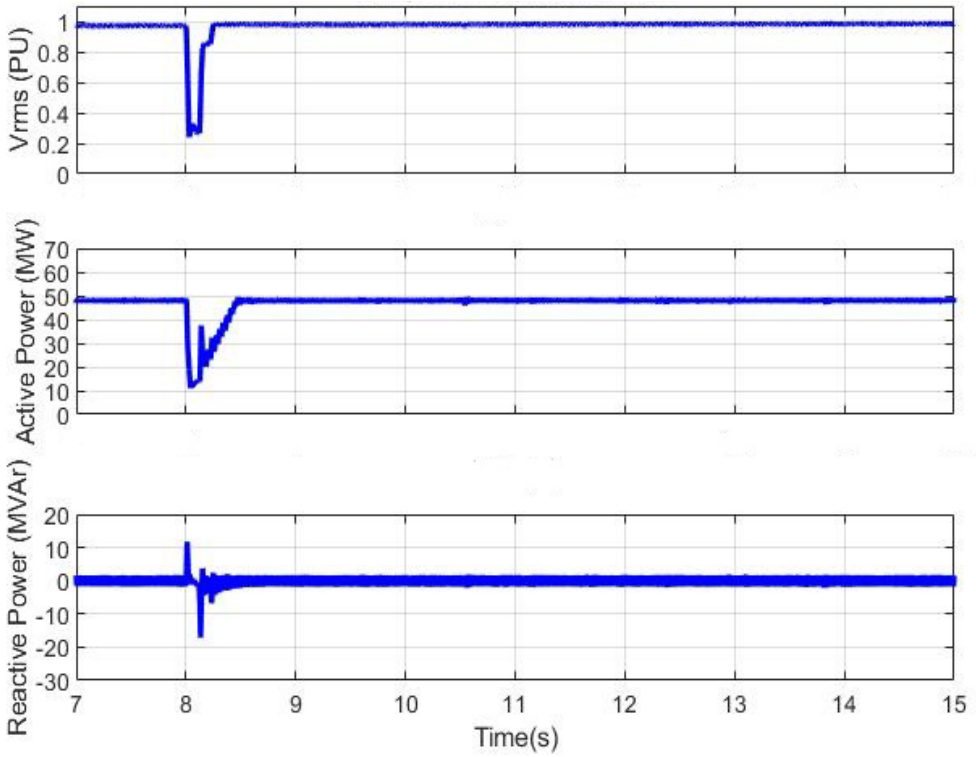

Figure 4.9: Response of WF B in Scenario 3.

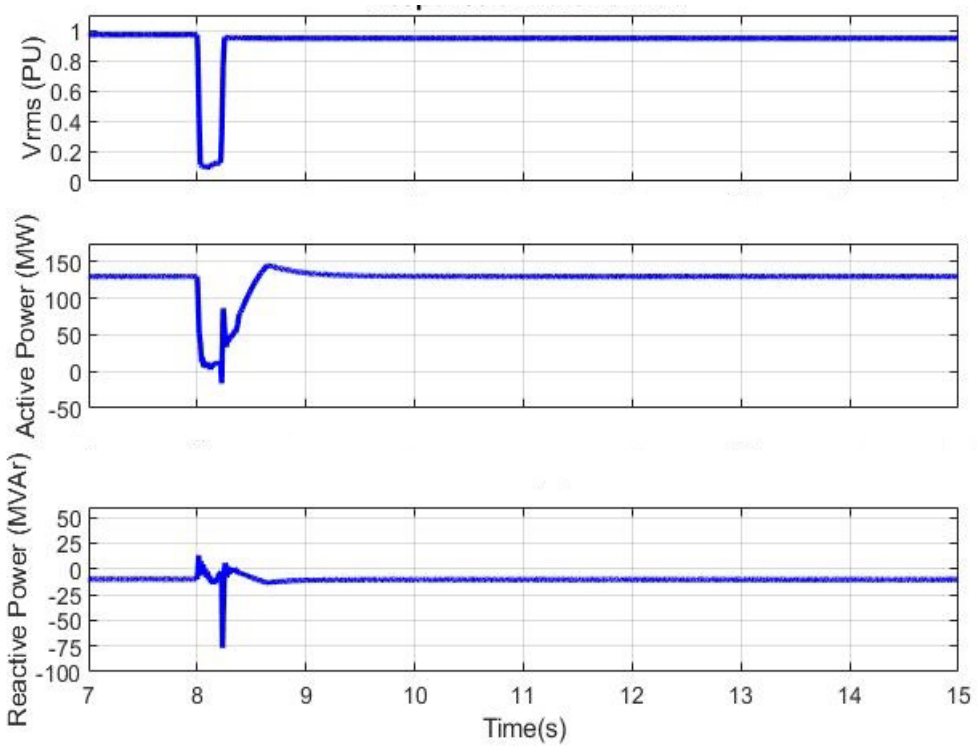

Figure 4.10: Response of WF E in Scenario 3.

Scenario 4: Network outage condition with a BESS system controlled as a 50 MVA Virtual Synchronous Machine (VSM)

The synchronous condenser of Scenario 3 was replaced by a comparable VSM, implemented on a Battery Energy Storage System (BESS). Simulation results shown in, Figure 4.11, Figure 4.12, and Figure 4.13 show that the wind plants and the system can recover successfully following the fault clearing. The close comparison of simulation results of the scenario with VSM (scenario 4) and the scenario with the synchronous condenser (Scenario 3) further validate the proposed VSM concept and its mathematical implementation in PSCAD/EMTDC software. The simulation results also verify the effectiveness of the VSM approach to mitigate stability issues of power electronic interfaced generation, when operating at weak grid locations.

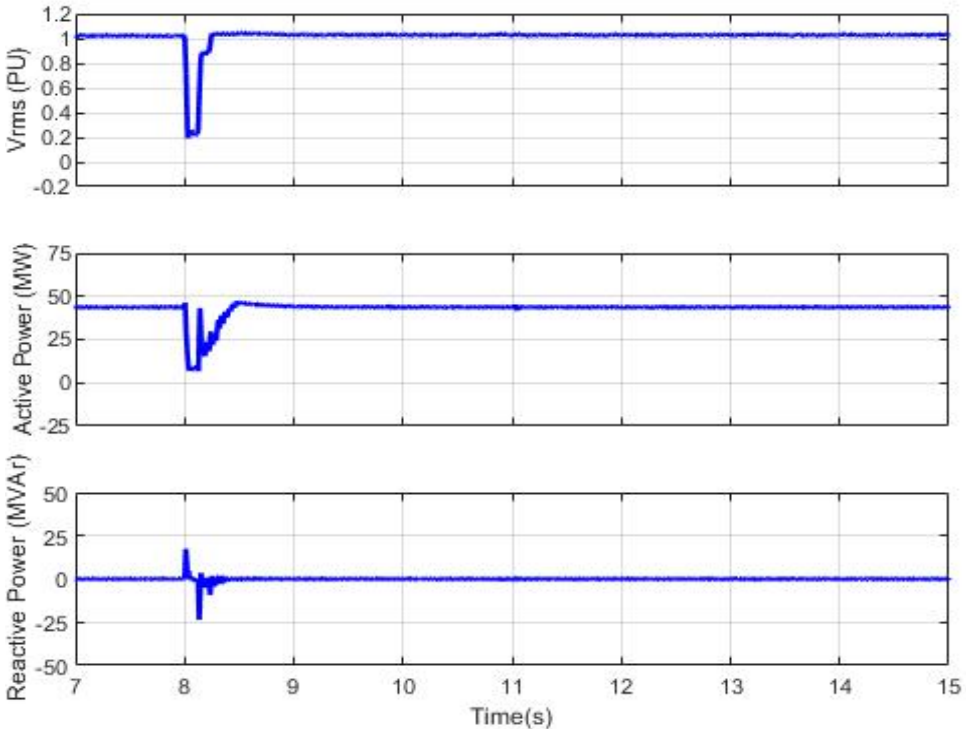

Figure 4.11: Response of WF A in scenario 4.

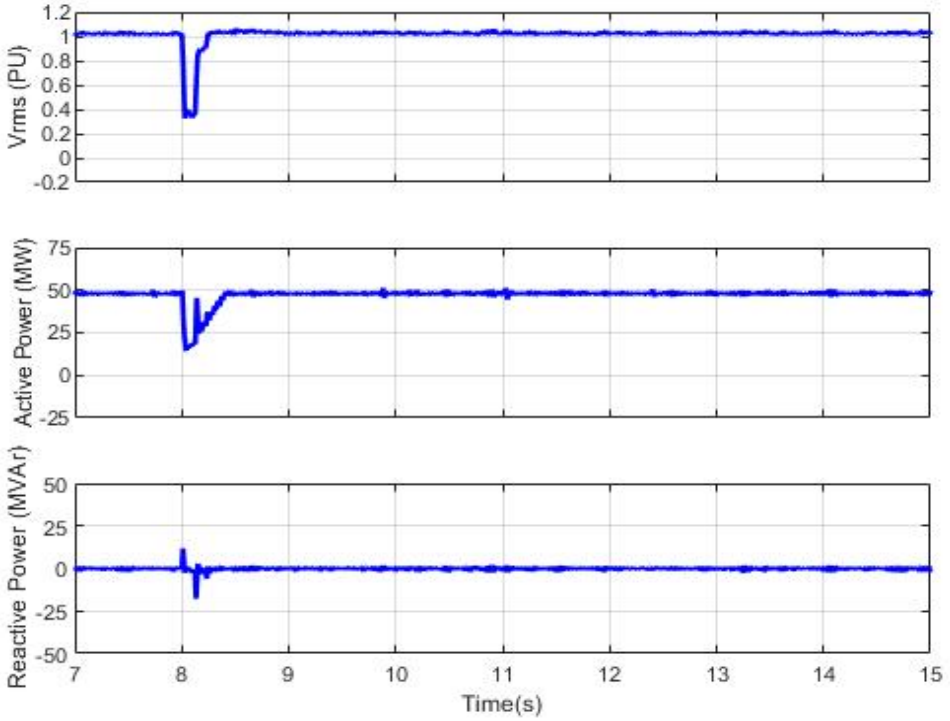

Figure 4.12: Response of WF B in Scenario 4.

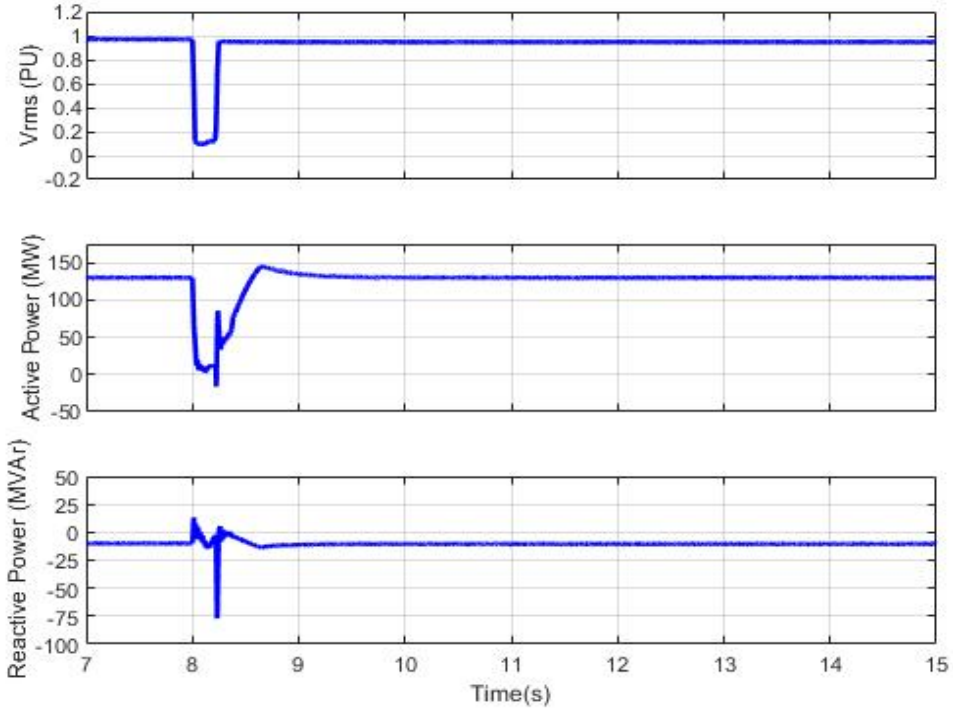

Figure 4.13: Response of WF E in Scenario 4.

The proposed Virtual Synchronous Machine (VSM) concept delivers system-wide benefits that go beyond immediate local improvements, as demonstrated in the research. Integrating the VSM approach into the broader European high-voltage network enhances overall system stability and resilience, even under challenging scenarios like network outages or the decommissioning of conventional synchronous generators.

4.1. Summary of Contribution

The integration of renewable energy into power systems presents significant challenges, particularly in weak grid locations where system stability is compromised. Conventional VSM methods have predominantly focused on grid-forming applications within isolated or microgrid networks, leaving a gap in their applicability to large-scale transmission systems. The investigations carried out in this chapter address this limitation by extending the VSM concept to transmission-level networks, with a focus on improving stability in scenarios of low system strength and high renewable energy penetration. Using a practical transmission network model based on a segment of the European grid, the proposed grid-following VSM approach demonstrates its ability to emulate the dynamic response of a synchronous machine. The results demonstrate its potential to enhance system stability and offer a novel solution for renewable integration challenges in weak transmission systems. This contribution bridges the gap in the literature, which previously lacked studies focused on VSM applications for large-scale transmission networks.

Based on the investigations carried out in this chapter, a journal paper titled "A Novel Virtual Synchronous Machine Implementation and Verification of Its Effectiveness to Mitigate Renewable Generation Connection Issues at Weak Transmission Grid Locations" was published in IET Renewable Power Generation, vol. 17, no. 10, pp. 2436-2457, 2022.

Chapter 5: Application of the VSM Approach to Control a Solar PV System

The VSM strategy illustrated in Figure 3.1 was implemented on a solar PV model in PSCAD/EMTDC transient simulation platform. The overall solar PV plant model consists of the main components shown in Figure 5.1. It should be noted that the inverter's current references (outputs of the VSM Emulator) are derived based on a real power and voltage input commands. Thus, it is important to design a Maximum Power Point Tracking (MPPT) controller to maintain a constant DC bus voltage during operation. A DC chopper circuit was also implemented to protect the inverter components from exposure to excessive DC-side overvoltage.

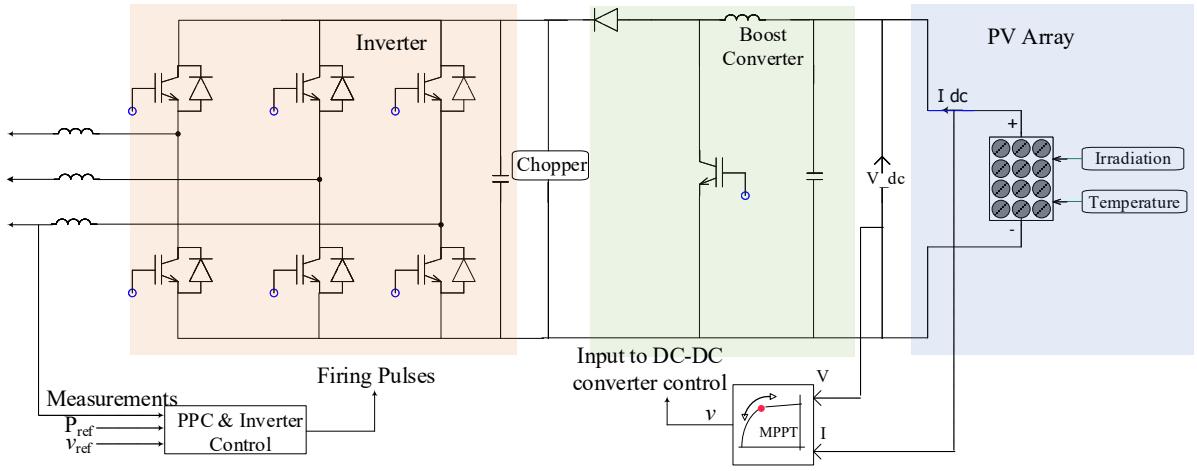

Figure 5.1: Main components of a solar PV plant.

The transmission test system shown in Figure 5.2 (network data as provided in Appendix A) is used to demonstrate the effectiveness of adopting the VSM concept to control a solar PV for improved power system stability.

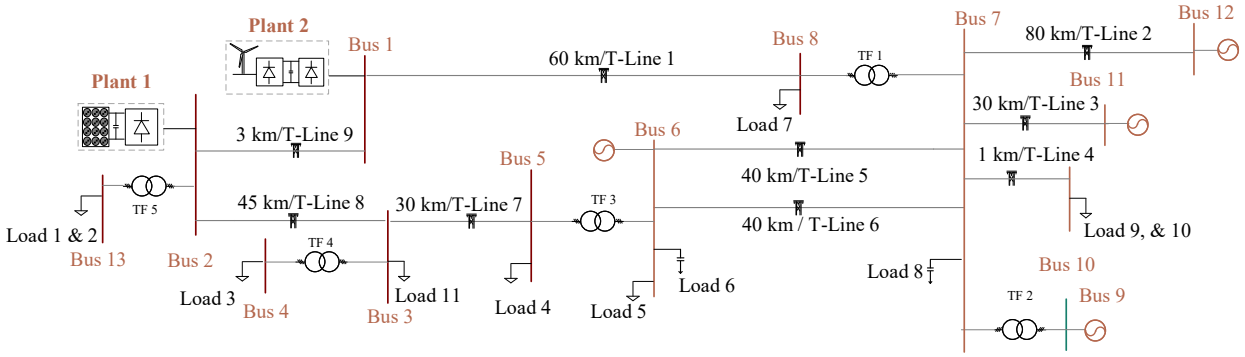

Figure 5.2: Transmission test system used for VSM performance verification.

The generation sources in the test system are as follows:

- Solar PV at Bus 2: 50 MW (Plant 1)
- Wind power plant at Bus 1: 70 MW (Plant 2)
- Thermal generation at Bus 6: 50 MVA

The VSM concept was implemented in a solar PV plant connected at Bus 2 (Plant 1). The response of the system was tested for a three-phase-to-ground solid fault on the transmission line from Bus 1 to Bus 8. The fault is applied at t = 10 s and is cleared by tripping the line breakers 100 ms (for Bus 1) and 120 ms (for Bus 8) after the fault's inception. The calculated Short Circuit Level (SCL) at Bus 1 under normal operation is 166 MVA (SCR of around 2.2 considering only the Wind farm). When the line from Bus 1 to Bus 8 is tripped, the SCL drops to around 73 MVA (SCR of around 1 considering only the Wind farm). This represents a 'weak system' condition at the POI for Plant 2 (and also for Plant 1).

Four control approaches were utilized to control the solar PV plant to investigate the stability of the system under a selected fault condition and to verify the performance of the VSM concept:

1. Control approach 1 - The solar PV plant inverters are controlled using reference signals generated based on a typical grid-following implementations shown in Figure 2.2.

2. Control approach 2 - The solar PV plant was replaced with a synchrous generator rated at 50 MVA.
3. Control approach 3 - The solar PV plant inverters were controlled based on the VSM implementation depicted in Figure 3.1.
4. Control approach 4 - Half of the inverters of the PV plant were controlled using VSM strategy and the other half of the inverters were operated based on typical grid-following implementations shown in Figure 2.2.

Control approach 1:

In this test, the solar PV plant inverters are controlled using reference signals generated based on a typical grid-following implementation. With this approach, the wind and solar PV plants were not able to ride through the fault if the output of Plant 2 was over approximately 50 MW. Figure 5.3 and Figure 5.4 show the response of Plant 2 and Plant 1 when the wind farm (plant 2) output is 50 MW. The responses of both PV plant and the wind farm are stable.

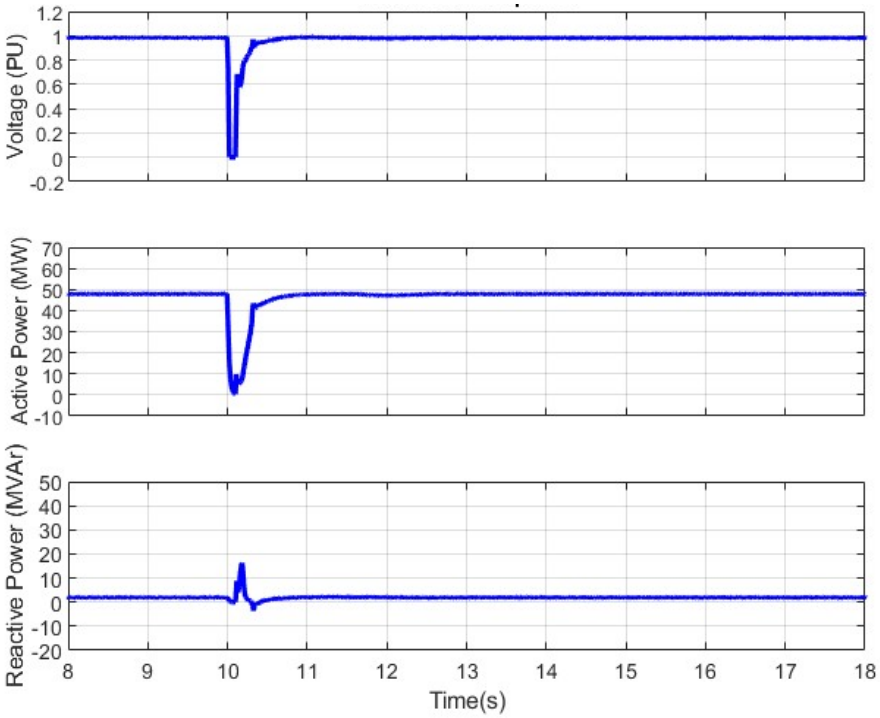

Figure 5.3: Response of plant 2: Wind farm output is 50 MW, and the solar PV output is 25 MW.

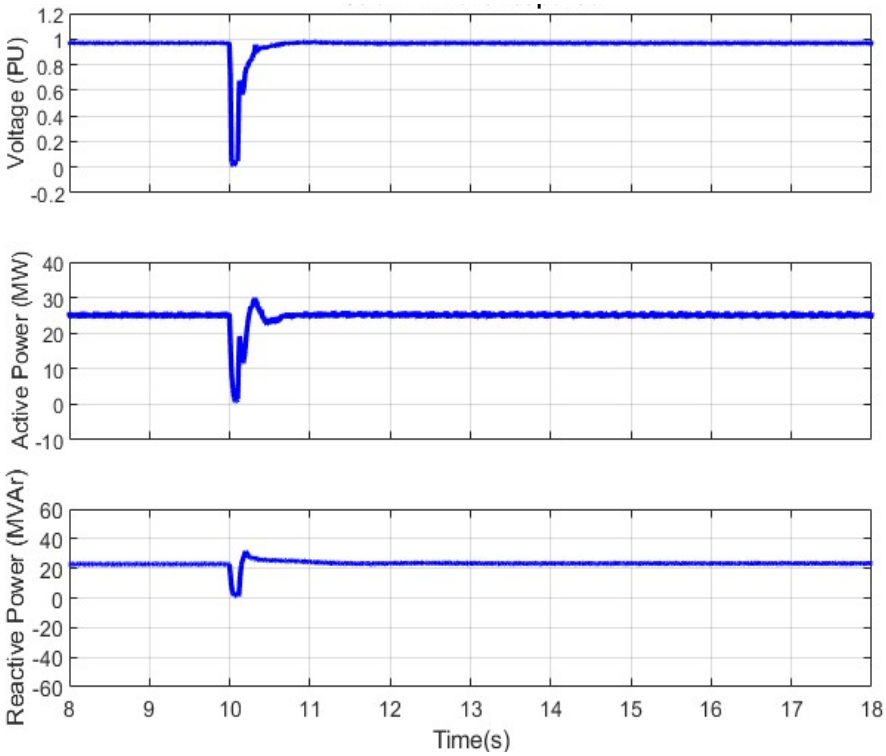

Figure 5.4: Response of plant 1: Wind farm output is 50 MW, and the solar PV output is 25 MW.

Figure 5.5 and Figure 5.6 show the response of Plant 1 and 2 when the wind plant output is 75 MW. The response of both solar PV and the wind plant are not acceptable.

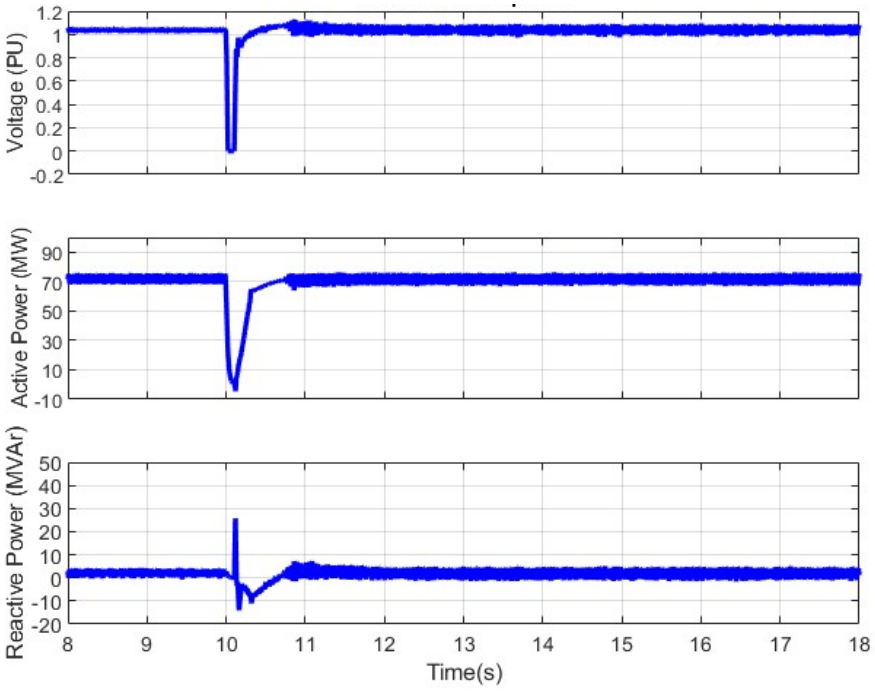

Figure 5.5: Response of plant 2: Wind farm output is 75 MW, and the solar PV output is 25 MW.

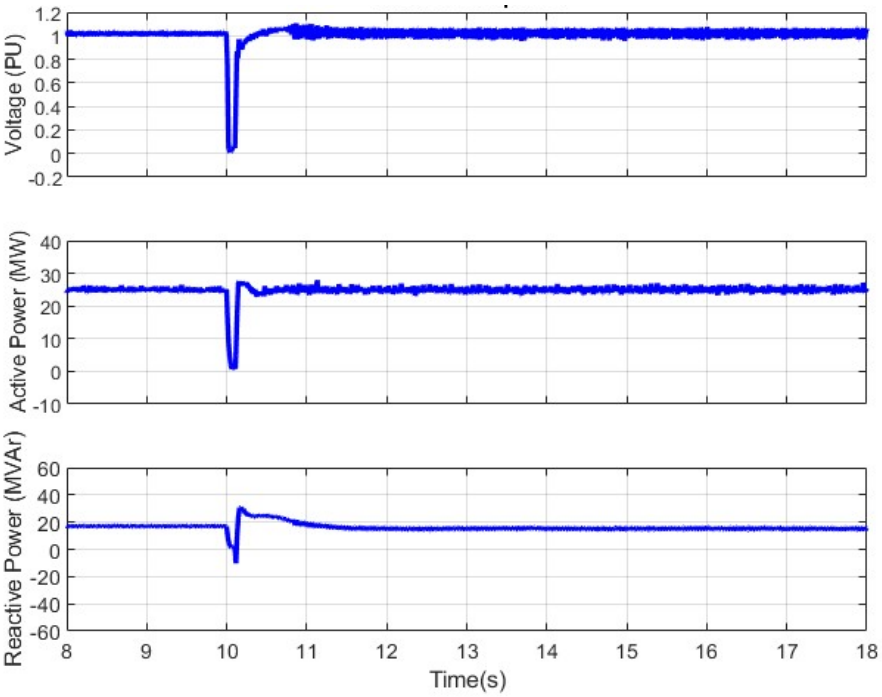

Figure 5.6: Response of plant 1: Wind farm output is 75 MW, and the solar PV output is 25 MW.

Control approach 2:

In this test, the solar PV plant was replaced with a synchrous generator rated at 50 MVA (connected to Bus 2). The synchronous machine improved the system's short circuit strength as well as the inertial response in the area. As a result, the overall response becomes stable when Plant 1 produces 60 MW. Wind plant and the solar plant responses are shown in Figure 5.7, and Figure 5.8.

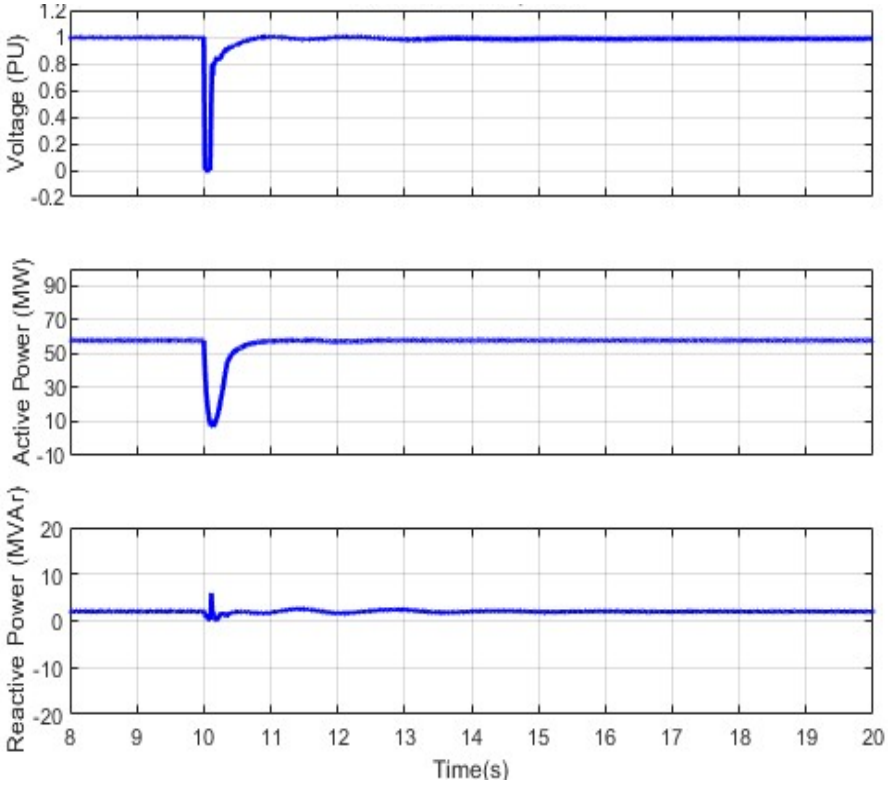

Figure 5.7: Response of plant 2: Synchronous machine is connected to Bus 2 (50 MVA unit dispatch level set to 40 MW).

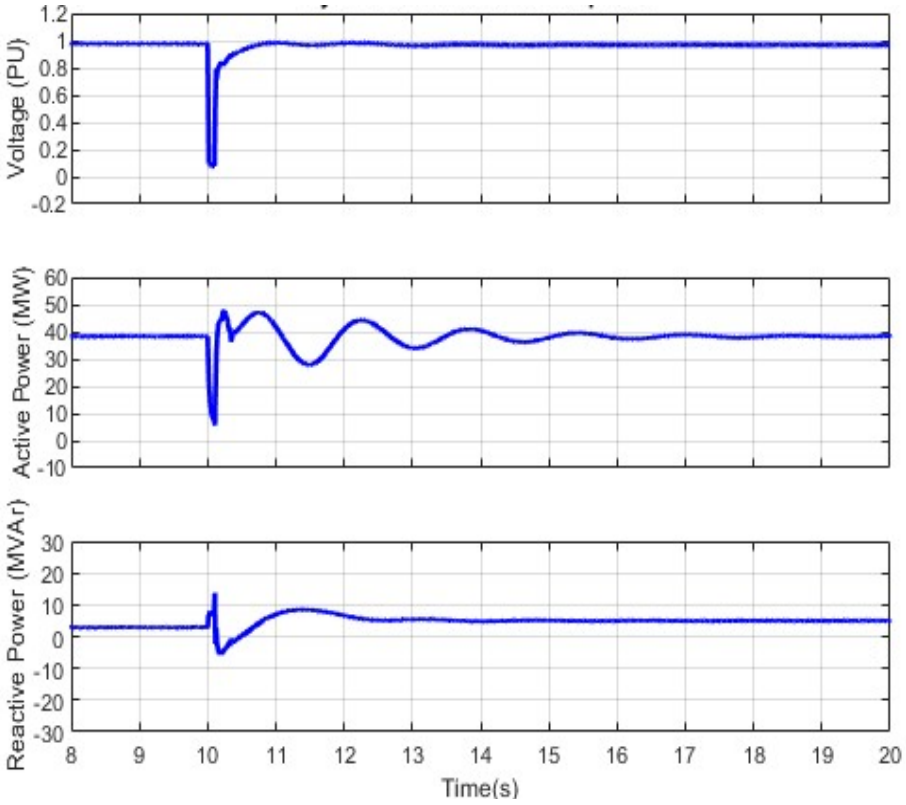

Figure 5.8: Response of synchronous machine: Synchronous machine is connected to Bus 2 (50 MVA unit dispatch level set to 40 MW).

Control approach 3:

In this test the solar PV plant inverters were controlled based on the VSM implementation depicted in Figure 3.1. The VSM (and hence the PV plant) rating was set to 50 MVA. The inverter current was limited to 1.1 pu of the inverter rating in order to ensure that inverter current ratings were not violated. Figure 5.9 and Figure 5.10 indicate a stable response.

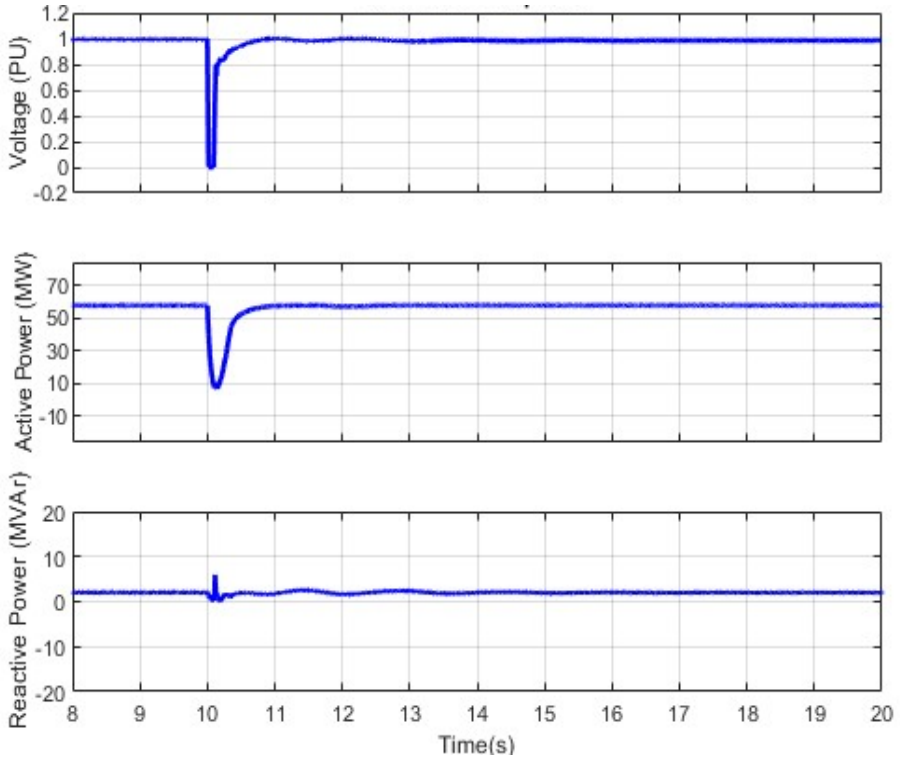

Figure 5.9: Response of plant 2: Solar PV inverter is controlled as a VSM.

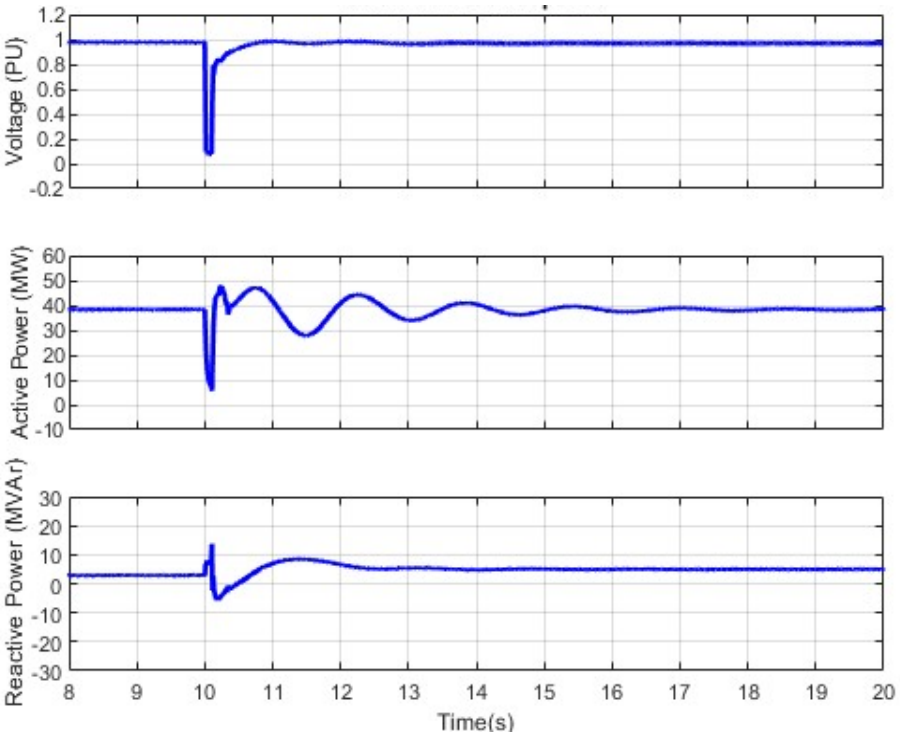

Figure 5.10: Response of plant 1: Solar PV inverter is controlled as a VSM.

Figure 5.11 and Figure 5.12 show a comparison of control approach 2 (Synchronous generator of 50 MVA at Bus 2) and control approach 3 (Solar PV plant of 50 MVA, controlled as a VSM at Bus 2) test's responses. The close comparison of responses further validates the VSM implementation and its effectiveness to improve stability.

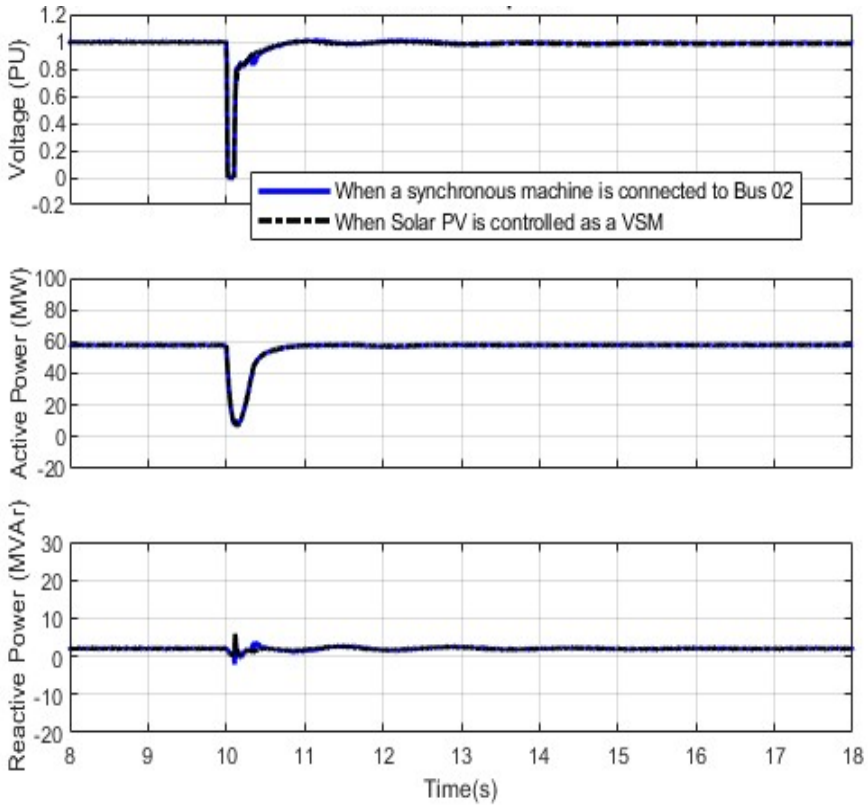

Figure 5.11: Response of plant 2: VSM–Synchronous generator comparison.

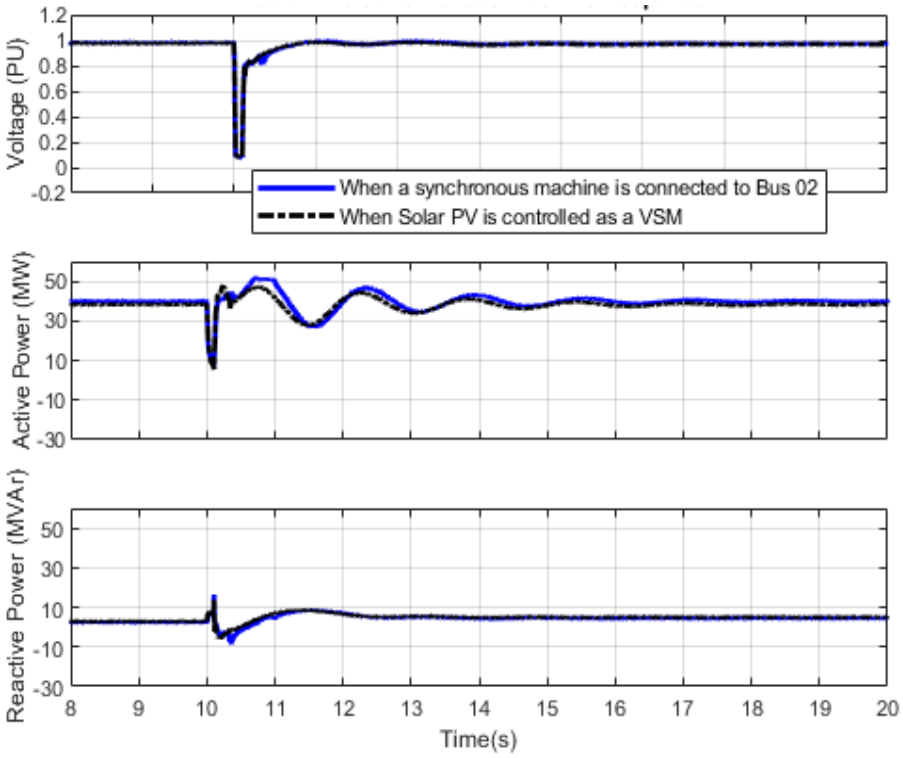

Figure 5.12: Response of plant 1: VSM–Synchronous generator comparison.

As an extension of 'control approach 3' the wind farm power output was increased to approximately 75 MW. The response is now stable as seen from results in Figure 5.13 and Figure 5.14.

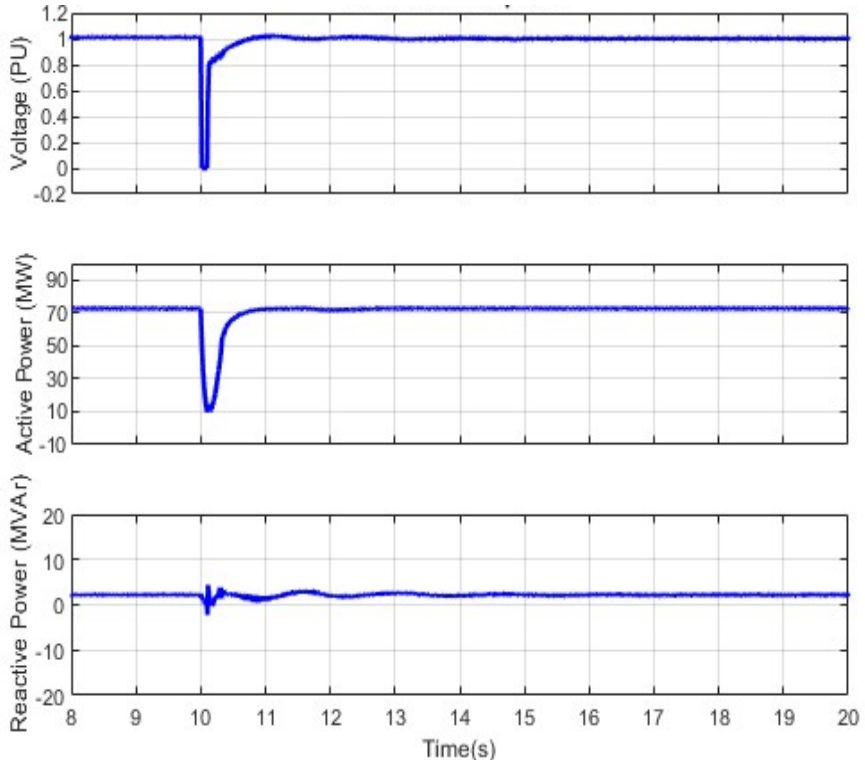

Figure 5.13: Plant 2 response: Solar PV inverter is controlled as a VSM. Wind farm power is set to 75 MW.

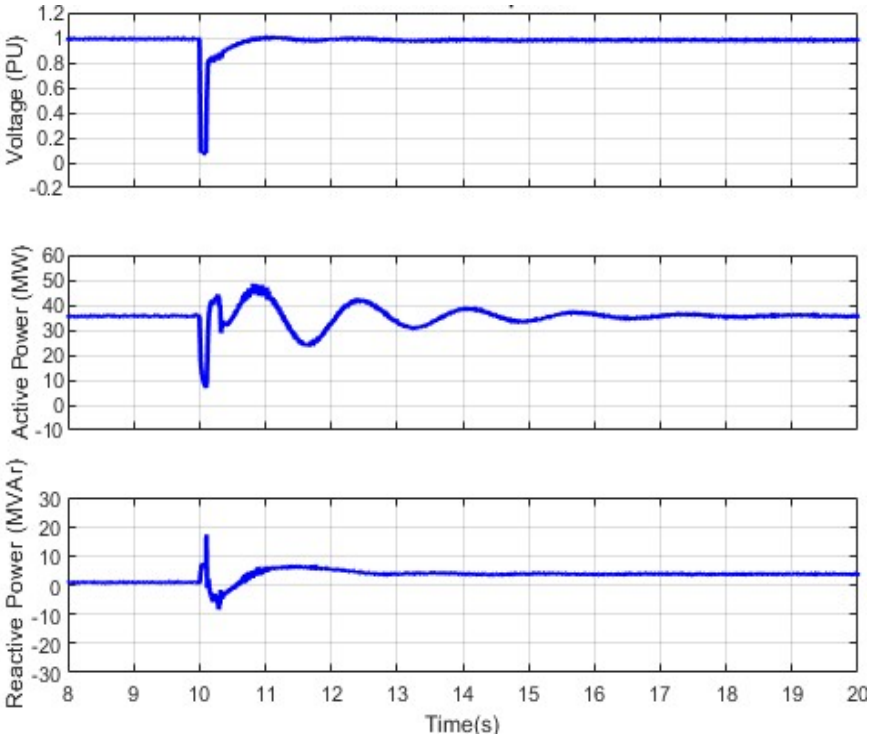

Figure 5.14: Plants 1 response: Solar PV inverter is controlled as a VSM. Wind farm power is set to 75 MW.

To evaluate the inertia emulation capability of the VSM control strategy, the operating conditions described in Scenarios 1 and 3 were considered. A 45 MW load was added to Bus 2 of the practical transmission test system (see Figure 5.2) at 10 seconds. The resulting frequency response at Bus 2 was recorded for scenario 1 and 3 and is presented in Figure 5.15.

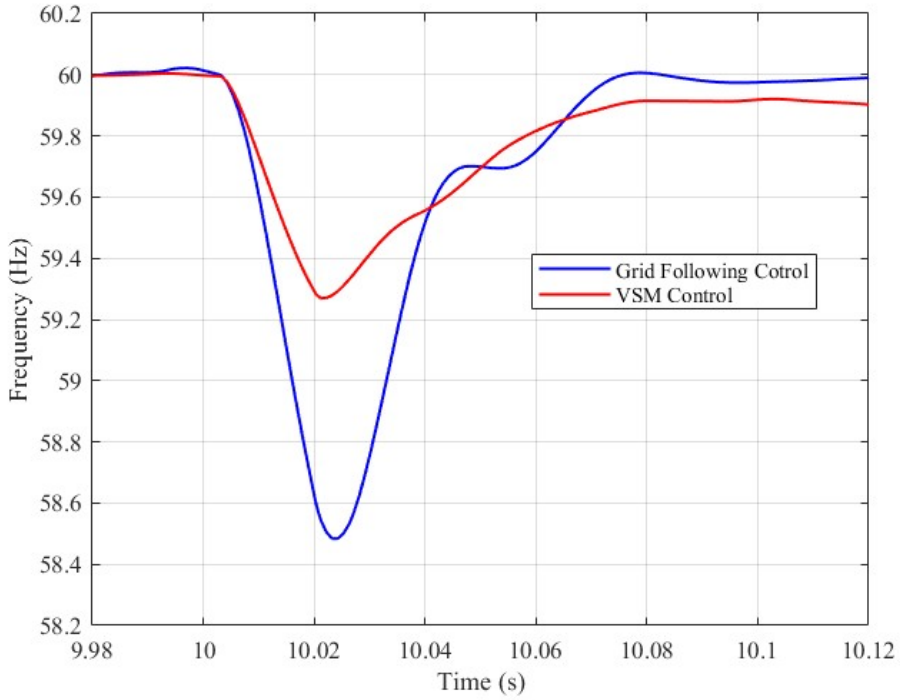

Figure 5.15: Frequency response comparison of the solar PV system operating in grid-following mode and Virtual Synchronous Machine (VSM) mode.

The simulation results demonstrate that the proposed VSM approach effectively emulates inertia, enhances frequency stability, and improves the dynamic response of inverter-based resources (IBRs).

5.1. Hybrid Method Taking Advantage of VSM Characteristics and Fast-Acting Response of a Typical Grid-Following Inverter

While typical IBRs do not provide inertial support to the grid, they do provide a number of superior characteristics compared to the dynamic response of a synchronous machine. These

include features such as fast reactive power injection and fast frequency control. Thus, there could be advantages in selecting a hybrid approach.

Control approach 4:

In order to demonstrate one such possibility, the VSM strategy was implemented in only half of the inverters of plant 1. The remaining inverters were designed as normal grid-following units with a control strategy as shown in Figure 2.2. The simulation results show that the system can recover from a three-phase-to-ground fault on the line from Bus 1 to Bus 8 when Plant 2 is producing 60 MW. The simulation results for the 'hybrid' case are shown in Figure 5.16 and Figure 5.17.

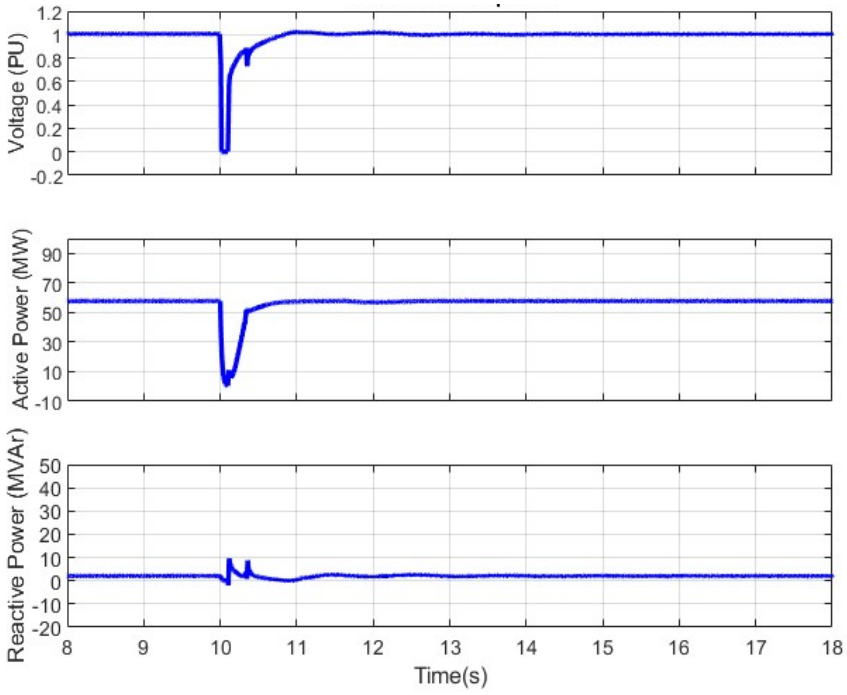

Figure 5.16: Plant 2 Response: Half of the inverters operate as a VSM, and half of the inverters operate conventionally.

This is an important finding as the fast voltage control features of an IBR plant can still be utilized (based on inverters operating on normal grid-following mode) to advantage while improving system inertial response (with part of inverters operating in VSM mode).

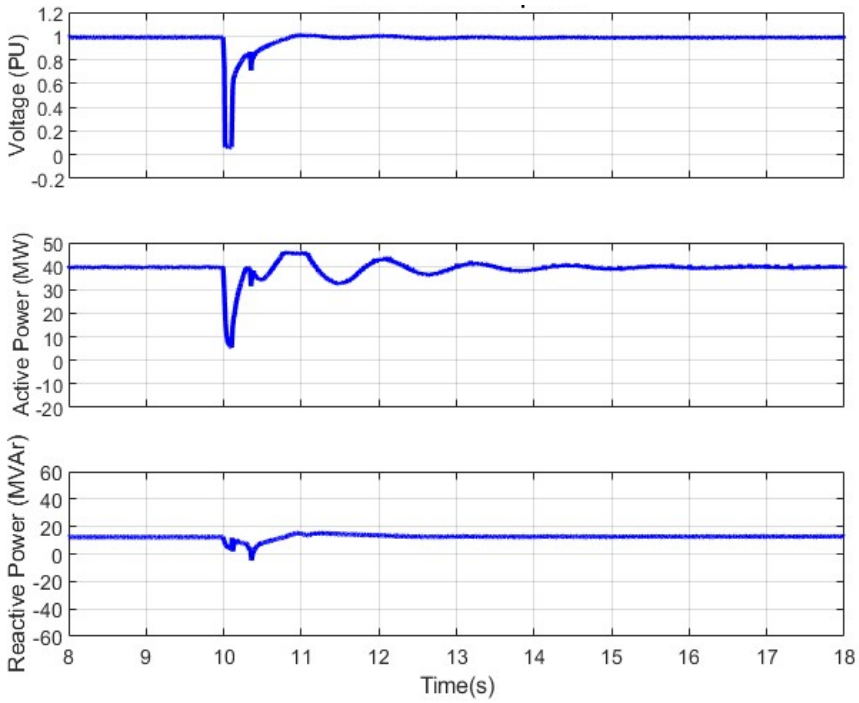

Figure 5.17: Plant 2 Response: Half of the inverters operate as a VSM, and half of the inverters operate conventionally.

5.2. Summary of Contribution

In this chapter, the VSM approach was applied to solar PV plant inverters, demonstrating significant improvements in system stability, particularly under weak grid conditions. The investigations revealed that the proposed VSM method effectively mitigates technical challenges such as fault recovery issues and unstable oscillations, which are common in networks with high levels of renewable energy integration.

Additionally, this chapter introduces a hybrid control method that integrates the advantages of grid-following and VSM-based controls. This innovative approach can be readily extended to hybrid systems combining solar PV and battery storage. By enhancing the resilience and stability of transmission networks with high renewable energy penetration, this method addresses some of the most pressing challenges in modern power systems, offering a robust and scalable solution for future grid operations.

Based on the investigations carried out in this chapter, a research paper titled "Application of the Virtual Synchronous Machine Approach to Control a Solar PV Power Plant for Improved System Stability" was presented at the CIGRE Canada Conference & Exhibition, Vancouver, BC, Canada, September 25–28, 2023.

Chapter 6: Performance Testing of a Solar PV System Controlled as a Virtual Synchronous Machine to Verify Grid Code Compliance

This chapter presents a comprehensive analysis of the functional response verification of an inverter operating as a VSM in grid-following mode. The proposed VSM control strategy addresses critical technical challenges associated with integrating IBRs into weak power grids. Modern grid codes outline essential performance requirements of IBRs, including voltage regulation, reactive power support, frequency control, and resilience during grid disturbances. An EMT-based testing procedure (generally referred to as Model Quality Tests or MQT) of a 50 MVA solar PV plant controlled as a VSM is presented. These tests ensure accurate model representation and IBR's compliance with regulatory standards. Furthermore, this chapter explores the adaptability of VSM controls in delivering essential functional features, such as inertial and fast frequency response, to enhance grid stability and operational efficiency. The test results highlight the ability of inverters operating as VSMs to meet essential grid code requirements, thereby enabling the reliable integration of renewable energy sources into power systems and supporting the transition toward sustainable energy.

6.1. Model Quality and Grid Compliance Tests

Modern grid codes are designed to ensure secure and efficient operation of power systems by addressing specific connection requirements for renewable plants, often imposing standards comparable to conventional power plants. Key mandates include voltage and reactive power

regulation, low voltage ride-through (LVRT) compliance, adherence to specifications during disturbances, and frequency control.

To ensure grid stability with increasing integration of IBRs, system operators require rigorous EMT-based MQTs before connection. These tests validate the accuracy of IBR models and their compliance with regulatory standards. Specifically, MQTs are designed to ensure that plant models are robust and compliant with system operator's requirements, including model guidelines, the grid code, and industry's best practices. These tests verify that the models accurately represent plant response across a range of operating conditions, meet minimum dynamic response requirements, and can be readily integrated into the national power system network model for planning, operation, and connection studies. Typically, both RMS and EMT models are evaluated. It is important to note that MQT acceptance does not constitute final plant design compliance or complete model validation, as models will be refined based on design modifications and field tests during commissioning. At a minimum, the required tests will be performed with the plant model connected to a simplified representation of the external system network, typically using a single machine-infinite bus configuration (see Figure 6.1).

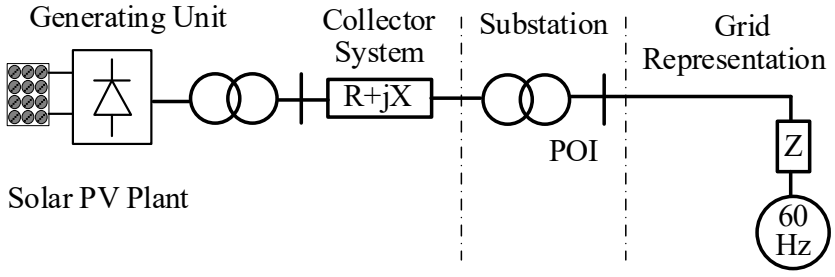

Figure 6.1: Test setup for plants with grid substation (POI: point of interconnection).

Performance requirements for some MQTs are mandated by system operators and are documented in publications such as AEMO [13], IEEE 2800 [14], and NSPI [15]. Similar tests are generally adopted industry wide. In this chapter, the steady-state and transient responses of the PV

plant model (shown in Figure 6.2) when controlled as a VSM are investigated. Specifically, the following conditions are addressed.

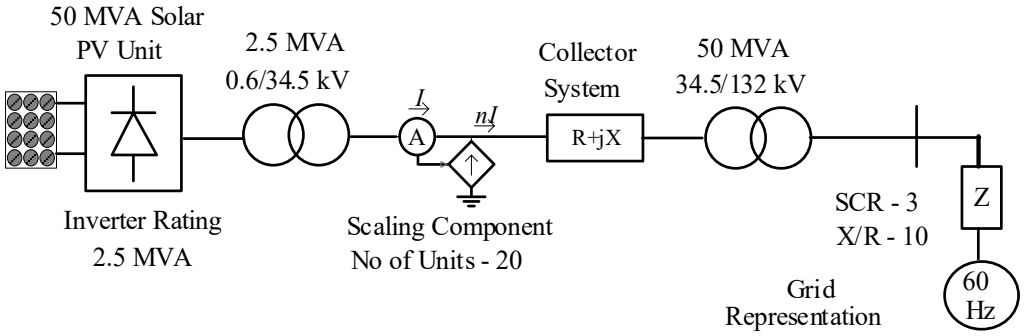

Figure 6.2: The solar PV test set up used to conduct MQTs.

The active power limit and the reactive power limits of the solar PV plant are set to 0.8 pu (about 40 MW), and +/- 0.75 pu (about 37.5 MVAr), respectively. The positive-sequence resistance, inductive reactance, and the capacitive susceptance of the collector system are 0.002019, 0.002306, and 0.01962 (pu/m) on a 100 MVA and 34.5 kV base.

6.1.1. Steady-state operation

In this test stable operation at full power and unity power factor under a range of system SCR conditions is assessed. This test verifies the plant's ability to deliver maximum power across varying SCRs. As low SCR conditions present the greatest challenge for inverter-based resources, the results shown in Figure 6.3 are for an SCR of 3. For comparison, a conventional PV plant using grid-following controls typically requires careful tuning to operate reliably below an SCR of 3. The results show the expected response.

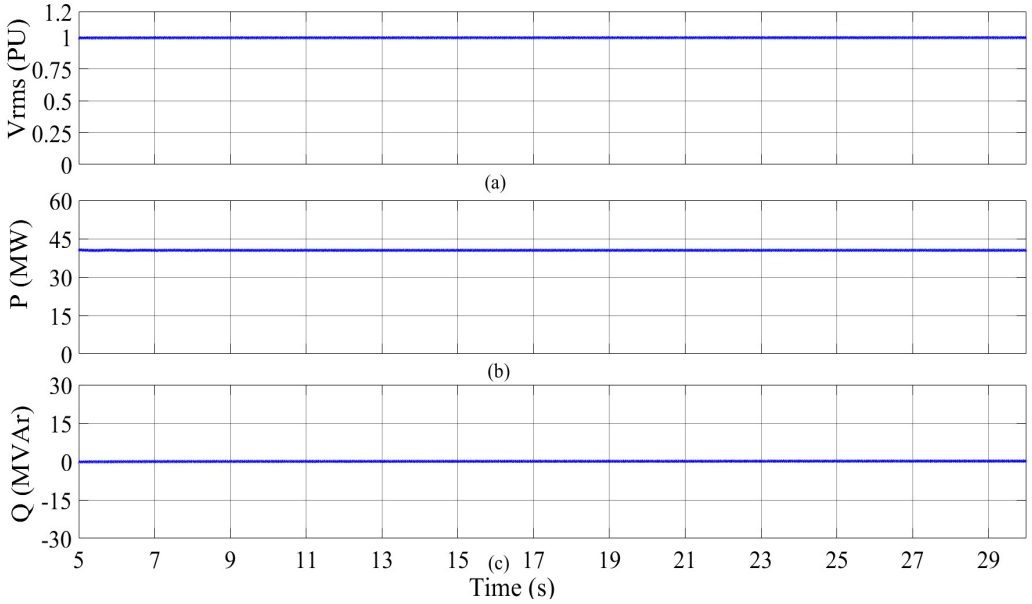

Figure 6.3: Plant response (a) voltage, (b) active power, (c) reactive power - Flat run test.

6.1.2. Steady-state operation under full power and leading power factor

For this test, the voltage at the POI is normally maintained at 1 pu. However, depending on the transformer impedance and collector system characteristics, adjusting the transformer taps may be necessary to keep the inverter's terminal low voltage within the manufacturer's specified range. In this specific case, the MV- side transformer tap was set to 1.05 pu to ensure the LV side voltage remained below 1.1 pu. This test, therefore, not only verifies the inverter's steady-state capability but also validates the selected transformer tap range. Furthermore, if the inverter's reactive power capability is insufficient to meet the POI reactive power requirements, additional fixed or variable shunt capacitors may be required to comply with grid code requirements. The Figure 6.4 shows the expected response.

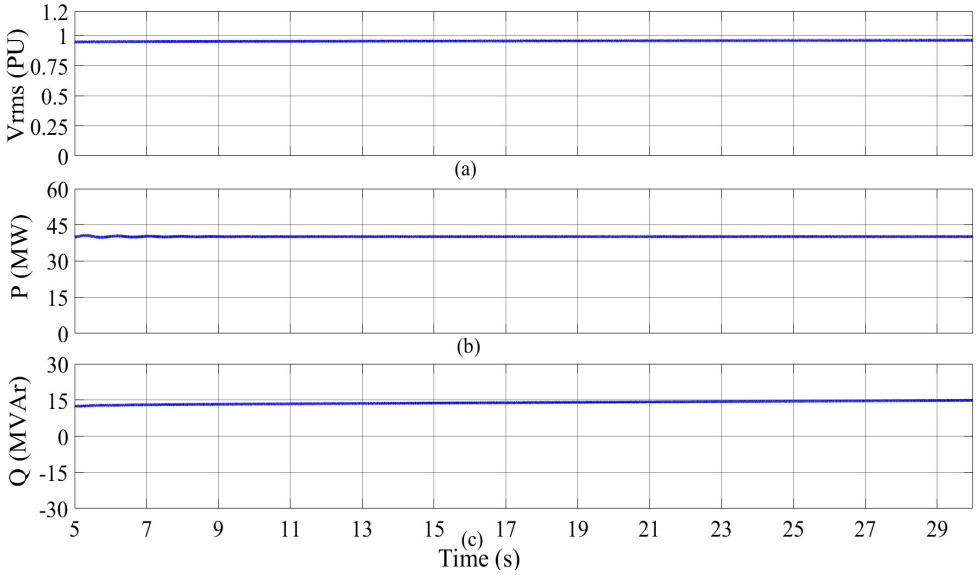

Figure 6.4: Plant response - Leading power factor test.

6.1.3. Steady-state operation under full power and lagging power factor

This test determines the required tap range of the main transformer and the need for additional shunt reactive equipment to meet the grid code. In this specific example, the MV- side transformer tap was set to 0.95 pu to maintain the LV-side voltage above 0.95 pu. The Figure 6.5 shows the expected response.

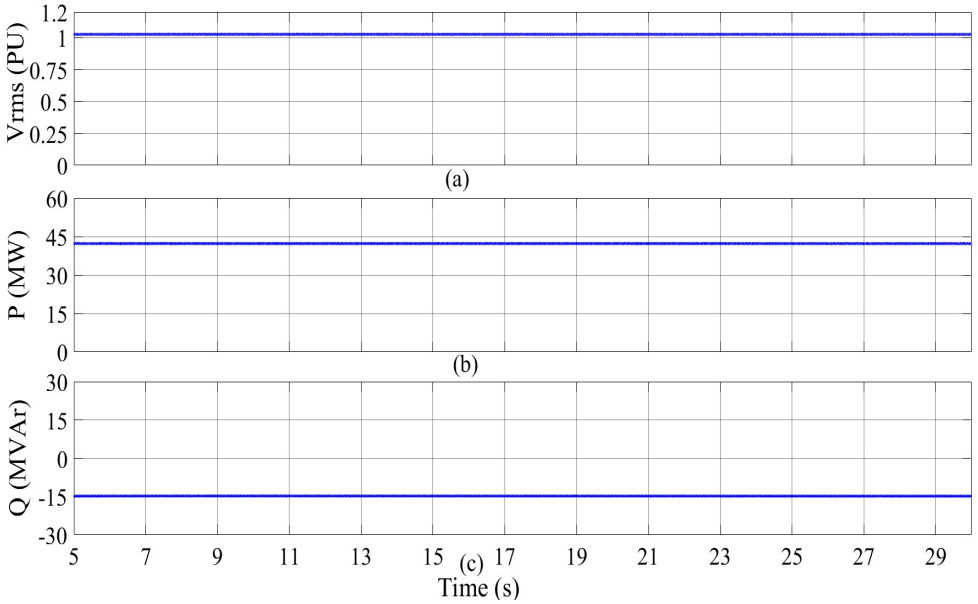

Figure 6.5: Plant response - Lagging power factor test.

6.1.4. Operation under low voltage condition (continuous)

Grid codes typically require inverters to remain connected if the voltage at the POI is above 0.9 pu. In this test the POI voltage was reduced to 0.9 pu. Figure 6.6 shows that the inverter remained connected supplying the rated power.

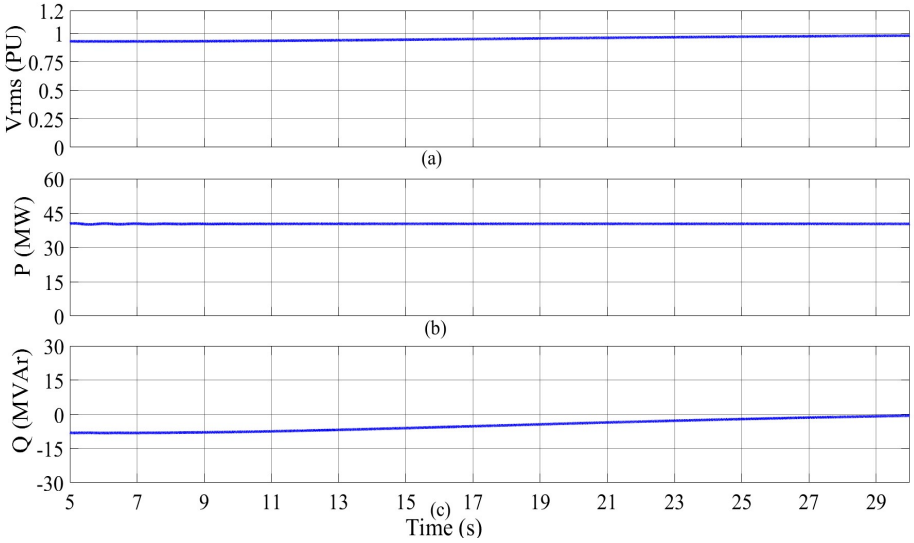

Figure 6.6: Plant response - Operation under low voltage test.

6.1.5. Operation under high voltage condition (continuous)

Typically, grid codes require the inverter to remain connected if the voltage at the POI is below 1.1 pu. The POI voltage was increased to 1.1 pu in this test.

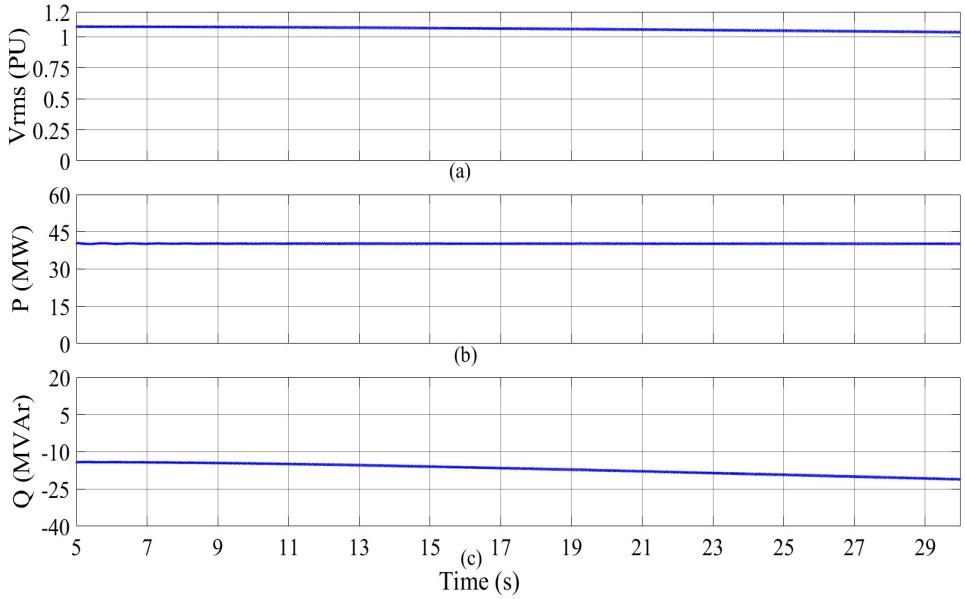

Figure 6.7: Plant response - Operation under high voltage test.

Figure 6.7 show that the inverter remained connected supplying the rated power and this is the expected response.

6.1.6. Operation at over-frequency conditions

In this test, the frequency was increased from 60 Hz to 61 Hz at a rate of 4 Hz/s. If an over-frequency response is required by the grid code, the active power output should decrease. The extent of the active power reduction is determined by the droop setting. The results shown in Figure 6.8 are as expected.

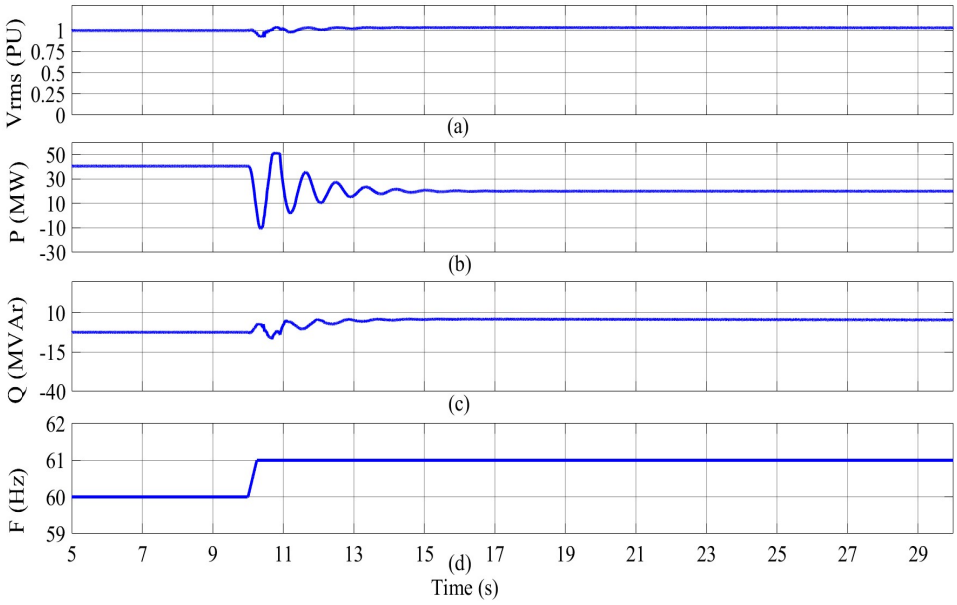

Figure 6.8: Plant response - Frequency step up test.

6.1.7. Operation under under-frequency conditions with headroom and verification of inertial response

In this test, the frequency was changed from 60 Hz to 59 Hz at a rate of 4 Hz/s. As required by grid codes for under-frequency response, the active power should increase. The test results (shown in Figure 6.9) demonstrate that the power output increased to the maximum rating of 40 MW from an initial operating value of approximately 36 MW. The magnitude of this active power increase is governed by a droop setting. To illustrate the VSM's inertial response, its performance is compared with that of a comparable synchronous machine. The observed difference in inertial response is expected due to the inverter current being limited by its rated capacity.

Beyond standard industrial model quality tests, additional tests are conducted to investigate the "un-curtailed inertia capacity" of the PV plant controlled as a VSM. In the tests shown in Figure 6.10, the VSM operates at 36 MW (with a 10% headroom), and its response is evaluated under three frequency drop scenarios: a drop to 59 Hz at a rate of 4 Hz/s, a drop to 59 Hz at a rate of 1 Hz/s, and a drop to 59.5 Hz at a rate of 4 Hz/s. Similarly, the tests depicted in Figure 6.11 examine

the VSM's response when operating at 20 MW (50% of its inverter's power rating) under the same frequency drop scenarios. In each scenario, the VSM's results are compared with the response of a comparable synchronous machine to demonstrate the VSM's inertial behaviour. The simulation results demonstrates that the inertial power injected to grid depends on four primary factors;

- The inverter's rated power capacity,
- Its pre-disturbance operating point,
- The magnitude of system frequency deviation during disturbances, and
- The rate-of-change-of-frequency (RoCoF).

This highlights the importance of considering these factors during the design stage to accurately determine the "un-curtailed inertia capacity" of the IBR.

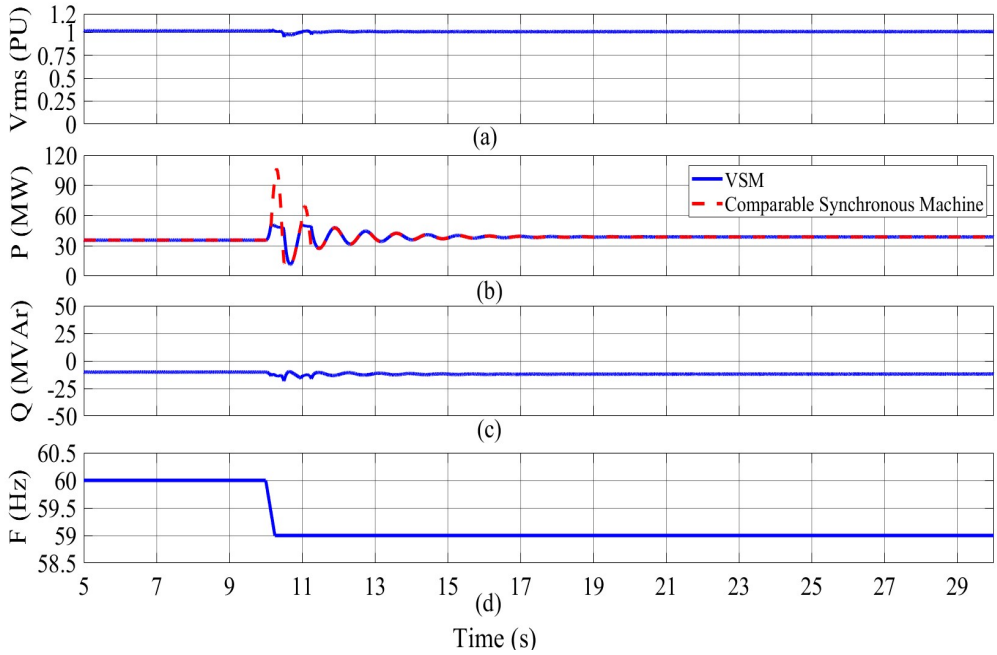

Figure 6.9: Plant response - Frequency step down test.

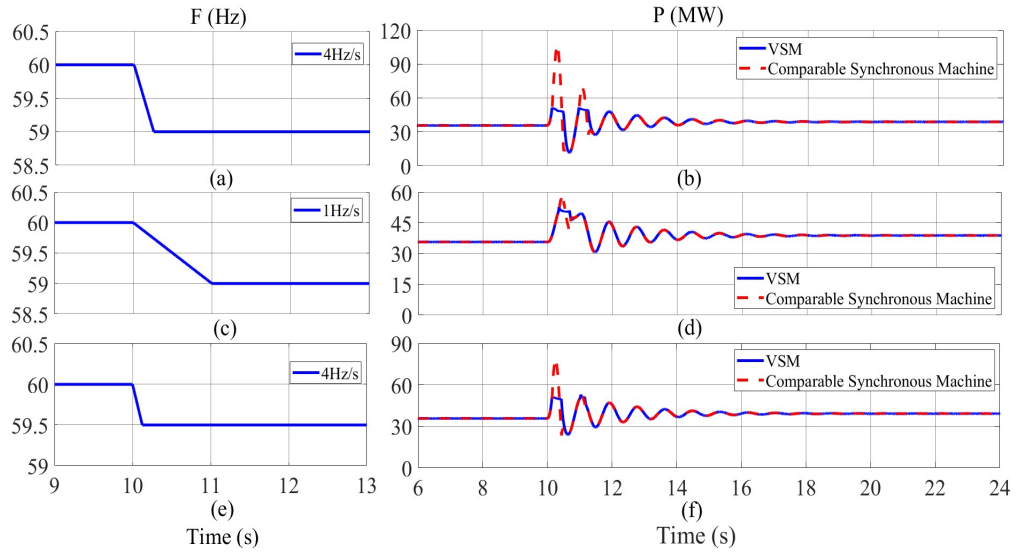

Figure 6.10: Plant response (full power) - Frequency step down (with different rate of changes) test.

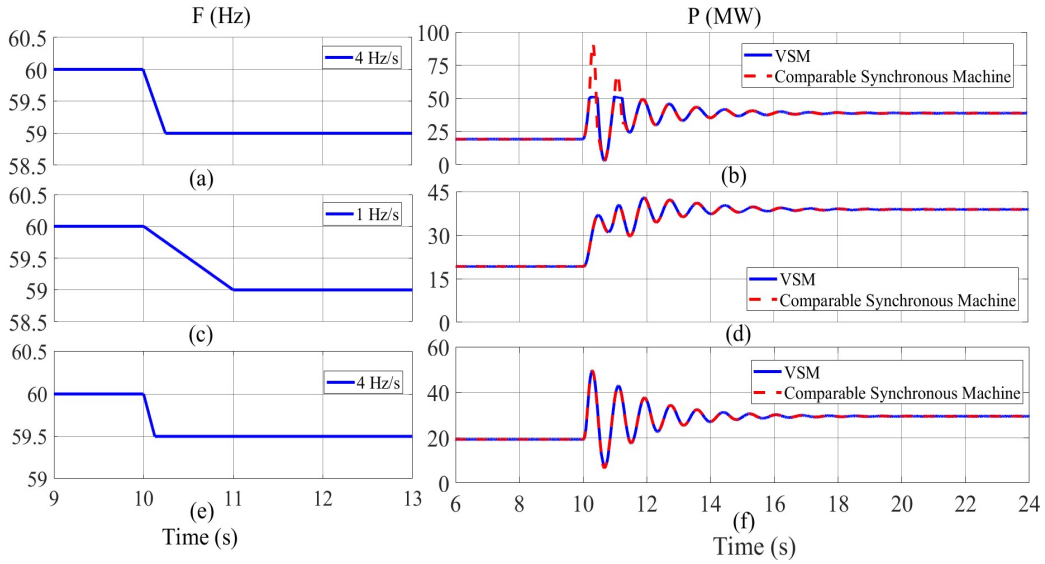

Figure 6.11: Plant response (Half power) - Frequency step down (with different rate of changes) test.

To further evaluate the effectiveness of the inertia emulation capability of the VSM control strategy, a 20 MW load was added at 6 seconds in the Solar PV SMIB test system (see Figure 6.2). The frequency response at the point of connection was recorded for both the VSM-controlled and the conventional grid-following-controlled solar PV. The simulation results are presented in Figure 6.12.

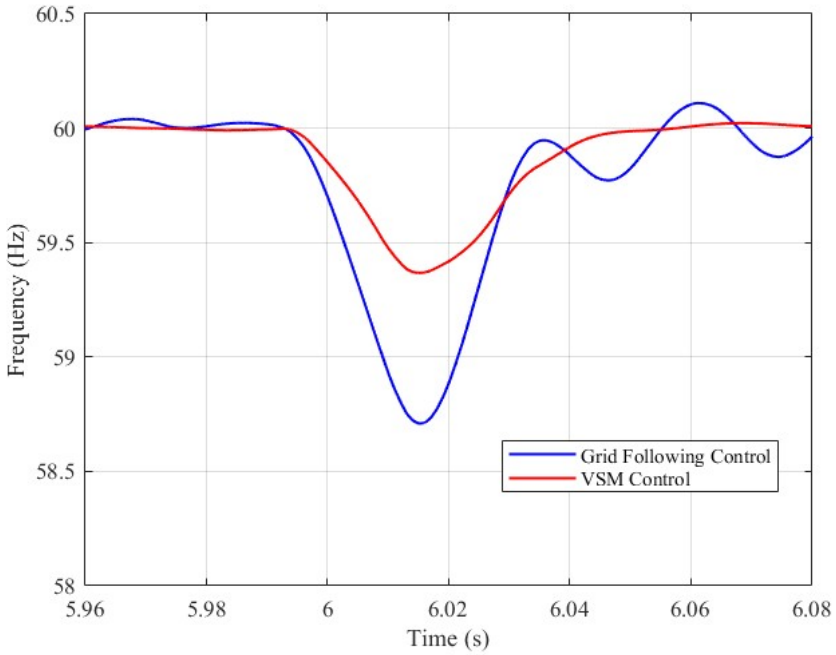

Figure 6.12: Frequency response comparison of the solar PV system operating in grid-following mode and Virtual Synchronous Machine (VSM) mode.

The simulation results demonstrate that the proposed VSM approach effectively emulates inertia, enhances frequency stability, and improves the dynamic response of the solar PV plant.

6.1.8. Response to voltage disturbances

6.1.8.1. Response to a voltage swell:

This test examines two reactive power operating modes: (i) voltage droop control mode and (ii) reactive power control mode. A voltage step from 1 pu to 1.1 pu is applied at the POI. In voltage droop control mode, the plant absorbs reactive power to provide voltage support. Conversely, in reactive power control mode, the plant maintains constant reactive power output despite the voltage change, as shown in the Figure 6.13.

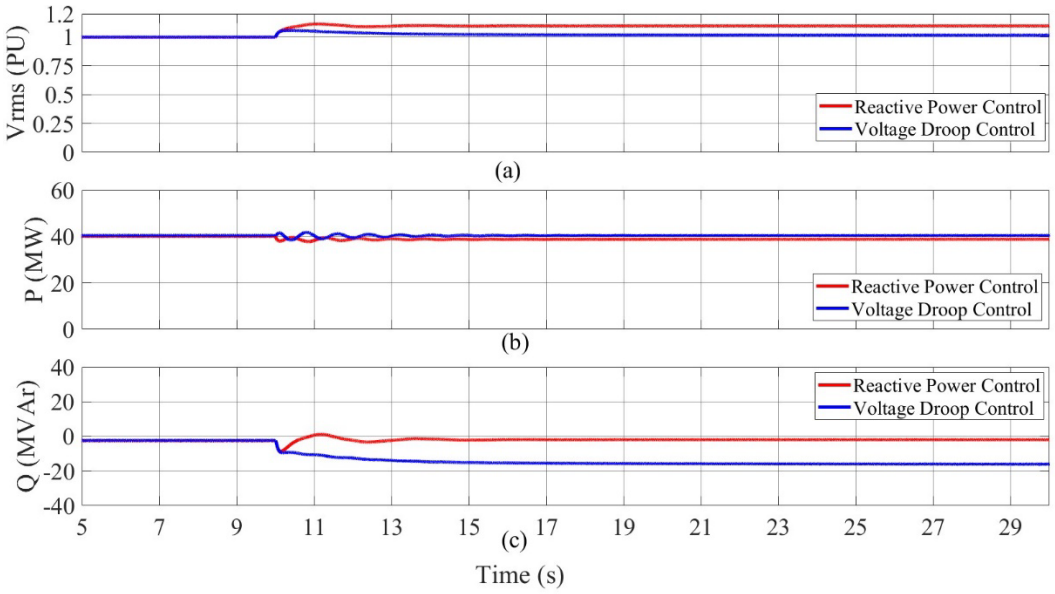

Figure 6.13: Plant response – Voltage step-up test.

6.1.8.2. Response to a voltage sag:

A voltage step is applied from 1 pu to 0.9 pu at the POI. In voltage droop control mode, the plant delivers reactive power to provide voltage control. Conversely, in reactive power control mode, the plant maintains a constant reactive power output despite the voltage change, as illustrated in the Figure 6.14.

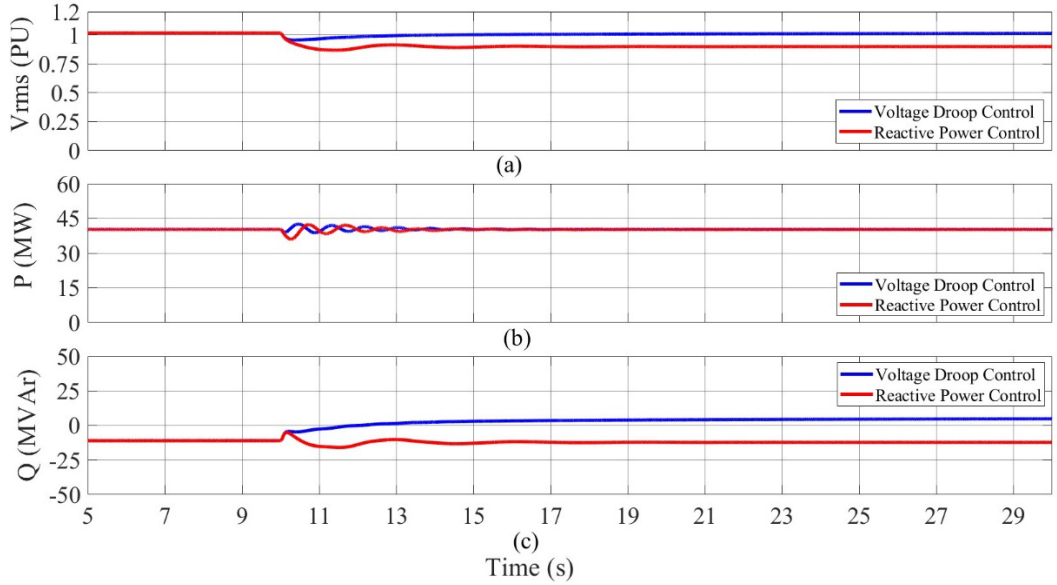

Figure 6.14: Plant response – Voltage step-down test.

6.1.8.3. Low-voltage ride-through (LVRT) response

The LVRT requirement is specified similarly to the HVRT profile. In addition, the LVRT response is also verified by testing the inverter's response following balanced and unbalanced faults. The response of the VSM following a balanced three-phase fault at the POI cleared in 0.12 seconds is shown in Figure 6.15.

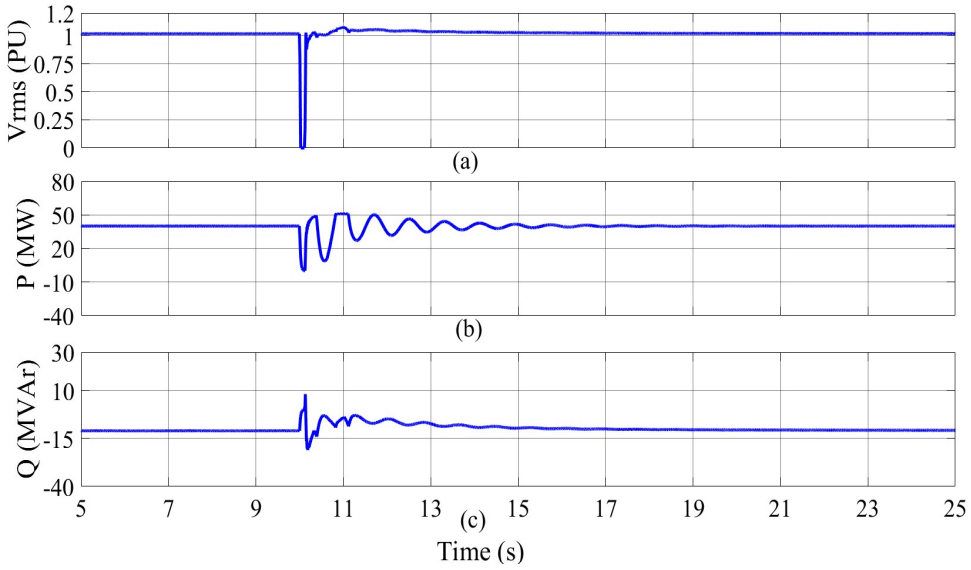

Figure 6.15: Plant response – Fault ride-though test.

6.1.8.4. High voltage ride-through (HVRT) response

Inverters are expected to remain connected for a specified duration during grid overvoltage conditions. This compliance is tested by applying a high voltage profile at the POI, as shown Figure 6.16. Simulation results are as expected.

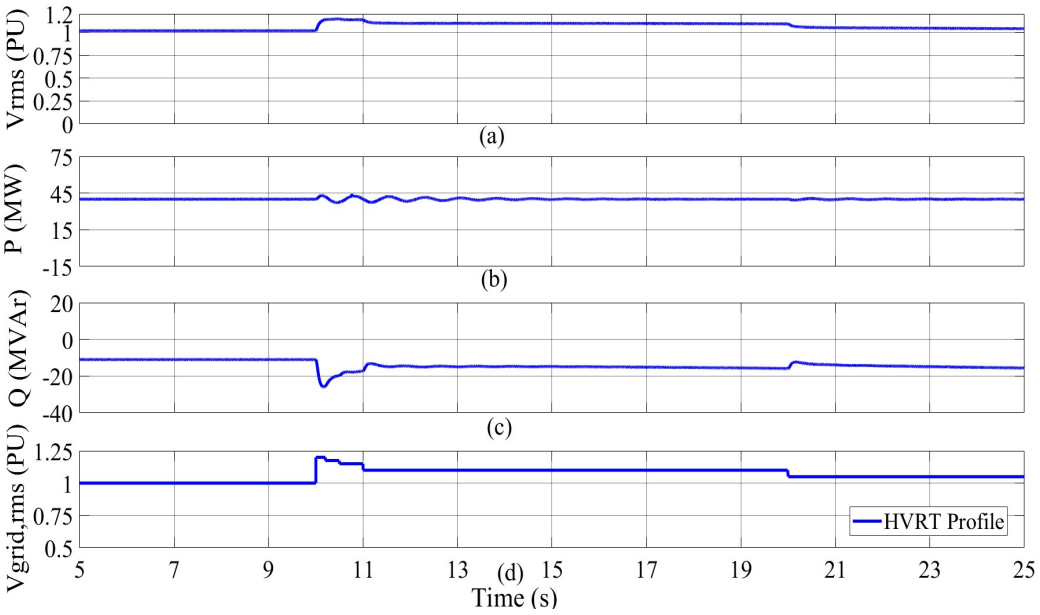

Figure 6.16: Plant response – HVRT Test.

6.2. Summary of Contribution

This chapter presented simulation-based tests that can be adopted to verify the performance of a grid-following solar inverter controlled as a VSM. Most tests described in this chapter are similar to those performed to test the compliance of normal grid-following inverters. The frequency step tests presented here must be performed specifically to verify the correct mimicking of a synchronous machine response. The frequency step response of the VSM is compared with the response of a comparable synchronous machine to verify the inertial response of the IBR. The close comparison of the response can be considered as validation of the VSM control design. However, it should be noted that there will be a difference between the response of the VSM and the comparable synchronous machine because of the current-limiting loops in an inverter control system. A detailed analysis was carried out to identify the factors that determine the inertial power that can be injected to the grid by an IBR of specific MVA rating. A concept of "un-curtailed inertia capacity" of an IBR is introduced.

Based on the investigations carried out in this chapter, a research paper titled “Performance testing of a solar PV system controlled as a virtual synchronous machine to verify grid code compliance," was presented in ACDC Global 2025 - 22nd IET International Conference on AC and DC Power Transmission, Birmingham, UK, Mar. 17–19, 2025 [5].

Chapter 7: Conclusions, Contribution and Future Work

7.1. Conclusions

Based on extensive simulation studies and theoretical analysis conducted in this research, the following key conclusions can be drawn:

- This research successfully demonstrated that inverter-based resources can be effectively controlled to emulate synchronous machine behavior through the Virtual Synchronous Machine concept. Importantly, the investigations conducted in this research proved the viability of implementing VSM control in grid-following inverter mode, expanding its potential applications in modern power systems.
- The proposed VSM approach addresses critical dynamic response challenges, particularly improving fault recovery performance for renewable generation equipment connected to weak grid locations.
- The VSM control concept demonstrates versatile implementation potential across various renewable energy systems, including battery energy storage systems (BESS), solar PV plants, and hybrid solar PV-battery installations. In addition, this research demonstrates that partial deployment of VSM control on select inverters within a plant can effectively combine the advantages of both VSM emulation and conventional grid-following operation.
- When operating as VSMs, inverter-based resources can effectively replicate the inertial response characteristics of synchronous machines. However, inherent differences emerge due to the current - limiting of inverter control systems, which safeguards power electronics during fault conditions. These operational constraints make it essential to evaluate the key

parameters governing an IBR's effective inertial contribution, collectively termed in this research as the "**un-curtailed inertia capacity**." Four primary factors determine this capacity: (1) the inverter's rated power capacity, (2) its pre-disturbance operating point, (3) the magnitude of system frequency deviation during disturbances, and (4) the rate-of-change-of-frequency (RoCoF). Understanding these dependencies enables optimal VSM tuning to maximize grid stability benefits while respecting the physical limits of power electronic systems.

7.2. Contributions

This research makes several contributions to the field of renewable energy integration and power system stability, in the context of large-scale penetration of inverter-based resources. The key contributions of the thesis are summarized below:

- This research introduces an innovative Virtual Synchronous Machine (VSM) control strategy specifically designed for grid-following inverters, addressing a critical gap in existing literature where most VSM implementations are limited to grid-forming approaches with simplified machine emulations. Unlike conventional methods, the proposed solution comprehensively captures both the electromagnetic and mechanical response characteristics of synchronous machines. This holistic emulation enables more accurate representation of full transient behavior while maintaining compatibility with standard grid-following inverter operations, offering new possibilities for stability enhancement in renewable-rich power systems without requiring fundamental changes to existing inverter configurations.

- The proposed VSM control strategy was implemented on a battery energy storage system and rigorously evaluated through comprehensive electromagnetic transient simulations. Using industry-standard EMT simulation platform (PSCAD/EMTDC), the method underwent extensive testing across multiple practical transmission network configurations to validate its performance under realistic grid conditions. These simulation studies demonstrated the controller's effectiveness in maintaining system stability while accurately emulating synchronous machine characteristics, confirming its applicability for real-world power system applications. The test results from various transmission network scenarios provide strong evidence of the method's robustness and scalability for large-scale renewable integration.
- This research significantly extends the applicability of Virtual Synchronous Machine technology by developing solutions specifically designed for large-scale transmission networks. While conventional VSM methods have primarily focused on grid-forming implementations in simple network setups or microgrids, the proposed approach addresses critical renewable integration challenges in weak grid locations at the transmission level. Through comprehensive testing and validation, the study demonstrates how VSM control can effectively enhance system stability and facilitate higher penetrations of inverter-based resources in bulk power systems, filling an important gap in existing research and practice.
- This research makes significant contributions to the development and validation of simulation-based assessment methods for grid-following solar inverters employing Virtual Synchronous Machine control. Through detailed electromagnetic transient simulations, the research establishes a comprehensive framework for evaluating VSM performance, with particular focus on comparative analysis of frequency responses between VSM-controlled

inverters and conventional synchronous machines. These investigations yield critical insights into inertial response characteristics and their emulation accuracy. Furthermore, the work introduces the novel concept of "un-curtailed inertia capacity" for inverter-based resources, providing a quantitative metric to assess the available inertial power contribution during grid disturbances. Together, these advancements not only deepen the technical understanding of VSM control dynamics but also establish practical methodologies for compliance testing of next-generation grid-supportive inverter technologies in renewable-rich power systems.

- While existing literature predominantly focuses on implementing Virtual Synchronous Machine concepts in Battery Energy Storage Systems, this research significantly advances the field by successfully applying the novel VSM approach to both battery storage systems and solar PV plants. The extension of VSM control to solar farm inverters represents a critical innovation, demonstrating measurable improvements in power system stability. Through comprehensive testing and validation, the results show that the proposed VSM implementation effectively mitigates key technical challenges in renewable integration, including enhanced fault recovery performance and damping of unstable oscillations. This breakthrough substantially broadens the practical applications of VSM technology, offering power system operators more flexible options for maintaining grid stability amid growing renewable energy penetration.
- This research introduces a hybrid control approach that combines the operational benefits of conventional grid-following strategies with the stability advantages of Virtual Synchronous Machine technology. The proposed method demonstrates successful scalability across hybrid renewable energy systems, offering a flexible solution that

maintains grid compliance while enhancing dynamic response capabilities. Importantly, this hybrid implementation preserves the fault ride-through performance of standard grid-following inverters while simultaneously providing VSM-based inertial support and damping characteristics. The approach has been validated for solar PV plants and shows potential for application to BESS-solar PV hybrid plant systems, representing a significant advancement in control strategies for modern renewable power plants.

The contributions made in this research have resulted in the following list of publications.

- R. T. Gunasekara, S. Filizadeh, and D. Muthumuni, "Battery Energy Storage System Controlled as a Virtual Synchronous Machine for Improved System Stability," in Proc. IEEE Power & Energy Society General Meeting (PESGM), Denver, CO, USA, 2022, pp. 1-5.
- R. T Gunasekara, D. Muthumuni, S. Filizadeh, D. Kho, B. Marshall, B. Ponnalagan, O. D. Adeuyi, "A novel virtual synchronous machine implementation and verification of its effectiveness to mitigate renewable generation connection issues at weak transmission grid locations," IET Renewable Power Generation, vol. 17, no. 10, pp. 2436-2457, 2022.
- R. T. Gunasekara, D. Muthumuni, and S. Filizadeh, "Application of the Virtual Synchronous Machine Approach to Control a Solar PV Power Plant for Improved System Stability," in Proc. CIGRE Canada Conference & Exhibition, Vancouver, BC, Canada, Sept. 25–28, 2023.
- R. T. Gunasekara, D. Muthumuni, and S. Filizadeh, "Performance testing of a solar PV system controlled as a virtual synchronous machine to verify grid code compliance," in Proc. 22nd IET International Conference on AC and DC Power Transmission, Birmingham, UK, Mar. 17–19, 2025.

7.3. Future work

This research has demonstrated the potential of the proposed VSM approach for improving system strength and stability, particularly in the context of high renewable energy penetration. However, several areas require further investigation to enhance the applicability and practicality of VSM technology.

- Cost Implications of Adopting VSM: A detailed analysis of the cost implications of adopting VSM technology is necessary. This includes examining the impact of system size, location, and hardware requirements on overall costs. Understanding the economic feasibility of large-scale VSM deployment is crucial for industry adoption, especially in comparison to alternative solutions.
- Extension of VSM to Type-3 Wind Farms and SSCI Mitigation: Further research is needed to explore whether the VSM concept can be extended to Type 3 wind farms, particularly to address sub-synchronous control interaction (SSCI) issues. Investigating the feasibility of using VSM to mitigate SSCI could lead to broader applications of this technology in wind farm control.
- Dynamic Switching Between VSM and Regular Mode: Investigating whether inverter control can dynamically switch between VSM and regular control modes based on the operating conditions of 'special protection systems (SPS)' would provide greater flexibility and adaptability. This capability could allow for the use of VSM during critical grid conditions, while maintaining the efficiency of regular control modes during normal operation.

These future research directions will help refine and extend the proposed VSM approach, making it more robust, cost-effective, and versatile for widespread adoption in transmission-level renewable energy plants.

References

[1] “Net-zero emissions by 2050.” Government of Canada. Accessed: Oct. 27, 2023. [Online]. Available: https://www.canada.ca/en/services/environment/weather/climatechange/climate-plan/net-zero-emissions-2050.html.

[2] “Australia's Long-Term Emissions Reduction Plan”, Australian Government, Department of Climate Change, Energy, the Environment and Water, Dec. 22, 2022. [Online]. Available: https://www.industry.gov.au/data-and-publications/australias-long-term-emissions-reduction-plan.

[3] “2050 long-term strategy.” European Commission - Climate Action, [Online]. Available: https://climate.ec.europa.eu/eu-action/climate-strategies-targets/2050-long-term-strategy_en.

[4] S. H. Huang, J. Schmall, J. Conto, J. Adams, Y. Zhang and C. Carter, "Voltage control challenges on weak grids with high penetration of wind generation: ERCOT experience," in Proc. San Diego, CA, USA, 2012 IEEE Power and Energy Society General Meeting, 2012, pp. 1-7.

[5] R. T. Gunasekara, D. Muthumuni, and S. Filizadeh, "Performance testing of a solar PV system controlled as a virtual synchronous machine to verify grid code compliance," in Proc. IET Int. Conf. AC DC Power Transmiss. (ACDC Global), Birmingham, UK, Mar. 17–19, 2025.

[6] EnBW Energie Baden-Württemberg AG, RWE Renewables International GmbH, Equinor ASA, Ørsted Wind Power A/S, Scottish Power Renewables (UK) Limited, Shell Global Solutions International B.V., SSE Renewables Developments (UK) Limited, Vattenfall Wind Power Ltd., and the Carbon Trust, "Wind Power as a Controllable Source of Power Generation - Work Package 1”, 2021.

[7] M. L. Zhang, H. T. Liu and X. B. Wang, "Research overview of sub-synchronous oscillation in DFIG-BASED wind farms connected to grid," in Proc. IET International Conference on AC and DC Power Transmission (ACDC 2016), Beijing, 2016, pp. 1-5.

[8] Y. Cheng, M. Sahni, D. Muthumuni and B. Badrzadeh, "Reactance Scan Crossover-Based Approach for Investigating SSCI Concerns for DFIG-Based Wind Turbines," *IEEE Transactions on Power Delivery,* vol. 28, no. 2, pp. 742-751, Apr. 2013.

[9] Y. Wang, C. Zhang, Y. Zhang, Y. Wang, P. Xu and X. Cai, "An Adaptive Voltage-Droop Gain Tuning Method for Optimizing VSC's Power Output Capability in Weak Grids," in Proc. 2023 IEEE 14th International Symposium on Power Electronics for Distributed Generation Systems (PEDG), Shanghai, China, 2023, pp. 218-222.

[10] A. Yazdani and R. Iravani, "A unified dynamic model and control for the voltage-sourced converter under unbalanced grid conditions," in Proc. 2006 IEEE Power Engineering Society General Meeting, Montreal, QC, Canada, 2006, pp. 1.

[11] Ha Thi Nguyen, Guangya Yang, A. H. Nielsen and P. H. Jensen, "Frequency stability improvement of low inertia systems using synchronous condensers," in Proc. 2016 IEEE International Conference on Smart Grid Communications (SmartGridComm), Sydney, NSW, Australia, 2016, pp. 650-655.

[12] Z. Seddik et al., "Power system stability improvement using shunt FACTS device controller based D-statcom," in Proc. 2023 Second International Conference on Energy Transition and Security (ICETS), Adrar, Algeria, 2023, pp. 1-5.

[13] L. Fan, D. Osborn, J. Miland and Z. Miao, "Regional transmission planning for large-scale wind power," in Proc. 2009 IEEE Power & Energy Society General Meeting, Calgary, AB, Canada, 2009, pp. 1-6.

[14] M. R. Fadli, K. M. B. Nahor, N. Hariyanto, R. Rahmani and F. S. Rahman, "Special Protection System (SPS) Designing and Testing Based on Vulnerability and Frequency Security Index: Case Study of Batam-Bintan System, Indonesia," in Proc. 2021 3rd International Conference on High Voltage Engineering and Power Systems (ICHVEPS), Bandung, Indonesia, 2021, pp. 569-574.

[15] S. Sithole, N. Mbuli and J. Pretorius, "Voltage regulation in the douglas area using shunt capacitor banks and controllable shunt reactors," in Proc. 2013 13th International Conference on Environment and Electrical Engineering (EEEIC), Wroclaw, Poland, 2013, pp. 85-90.

[16] C. R. Sarimuthu, V. K. Ramachandaramurthy, K. R. Agileswari, and H. Mokhlis, "A review on voltage control methods using on-load tap changer transformers for networks with renewable energy sources," *Renewable and Sustainable Energy Reviews*, vol. 62, pp. 1154-1161, 2016.

[17] C. Schauder, "Vector analysis and control of advanced static VAr compensators," in Proc. International Conference on AC and DC Power Transmission, London, UK, 1991, pp. 266-272.

[18] Di Wu et al., “Assessing Impact of Renewable Energy Integration on System Strength Using Site-Dependent Short Circuit Ratio,”, *IEEE Trans. on sustainable energy*, vol. 9, no. 3, Jul. 2018.

[19] A. I. Aldaoudeyeh, "Weak Power Grid Analysis for Renewable Energy Sources Integration," Ph.D. dissertation, Dept. Agriculture and Applied Science, North Dakota State Univ, Jun. 2019.

[20] S. L. Lorenzen, A. B. Nielsen and L. Bede, "Control of a grid connected converter during weak grid conditions," in Proc. 2016 IEEE 7th International Symposium on Power Electronics for Distributed Generation Systems (PEDG), Vancouver, BC, Canada, 2016, pp. 1-6.

[21] S. Achilles, J. MacDowell, C. Smith, "Integrating Inverter-Based Resources into Low Short Circuit Strength Systems, Reliability Guideline," North American Electric Reliability Corporation (NERC), Dec. 2017.

[22] "IEEE Guide for Planning DC Links Terminating at AC Locations Having Low Short-Circuit Capacities," IEEE Standard 1204, vol., no., pp.1-216, 21 Jan. 1997.

[23] R. T. Gunasekara, S. Filizadeh and D. Muthumuni, "Battery Energy Storage System Controlled as a Virtual Synchronous Machine for Improved System Stability," in Proc. 2022 IEEE Power & Energy Society General Meeting (PESGM), Denver, CO, USA, 2022, pp. 1-5.

[24] C. Hardt, D. Premm, P. Mayer, F. Mosallat, and S. Goyal, "Practical experience with mitigation of sub-synchronous control interaction in power systems with low system strength," *CIGRE Science & Engineering*, vol. 21, pp. 5–14, Jun. 2021.

[25] "The Black System Event Compliance Report - Investigation into the Pre-event, System Restoration, and Market Suspension aspects surrounding the 28 September 2016 event", Australian Energy Regulator (AER), Melbourne. Accessed: Dec. 03, 2023. [Online]. Available: https://www.aer.gov.au/system/files/Black%20System%20Event%20Compliance%20Report%20-%20Investigation%20into%20the%20Pre-event%20System%20Restoration%20and%20Market%20Suspension%20aspects%20surrounding%20the%2028%20September%202016%20event.pdf.

[26] S. D'Arco and J. A. Suul, "Virtual synchronous machines-Classification of implementations and analysis of equivalence to droop controllers for microgrids," in Proc. 2013 IEEE Grenoble Conference, Grenoble, France, Jun. 2013, pp. 1–7

[27] S. P and T. M. M., "A Droop Controller Based Active Power Sharing of Parallel Inverter Islanded Microgrid," in Proc. 2022 International Conference on Futuristic Technologies in Control Systems & Renewable Energy (ICFCR), Malappuram, India, 2022, pp. 1-6.

[28] S. D'Arco and J. A. Suul, "Equivalence of Virtual Synchronous Machines and Frequency-Droops for Converter-Based MicroGrids," *IEEE Transactions on Smart Grid*, vol. 5, no. 1, pp. 394-395, Jan. 2014.

[29] Y. Chen1, R. Hesse, D. Turschner and Hans-Peter Beck, "Comparison of methods for implementing virtual synchronous machine on inverters." in Proc. 2012 International conference on renewable energies and power quality, Santiago de Compostela (Spain), Mar. 28-30, 2012, pp. 734-739.

[30] K. Sakimoto, Y. Miura and T. Ise, "Stabilization of a power system with a distributed generator by a Virtual Synchronous Generator function," in Proc. 8th International Conference on Power Electronics, ECCE Asia, 2011, pp. 1498-1505.

[31] V. Thomas, S. Kumaravel and S. Ashok, "Reduction of Frequency Oscillations in Solar PV Microgrid using Virtual Synchronous Machine," in Proc. 2019 International Conference on Power Electronics Applications and Technology in Present Energy Scenario (PETPES), 2019, pp. 1-5.

[32] K. Sebaa, Y. Zhou, Y. Li, A. Gelen and H. Nouri, "Low-frequency Oscillation Damping Control for Large-scale Power System with Simplified Virtual Synchronous Machine," *Journal of Modern Power Systems and Clean Energy*., vol. 9, no. 6, pp. 1424-1435, Nov. 2021.

[33] M. Baruwa and M. Fazeli, "Impact of Virtual Synchronous Machines on Low-Frequency Oscillations in Power Systems," *IEEE Transactions on Power Systems*, vol. 36, no. 3, pp. 1934-1946, May. 2021.

[34] J. Alipoor, Y. Miura and T. Ise, "Power System Stabilization Using Virtual Synchronous Generator with Alternating Moment of Inertia," *IEEE Journal of Emerging and Selected Topics in Power Electronics*, vol. 3, no. 2, pp. 451-458, Jun. 2015.

[35] C. Li, I. Cvetkovic, R. Burgos and D. Boroyevich, "Assessment of Virtual Synchronous Machine based Control in Grid-Tied Power Converters," in Proc. 2018 International Power Electronics Conference (IPEC Niigata 2018 -ECCE Asia), 2018, pp. 790-794.

[36] T. Kerdphol, M. Watanabe, Y. Mitani, D. Turschner and H. -P. Beck, "Stability Assessment of Multiple Virtual Synchronous Machines for Microgrid Frequency Stabilization," in Proc. 2020 IEEE Power & Energy Society General Meeting (PESGM), Montreal, QC, Canada, 2020, pp. 1-5.

[37] M. P. N. van Wesenbeeck, S. W. H. de Haan, P. Varela and K. Visscher, "Grid tied converter with virtual kinetic storage," in Proc. IEEE Bucharest PowerTech, Bucharest, Romania, 2009, pp. 1-7.

[38] Khan, S. Aziz, Wang, Mengqi, Su, Wencong, Liu, Guanliang and Chaturvedi, Shivam, "Grid-Forming Converters for Stability Issues in Future Power Grids", *Energies*, 15, issue 14, p. 1-18, 2002.

[39] "Application of Advanced Grid-scale Inverters in the NEM", Australian Energy Market Operator, AU, Aug. 2021.

[40] P. M. Anderson, A. A. Fouad, "The Synchronous Machine," in *Power System Control and Stability*, 2nd edn. Hoboken, NJ, USA, of John Wiley & Sons, inc., 2006, ch.6, pp. 83-148.

[41] "Dynamic models for fossil fueled steam units in power system studies," *IEEE Transactions on Power Systems*, vol. 6, no. 2, pp. 753-761, May 1991.

[42] *IEEE Recommended Practice for Excitation System Models for Power System Stability Studies*, IEEE Standard 421.5, 10 Aug. 2016.

[43] Q. Zhong and G. Weiss, "Synchronverters: Inverters That Mimic Synchronous Generators," *IEEE Transactions on Industrial Electronics*, vol. 58, no. 4, pp. 1259-1267, April 2011.

[44] R. T. Gunasekara et al., "A novel virtual synchronous machine implementation and verification of its effectiveness to mitigate renewable generation connection issues at weak transmission grid locations", *IET Renewable Power Generation*, vol. 17, no. 10, p. 2436-2457, 2022.

[45] R. T. Gunasekara, D. Muthumuni, S. Filizadeh, “Application of the Virtual Synchronous Machine Approach to Control a Solar PV Power Plant for Improved System Stability,” in CIGRE Canada Conference & Exhibition Vancouver, BC, Sept.25 – 28, 2023.

[46] Rathnayake, et al. “Grid Forming Inverter Modeling, Control, and Applications.” *IEEE Access*, vol. 9, 2021, pp. 114781–807.

[47] R. Aljarrah, B. B. Fawaz, Q. Salem, M. Karimi, H. Marzooghi and R. Azizipanah-Abarghooee, "Issues and Challenges of Grid-Following Converters Interfacing Renewable Energy Sources in Low Inertia Systems: A Review," *IEEE Access*, vol. 12, pp. 5534-5561, 2024.

[48] S. Chakraborty, A. Hoke and B. Lundstrom, "Evaluation of multiple inverter volt-VAR control interactions with realistic grid impedances," in Proc. 2015 IEEE Power & Energy Society General Meeting, Denver, CO, USA, 2015, pp. 1-5.

Appendix A

The practical transmission test system data for transformers, transmission lines, and boundary buses are presented below.

Table 8.1: Transformer data of the test system

Transformer	**Rating**	**X (pu)**	**Voltage level (kV)**
TF 1	150 MVA	0.1	66/132
TF 2	300 MVA	0.1	132/275
TF 3	125 MVA	0.1	66/132
TF 4	100 MVA	0.1	22/66
TF 5	75 MVA	0.1	22/66

Table 8.2: Transmission line data of the test system

T Line	**R (pu/m)**	**X (pu/m)**	**Y (pu/m)**	**Length**	**Voltage**
T Line 1	9.20E-06	1.15E-05	4.40E-07	60 km	66 kV
T Line 2	8.60E-07	2.90E-06	5.60E-07	80 km	132 kV
T Line 3	8.60E-07	2.90E-06	5.60E-07	30 km	132 kV
T Line 4	8.60E-07	2.90E-06	5.60E-07	1 km	132 kV
T Line 5	8.60E-07	2.90E-06	5.60E-07	40 km	132 kV
T Line 6	8.60E-07	2.90E-06	5.60E-07	40 km	132 kV
T Line 7	9.20E-06	1.15E-05	4.40E-07	30 km	66 kV
T Line 8	9.20E-06	1.15E-05	4.40E-07	45 km	66 kV
T Line 9	9.20E-06	1.15E-05	4.40E-07	3 km	66 kV

Table 8.3: Load data of the test system

Load	**Bus No**	**P (MW)**	**Q (MVAr)**	**Voltage**
Load 1,2	Bus 13	23	1.8 (Inductive)	22 kV
Load 3	Bus 4	3	1.5 (Inductive)	22 kV
Load 4	Bus 5	90	7.5 (Inductive)	66 kV
Load 5	Bus 6	1.8	2.7 (Capacitive)	132 kV
Load 6	Bus 6	0	10 (Capacitive)	132 kV
Load 7	Bus 8	31.5	51 (Inductive)	66 kV
Load 8	Bus 7	0	40 (Inductive)	132 kV
Load 9	Bus 10	18	0	132 kV
Load 10	Bus 10	0	15 (Inductive)	132 kV

Table 8.4: Equivalent Source Data

Bus	**Source Impedance**	**Terminal Voltage (pu)**	**Phase Angle (deg)**	**Initial P, Q**
9	55∠80	1.03	10.75	-106 MW, 28 MVAr
10	170∠85	1.02	18.35	14 MW, -14MVAr
11	40∠85	1.03	19.9	213 MW, 12 MVAr